

## RESEARCH ARTICLE

# A novel approach for early detection of impending voltage collapse events based on the support vector machine

Huy Nguyen Duc<sup>1</sup>  | Innocent Kamwa<sup>2</sup> | Louis-A Dessaint<sup>3</sup> | Huy Cao-Duc<sup>4</sup>

<sup>1</sup>Electric Power Systems, School of Electrical Engineering, Vietnam

<sup>2</sup>Power Systems and Mathematics, Hydro-Quebec, Canada

<sup>3</sup>Electrical Engineering, Ecole de technologie supérieure, Canada

<sup>4</sup>Power System Planning, Institute of Energy, Vietnam

## Correspondence

Huy Nguyen Duc, Electric Power Systems, School of Electrical Engineering, Vietnam.  
Email: huy.nguyenduc1@hust.edu.vn

## Funding information

Vietnam National Foundation for Science and Technology Development (NAFOSTED), Grant/Award Number: 102.05-2013.27

## Summary

This paper proposes an approach to detect the possibility of long-term voltage instability, based on online measurement of system bus voltages. An optimization framework is proposed to determine the maximum loading points, with different load increase patterns and different levels of reactive power output. The operating conditions so obtained are used as the training database for an artificial intelligence classifier based on the support vector machines. In an online application, the support vector machine classifier helps in detecting the probability of some generators operating at high reactive power output, which is an important indicator of an impending voltage collapse. The proposed framework is tested with the IEEE 39 bus and the Nordic 32 bus systems. The test results demonstrate that the proposed scheme gives reliable prediction of the power system long-term voltage stability.

## KEYWORDS

long-term voltage collapse, multiclass classification, power system stability, reactive power reserve, support vector machine

## 1 | INTRODUCTION

Cascading failures and blackouts are the severest possible contingencies in the operation of large electric power systems. The cascading event is generally triggered by the failure of a critical component, which can lead to cascaded tripping, loss of control at certain parts of the power system, and eventually to islanding or total blackout. To reduce the risk of cascading failures, many efforts have been made to develop more efficient real-time algorithms for stability analysis and to improve power dispatcher's situational awareness. However, large-scale power grid failures continue to occur, as evidenced by the North America blackout<sup>1</sup> in 2003, the blackout of the India power system<sup>2</sup> in 2012, and the blackout in the Southern grid of Vietnam<sup>3</sup> in 2013.

A lot of research has been done on improving the accuracy and effectiveness of online stability analysis.<sup>4,5</sup> For long-term

voltage stability evaluation, the condition of the load flow Jacobian is considered to be a good indicator of the power system operating condition (OC). The reconstruction of the Jacobian matrix from online measurements requires a substantial amount of data and the convergence of State Estimation algorithms. Several alternative solutions to the estimation of the Jacobian matrix have been proposed. Previous studies<sup>6-9</sup> proposed a Thevenin representation of the power system at important tie lines. The degradation of steady-state performance can be detected by the changes in the Thevenin circuit parameters. Glavic et al<sup>10,11</sup> proposed the construction of a reduced order model of the system that represents the network dynamics and the dynamics of Over Excitation Limiter (OEL) devices. A framework for data filtering and for computing voltage sensitivities from synchrophasor data was proposed in 1 study<sup>12</sup> to assess the voltage stability condition.

**List of abbreviations:** OC, Operating Condition; OEL, Over Excitation Limiter; OLTC, On-Load Tap Changer; OPF, Optimal Power Flow; SVM, Support Vector Machine.

One important event in the developing process of voltage collapse is the loss of voltage control, when the system's voltage level continues to decrease even with more reactive injection from the generators. In small-signal stability analysis, this is explained by the fact that there is an eigenvalue that changes sign.<sup>10,13</sup> It has been shown that at this point, the determinant of the system Jacobian matrix also changes sign.<sup>14</sup> An alternative solution to using Jacobian matrix is based on sensitivity evaluation. Another study<sup>10</sup> estimates the sensitivity of reactive injection regarding load reactive demand. This approach has been shown to detect instability condition earlier than the impedance-based methods.<sup>11</sup>

It is well understood that reactive reserve and OEL devices play very important roles during the process of voltage collapse. Once the OEL is activated, it severely limits its generator reactive output, which causes a reduction in reactive support for the neighboring area. Therefore, one reasonable approach to anticipating the voltage collapse is by monitoring the state of OEL devices in the system. Alternatively, the reactive reserve of the whole system can be monitored. Several studies suggest the use of reactive reserve to predict the system voltage stability condition.<sup>15-17</sup> One study<sup>15</sup> shows that there is a quasilinear relationship between Var reserve and the maximum load margin for a given pattern of load increase. Multilinear regression models have been developed to predict the load margin, based on generators' reactive reserves.<sup>16</sup>

The approach of determining the relationship between the reactive reserve and the maximum loading point, as in previous studies,<sup>15-17</sup> also has some drawbacks. First, the maximum loading point, as well as the relevant generators, may change considerably depending on the load increase pattern. Second, the maximum loading point also depends on how the generators respond to the increase in active power load. This represents another source of uncertainty. Third, in the power flow-based framework to determine the maximum loading point, the generators' reactive reserves are determined by their capability curves. Under actual OCs, a generator can produce reactive power beyond its rated value for a short period of time, before corrective actions are issued to alleviate its reactive power burden. To derive a more realistic generation response, a quasi-static simulation (QSS) approach, which models the OELs, and also the speed governors, can be used.<sup>18</sup> The study in Capitanescu and Cutsem<sup>19</sup> used this approach to determine marginally stable OCs. One important feature of the QSS-based approach is that it can take into account the operating states in which several generators work above their reactive power limits (before the OELs are activated).

The recent advances in synchronized measurement technology PMU allow for better monitoring of the power system in real time. Phasor measurement unit-based algorithms have been proposed to detect transient instability<sup>20-22</sup> and voltage instability.<sup>15,23</sup> To evaluate the stability level of the OCs, online measurements can be compared with the results of off-line stability analysis. Several data mining tools, such as

artificial neural networks, support vector machines (SVMs), decision tree (DT), and random forests can be used in this regard.<sup>24-28</sup> The accuracy and effectiveness of an online algorithm based on data mining depend on the appropriate choice of the training database and, even more importantly, on the engineering relevance of the features selected as inputs to decision making. Most of the existing works on artificial intelligence (AI)-based voltage stability assessment use input data obtained from static power flow solution, in which the loads are gradually increased until the load margin is reached. In fact, the dynamics of voltage collapse events are quite more complex, involving several power system control and protection devices. Therefore, the input data from time-domain simulation are more suitable to evaluate the effectiveness and accuracy of online voltage stability assessment algorithm.

In this paper, a novel method for online detection of impending long-term voltage instability condition is proposed. The voltage stability assessment is based on the SVMs, which estimates the reactive output levels from generators using a probabilistic assessment framework. The accuracy and effectiveness of the proposed framework are tested using time-domain simulation results of voltage collapse events. The following are the main contributions of the paper:

1. A novel method for assessing the reactive power outputs from generators is proposed, based on system-wide voltage profile and an AI classification engine.
2. An optimal power flow (OPF) framework is proposed to generate training data for the classification engine.
3. A multiclass classification approach is proposed. The multiclass classifier allows the grid dispatcher to monitor the progressive degradation of stability level and thus determine the stability level with higher degree of certainty.

The remainder of the paper is organized as follows: Section 2 presents an overview of the methods and algorithms being used for predicting voltage instability. The proposed algorithm is presented in Section 3. Test results for the New England system and the Nordic 32 bus test system are presented in Section 4. A performance comparison between the proposed approach and the sensitivity-based approach is also presented in this section.

## 2 | REACTIVE RESERVE MARGIN AND VOLTAGE STABILITY

### 2.1 | The process of long-term voltage collapse

Much research has been done on the mechanism of voltage collapse and power grid blackout. A common scenario of long-term voltage collapse can be described as follows<sup>29</sup>:

- The power system experiences very heavy power transfer on important tie lines, and the reactive outputs of generators

are at high level. An initial event, such as tripping of a transmission line, disconnection of a generation unit causes further burden on the power grid.

- The on-load tap changers (OLTCs) get activated, which helps in recovering the voltage at load buses. As a result, the load demand is recovered. However, the load recovery process places additional reactive power burden on the generators. At this point, one of the generators may reach reactive power limit.
- If the overloaded condition of the excitation system is not alleviated, the Over Excitation Protection (OEL) will trip. As a result, the reactive burden will be shifted to the nearby generators. Hence, OEL devices of these generators might also be activated.
- Eventually, the power system reaches a state where there is severe loss of voltage control. The voltage will decay rapidly, leading to voltage collapse and cascaded tripping of protective relays.

The voltage collapse phenomenon described above is initiated by a loss of voltage control in the system. In the process of voltage decay, more and more reactive power is injected into the system. As a result, the voltages at several system buses get increasingly lower. Therefore, the main input variables for voltage stability analysis can be bus voltage magnitudes, reactive power flows, or branch currents.<sup>15</sup>

## 2.2 | Reactive reserve and voltage profile

In this work, we propose to use system bus voltage magnitudes to determine reactive power output from system generators. The proposed algorithm for voltage stability evaluation can be explained by analyzing a simple radial power system, which consists of 5 buses: The generator is at bus 1, and the load is at bus 5. We want to evaluate how much the load at bus 5 can be increased, with a constant power factor. The maximum load margin depends on the generator's active and reactive limit. With the active power limit relaxed, there are 4 possible results as shown in Figure 1:

- If the generator's reactive limit is set at 100% of its rated capacity, then at the maximum loading point, the voltage profiles are 1A and 2A, when the generator voltage is set at 1.1 and 1.02 pu, respectively.
- If the generator's reactive limit is increased to 130% of its rated capacity, then at the maximum loading point, the voltage profiles are 1B and 2B, when the generator voltage is set at 1.1 and 1.02 pu, respectively.

Cases 1A and 2A are stressed OCs, where an action would be necessary to reduce the reactive power burden of the generator. Cases 1B and 2B are very critical OCs, because the generator's reactive output is much higher than its rated capability. If no action is taken in time, the OEL protection will

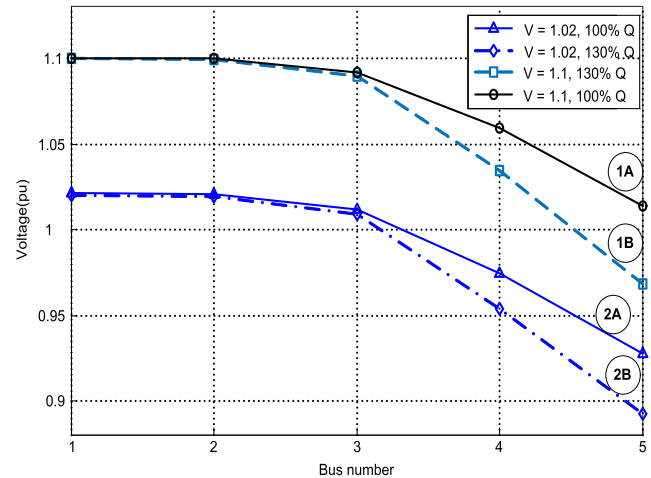


**FIGURE 1** Illustration of the proposed concept: reactive output and voltage profile

get activated and reduce generator's reactive output, which may result in voltage instability. The objective of the proposed algorithm is to differentiate between voltage profiles of cases A and B. It can be seen from this very simple example that cases B have higher voltage loss, because of higher  $I^2X$  loss in the system. The classification of actual systems will be much more complicated, because the system may have meshed structure, and the load increase patterns can be diverse. Moreover, there will be additional complexity if there are bus voltages regulated by OLTCs.

## 3 | PROPOSED ALGORITHM

### 3.1 | The proposed framework

This paper proposes the use of an AI classifier based on the SVM to detect the impending voltage collapse events. Based on online measurements of system bus voltages, the AI classifier will estimate the probability of generators working at a high reactive output. The main requirements for this classification engine are as follows:

1. It must be able to differentiate the OC, in which the system still has ample reactive reserve, from the OCs in which reactive reserves are depleted.
2. The margin of separation between these 2 classes of training instances must not be too large. That is, some amount of overlapping should be allowed. If the difference between the voltage profiles of the 2 classes is clear, then the advantage of the engine is reduced: even though we get very good training result (very low false classification rate), the engine would trigger the alarm signal about depleting reactive reserve when it is already too late.

With the above-mentioned requirements, the 2 following extreme OCs for loading margin calculations are important in database generation:

- Operating conditions representing cases 2A in Figure 1: The system still has a large amount of reserve, but the voltage set points of generators (or sink buses) are set low (1-1.05 pu). This might be considered a suboptimal OC, since the line charging capacitances are not used effectively. However, these OCs are still common in practice.
- Operating conditions representing cases 1B in Figure 1: The system draws very large amount of reserve, eg, 130% percent of the rated reactive capability at some generators, and the generator voltage set points are set very high to maximize reactive support from line charging capacitances.

As the reactive power burden increases in the system, the generator operating point will reach the reactive limit. Thus, the maximum loading point can be determined by gradually increasing the load demand, following a specific pattern, until the load flow fails to converge. In practice, the grid dispatchers and power plant operators can anticipate the OC at reactive limit and perform local corrective actions to relieve the reactive burden of highly stressed generators. Once the appropriate corrective actions are performed, the reactive burden can be shifted towards nearby generators (load shedding is avoided). With this consideration, the maximum loading point that the system can provide, under a given load increase pattern, can be best determined using an OPF framework. To determine the maximum loading point at load buses  $k \in C_k$ , the optimization problem is formulated with the following objective function:

$$\sum_{k \in C_k} P_{lk} \rightarrow \max \quad (1)$$

subject to

$$g(x) = 0 \quad (2)$$

$$Q_{lk} = \lambda_k P_{lk} \quad (3)$$

$$h(x) \leq 0 \quad (4)$$

$$U_{g, \min} \leq U_g \leq U_{g, \max} \quad (5)$$

$$P_{g, \min} \leq P_g \leq P_{g, \max} \quad (6)$$

$$Q_{g, \min} \leq Q_g \leq Q_{g, \max} \quad (7)$$

where  $P_{lk}$  is the active load demand at load bus  $k$ ,  $C_k$  is the set of load buses,  $x = [\theta, U_m, P_g, Q_g]^T$  is the vector of optimization variables,  $U_m$  is the vector of system bus voltage magnitudes, and  $U_g \in U_m$  is generator bus voltages. Equation 2 represents the load flow constraints, and Equation 4 the branch flow constraints. The generator voltage and active and reactive power are subject to constraints 5 to 7. The branch flow and voltage constraints should be relaxed to find the maximum loading point that stresses the generators'

capability to their limits. Besides, the lower voltage limit at load buses are also relaxed.

Problem 1 will be solved with different load increase patterns, by varying the coefficient  $\lambda_k$ . With this approach, the obtained maximum loading point will have several generators working at their reactive limits. The system bus voltages at this maximum loading point will be used as the training data for an AI-based classifier. The reason for using an OPF-based algorithm is as follows: With an optimal dispatch of the system's active and reactive power, the generators still have to produce high amounts of reactive power. Therefore, it is safe to conclude that the OC is very critical, and corrective actions are needed. The proposed framework is thus composed of 2 components: (1) The OPF problem is solved to determine how to optimally dispatch generators for a given load increase scenario; (2) the AI engine is used to identify whether the actual operating point (in terms of voltage profile) is a close match with one of these optimal solutions. It can be seen that the OPF is formulated such that in the optimal solution, the generators' reactive outputs reach their limits. Therefore, the tap changers will not have a significant impact on the optimal results.

As discussed in Section 1, the QSS approach gives more accurate estimates of the generation response to a certain load increase scenario. However, long-term power system dynamics are always influenced by human intervention. Hence, a static approach based on OPF is proposed, so that the dispatchers' corrective actions can be modeled. It should be noted that the grid dispatchers might not have sufficient time and system information to determine the best corrective actions.<sup>30</sup> However, an operating point based on OPF still represents the actual long-term condition more accurately than the one obtained from time-domain simulation without any corrective action.

To account for the situations in which some generators operate temporarily in overexcitation mode, the reactive limit in Equation 7 was set at different values (96%-130%). The optimal solutions obtained with 96% reactive output limit represent OCs of cases A, and those obtained with 120% to 130% reactive output limit represent OCs of cases B in Figure 1.

The process of database creation is illustrated in Figure 2. The load increase scenarios at load buses are varied with different load increase patterns. Besides, for each training instance, the maximum voltage set point  $U_g$  was imposed randomly at each generator (from 1.02 to 1.1 pu). As discussed in the work of Capitanescu,<sup>30</sup> when the objective of the OPF is to maximize the reactive reserve, the optimal solution often results in several generators working at its highest voltage set point. In practice, the power plants are not always operated at 1.1 pu voltage set point. Thus, we choose to vary the upper bound of set point voltage (Equation (5)), so that a wider range of realistic OCs can be created. Since the generators' voltage set points and the load increase patterns are

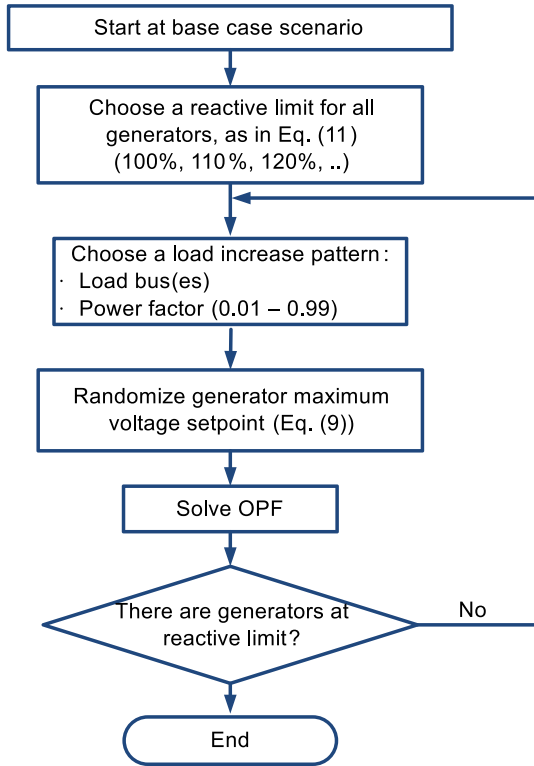


**FIGURE 2** Framework for database generation. OPF, optimal power flow

varied, the proposed approach can take into account a wide range of possible OCs. However, the training dataset will be complex and it is difficult to achieve a highly accurate classification rate, because there are significant overlaps between the instances of different classes. Given this difficulty, it is important that the condition of depleted reactive reserve is detected accurately and early, so that mitigation actions such as load shedding and blocking of OLTCs<sup>31</sup> can be more effective.

### 3.2 | Classification based on AI tools

The previous section has shown that it might be possible to assess the level of reactive outputs from the system generators by observing the system voltages and using a pattern recognition-based approach. In this work, we propose to use SVMs for classification task. The SVM have been used successfully to classify OCs, based on transient stability criteria.<sup>20,32</sup> A linear SVM can be described by Equation 8:

$$f(x) = \text{sign}(\mathbf{w}^T x + b) \quad (8)$$

The concept of a linear SVM is illustrated in Figure 3. The obtained optimal hyperplane separates the input space with a maximum possible margin. Instances that satisfy  $\mathbf{w}^T x + b > 1$  and  $\mathbf{w}^T x + b < -1$  belong to classes (label) “+1” and “-1”, and those that satisfy  $\mathbf{w}^T x + b = \pm 1$  are called the support vectors. The vector  $\mathbf{w}$  is called the weight vector.

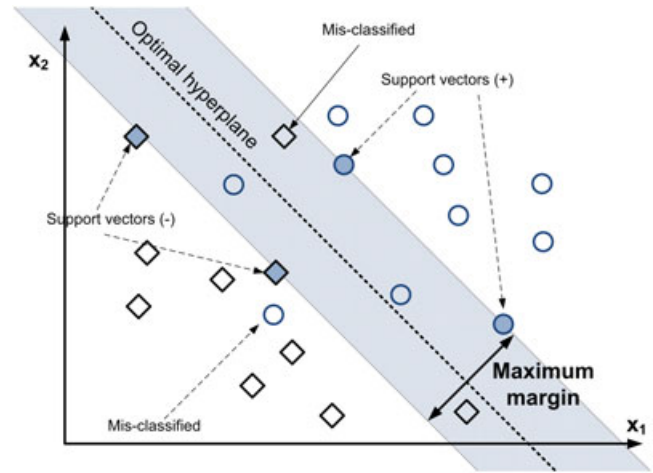


**FIGURE 3** Concept of support vector machines. The optimal hyperplane separates 2 classes of instances: square and circle. The dark-filled instances are called support vectors

The objective of training the SVM is to maximize the margin  $\frac{2}{\|\mathbf{w}\|}$ , which is equivalent to minimizing  $\|\mathbf{w}\|$ . The optimization problem is formulated as follows:

$$\min_{\mathbf{w}, b, \xi} \frac{1}{2} \mathbf{w}^T \mathbf{w} + C \sum_{i=1}^l \xi_i, \quad (9)$$

subject to

$$\begin{cases} y_i(\mathbf{w}^T \phi(x_i) + b) \geq 1 - \xi_i \\ \xi_i \geq 0. \end{cases} \quad (10)$$

In Equation 10, the function  $\phi(x)$  represents a nonlinear mapping, which maps the input vector  $x$  into a higher dimensional space. With appropriate selection of the kernel function, the classification problem becomes linearly separable in the new higher dimensional space. To allow for some misclassification, a penalty on error term  $C$  is used in Equation 9. The SVM concept can be expanded for multiclass classification. The common strategy for multiclass classification is comparing one-against-one or one-against-all.<sup>33</sup> In this work, the LibSVM package<sup>34</sup> was used for SVM training. Besides giving a predicted label for an input instance, the probability of this label (ie, its degree of certainty) can also be estimated. In the developing process of voltage instability, the SVM engine will give the highest probability first to a normal state, then to the highly stressed state, and finally to the critical state. This progression can be a more reliable indication of a gradual decrease in voltage stability level. This probabilistic assessment is very useful in the proposed framework, because the training dataset is deliberately created such that there is significant overlaps between classes, as discussed in Section 3.1.

Besides the SVM, several other classification tools can be used in the proposed framework. Currently, the state-of-the-art classification engines are as follows<sup>35</sup>: the probabilistic neural networks, the DT and its variants, such

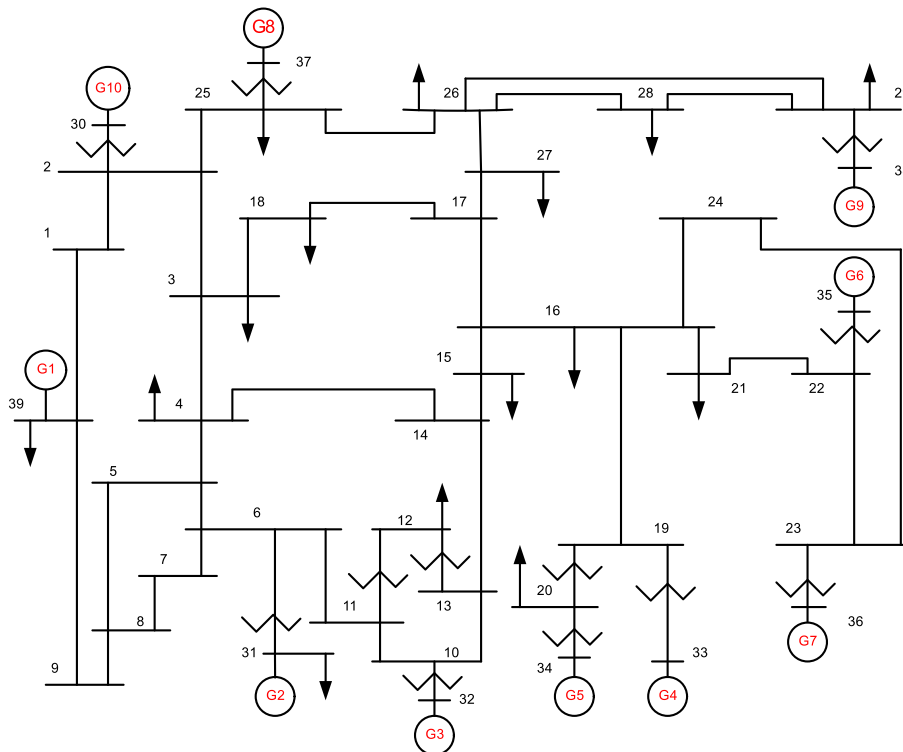


**FIGURE 4** The New England system

as random forest and bagged trees, etc. The DTs have been used successfully for transient stability classification.<sup>21,24</sup> The main principle of these tools is that a group of “weak learners” can form a more accurate predictor. Each ensemble consists of several DTs, which are trained with different subsets of the training data. Similar to the probability estimation of the SVM, these classification engines also estimate the probability of the prediction label, using different scoring systems.

## 4 | TEST RESULTS AND PERFORMANCE COMPARISON

### 4.1 | The New England system

The proposed algorithm was first applied for the New England (IEEE 39 bus) system, as shown in Figure 4. For this system, 2 classes of reactive output levels—the first one 110% and the second one 130%—were prepared for SVM training. The OPF calculation was conducted using MATPOWER.<sup>36</sup> For SVM input features selection, only the voltages of 230-kV buses were selected. A total of 600 OCs were created. As the difference between the voltage profiles of the 2 classes was large, the achieved classification accuracy was almost 100%. The contingency considered for this system was the loss of a generation unit at bus 38. The simulations were performed using PSS/E software. In the dynamic simulation, the loads are represented as ZIP model. The system voltage response to the tripping of the generator at bus 38 is shown in Figure 5.

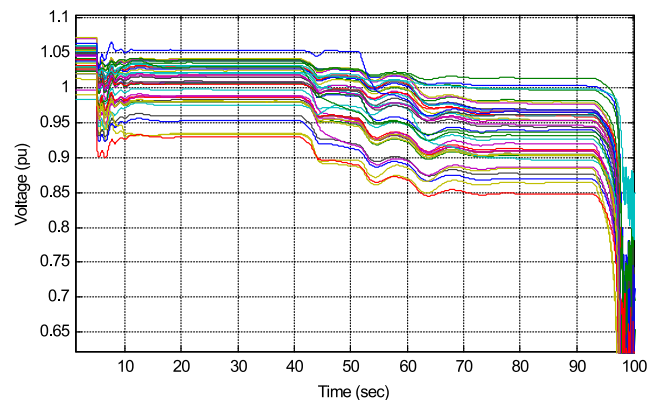


**FIGURE 5** Voltage response of New England system, with loss of generator at bus 38

The reactive power outputs of all the system generators and the timing of OEL actions are shown in Figure 6.

The tripping of the generating unit at bus 38 resulted in voltage collapse at around 100 seconds (see Figure 5). As can be seen in Figure 5, the tripping of the generating unit at bus 38 resulted in voltage collapse at around 100 seconds. It is evident from Figure 6 that while the OEL was under activation at one generator, the other generators in the system had to take on additional reactive power burden. The cascaded operations of OEL devices have led to voltage collapse.

Figure 7 shows the probability estimation of reactive reserve margin, in function of time. Voltage signals were

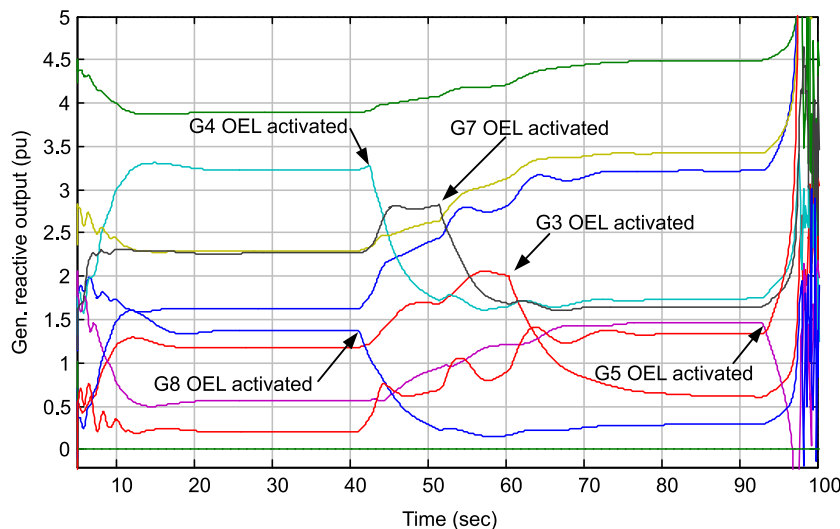


**FIGURE 6** Generator reactive output, with loss of generator at bus 38. OEL, Over Excitation Limiter

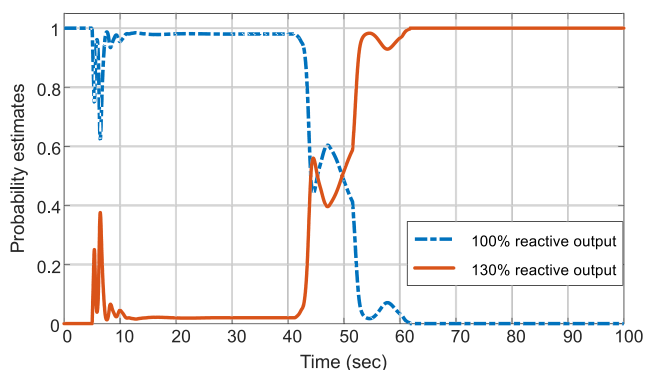


**FIGURE 7** Probabilities reactive output level, with loss of generator at bus 38

sampled at every 0.1 second and sent to the SVM engine. To evaluate the effect of transient responses on the performance of the SVM, no attempt was made to filter the voltage waveform.

It can be seen from Figure 7, that after the OEL activations at generators G8 (bus 37) and G4 (bus 33), the probability of instability rose very rapidly. The violation of 130% reactive reserve margin can be confirmed with high certainty (more than 80%) at around 50 seconds. At this instant, some system bus voltages also started to decrease below 0.9 pu, as shown in Figure 5. There was ample time for mitigation action, as the voltage collapse did not happen until 50 seconds later. At  $t = 5$  seconds, where the generator G9 tripped, the system transient caused severe disturbance to the probability evaluation. Therefore, a low-pass filter should be applied at bus voltages to avoid false classification. The other alternative is to wait until the probability estimates become quite consistent, before applying corrective actions.

## 4.2 | The Nordic 32 bus system

The foregoing New England system example is a simple demonstration of the proposed algorithm. With this system, the classification problem is rather simplified, because there were no OLTC actions considered. To verify the effectiveness of the proposed algorithm when there are OLTCs, we applied it to the Nordic 32 bus test system. This system was created by CIGRE for the analysis of long-term voltage instability.<sup>37</sup> Long-term voltage stability simulations for this system have been reported extensively in the literature.<sup>10,38</sup> The single-line diagram of the Nordic 32 bus test system is shown in Figure 8.

### 4.2.1 | Database generation and training

For this system, we created 3 following classes of reactive reserve margins:

- Class 1—“100% reactive power output.” For this class, 2 sets of optimization solutions were used: one with generators’ reactive limit set to 100% and the other with generators’ reactive limit set to 96%.
- Class 2—“110% reactive power output.”
- Class 3—“120% and higher reactive power output.” For this class, 2 sets of optimization were performed. The first one with generators’ reactive limit extended to 120% of their rated capacity, and the second one extended to 130%.

A total of 1600 OCs were created for these 3 classes. The voltage magnitudes at all 400 kV and load buses were used as input for the SVM. The performance matrix of the SVM classifier for 3 data classes is shown in the Table 1. Unsurprisingly, the classification accuracy of class 2, which lies between the other 2 classes, is the lowest. As discussed in Section 3, the database is created such that there are significant overlaps between classes. Thus, the classification

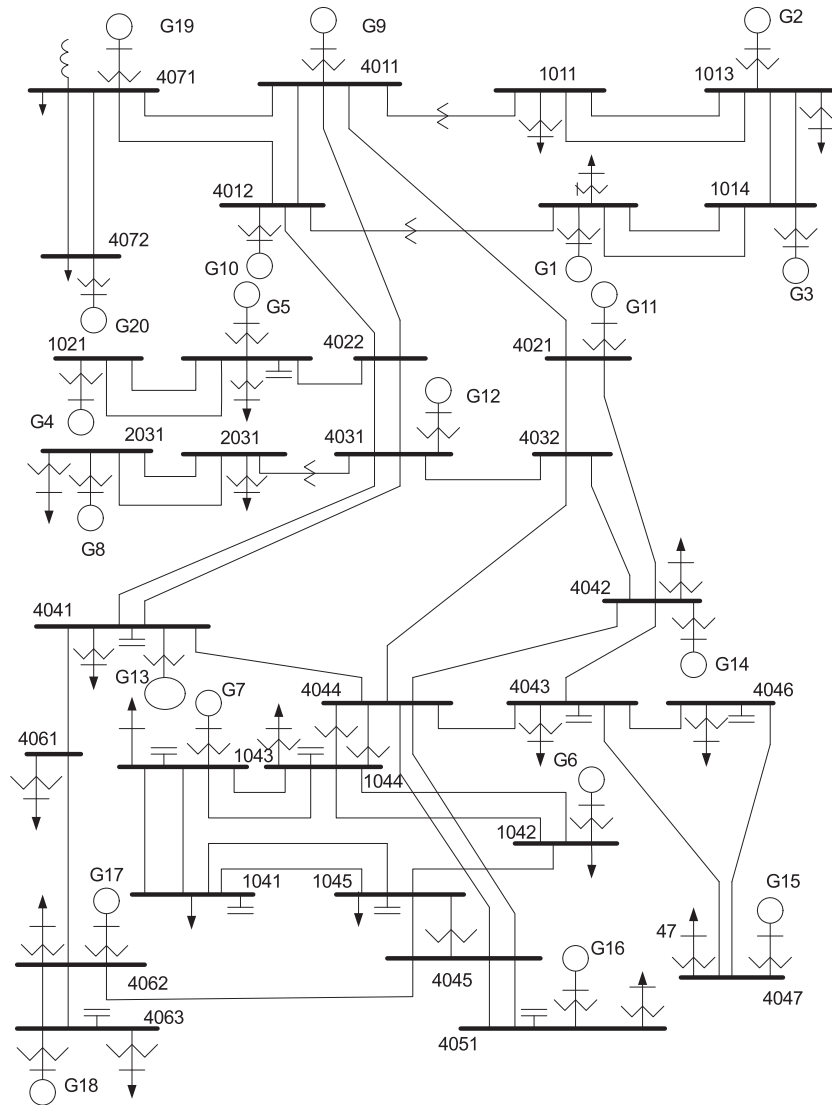


**FIGURE 8** The Nordic 32 bus system

**TABLE 1** Performance of the SVM for 3 data classes

Data	Classified as 1	Classified as 2	Classified as 3
Class 1 (100%)	97.22 %	2.78 %	0%
Class 2 (110%)	5.05 %	93.18 %	1.77%
Class 3 ( $\geq 120\%$ )	2.52 %	3.14 %	94.34%

Abbreviation: SVM, support vector machine.

accuracy as shown in Table 1 can be considered very good, with a very small false negative rate (class 3 being classified as class 1) and zero false positive rate (class 1 being classified as class 3).

#### 4.2.2 | Case 1: unstable long-term dynamics

The disturbance considered in this case was the tripping of the generator at bus 4047, at  $t = 50$  seconds. The system voltage response is shown in Figure 9. After the tripping of

the generator, the system suffered low voltage, which led to several OLTC operations. As a result, the system's reactive reserve reduced gradually. Finally, several OEL relays timed out. The OELs at generator buses 1042, 1043, 4042, and 4031 timed out at 139, 139, 142, and 156 seconds, respectively. After 200 seconds, the system suffered a very low voltage profile and unstable power oscillation. Voltage collapse finally occurred at  $t = 242$  seconds.

The probabilities of different reactive margin levels are shown in Figure 10. Again, as the voltages were not subjected to filtering, we could observe the oscillations in the probability estimation, due to OLTC switchings. After the tripping of the unit at bus 4047, the probability of "120+% reactive level" started increasing. At around 125 seconds, its probability became significantly higher than that of the 2 other labels, which evidently indicated that excessive reactive power was being drawn from the remaining generators. It is worth noting that, at this time, no OEL relays timed out yet. As the

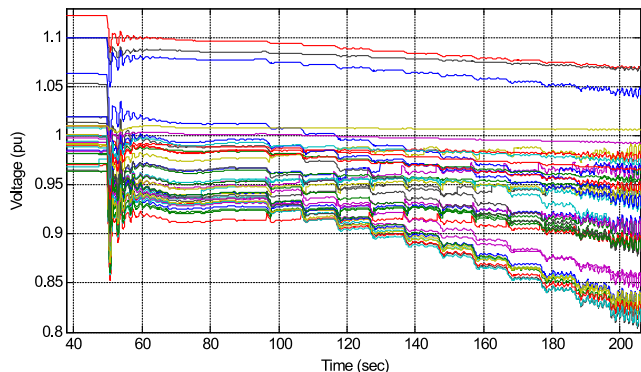


**FIGURE 9** Voltage response of Nordic system, with loss of generator at bus 4047

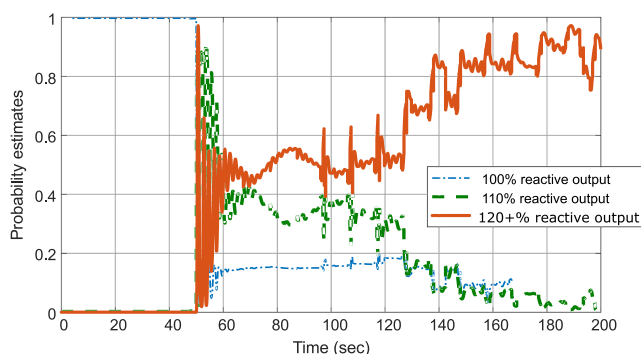


**FIGURE 10** Probability of reactive output levels, with loss of generator at bus 4047

system’s voltage condition deteriorated, the certainty level of the “120+% reactive output” class also increased. Besides, most bus voltages remained at higher than 0.9 pu, which is above the practical voltage level for most undervoltage load shedding relays.

From a comparison of the changes in probability prediction of the Nordic 32 bus system (see Figure 10) with those of New England system (see Figure 7), it becomes evident that the probability estimates change much more slowly in the case of the Nordic 32 bus system. As there is little difference between the voltage profiles of different input classes, the SVM engine cannot estimate, with high certainty, the reactive reserve level of the system during the first cascading OLTC actions. However, when the probability of 120+% reactive output was high, there was still a large time window for the grid dispatcher to initiate corrective actions. In the case of the New England system, the “130% reactive output” was detected with high certainty, but only when the system voltages were already quite low, and the system was close to voltage collapse. This comparison suggests that a multiclass classification approach should be used to detect the progressive evolution of voltage collapse.

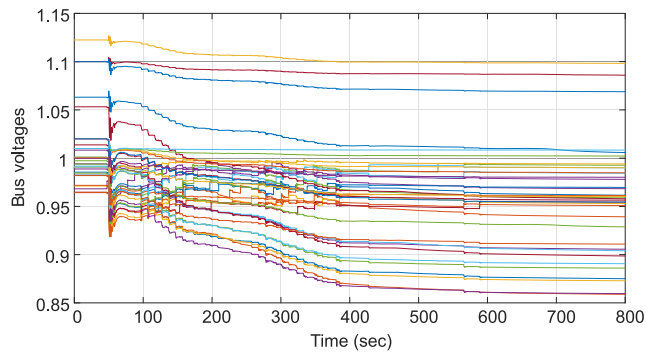


**FIGURE 11** Voltage response of Nordic system, with loss of line 4030 to 4044

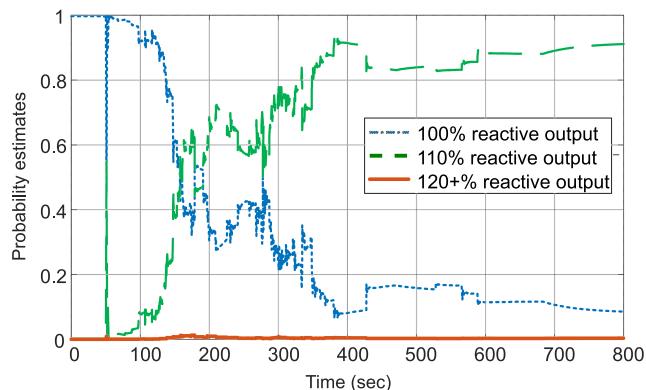


**FIGURE 12** Probability of reactive output levels, with loss of line 4030 to 4044

### 4.2.3 | Case 2: marginally stable long-term dynamics

In this case, the system was simulated with line 4030 to 4044 tripped at  $t = 50$  seconds. This event triggered several OLTC actions at load buses. However, the generators’ reactive reserves were not depleted, and the system stabilized at 800 seconds, without any further OLTC action. The system voltages are shown in Figure 11. It is noteworthy that many bus voltages settled at 0.85 to 0.9 pu.

The reactive power margin probability evaluation is shown in Figure 12. The probability of generators working at 110% reactive limit is highest, which indicates a highly stressed condition.

### 4.3 | Comparison with the sensitivity-based approach

The results presented in the previous sections showed good performance of the proposed framework, which allows detecting early the voltage collapse events. In this section, we present briefly a performance comparison between the proposed framework and the sensitivity-based method.<sup>10</sup> The sensitivity-based method relies on estimations of the change

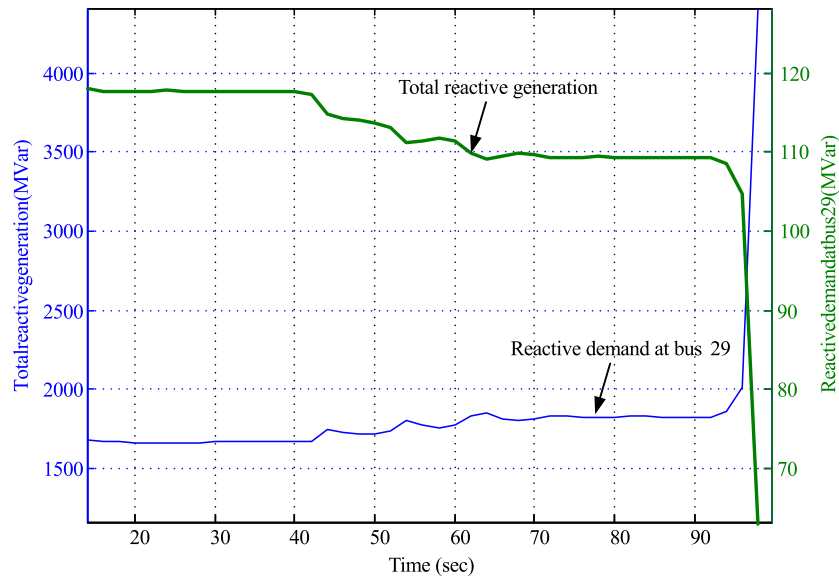


**FIGURE 13** Performance of the sensitivity-based method on the New England system

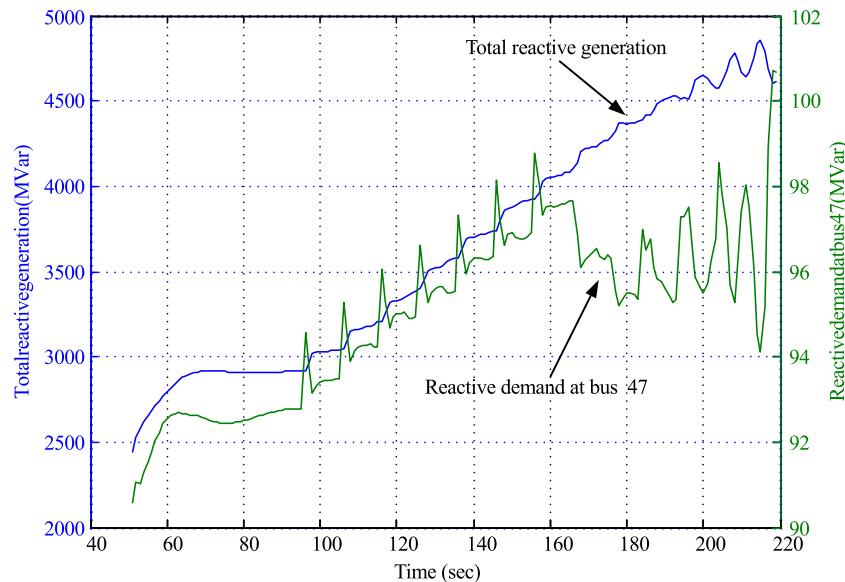


**FIGURE 14** Performance of the sensitivity-based method on the Nordic 32 bus test system

in total reactive generation and the change in reactive demands at load buses. The principles of the sensitivity method proposed in 1 study<sup>10</sup> are as follows:

- Monitor the power system parameters (voltage, currents, and branch flows) and the status of OEL relays.
- Establish a reduced order dynamic model of the system based on the measurements mentioned above.
- Assess the sensitivity of total reactive generation ( $Q_g$ ) regarding the reactive demand at load buses ( $Q_l$ ). If this sensitivity measure changes to a negative sign, a voltage instability condition is indicated, because the negative sensitivity is equivalent to the appearance of an unstable eigenvalue.

The performance of this method is thus dependent on the accuracy of the measurements and the accuracy of the identification method to derive a reduced system model. In this comparative study, we assume that a perfect measurement and a perfect identification result can be achieved. Therefore, the effectiveness of the sensitivity-based method will be assessed based on observation of raw data obtained from time-domain simulation. Another assumption is that we know exactly the weakest bus where the sensitivity measure would change sign. For the simulation scenario of the New England system, it is obvious that bus 29 is the weakest bus, since the active and reactive demand from this bus need to be supplied from remote generation buses, after the generator at bus 38 is

tripped. Figure 13 presents the total reactive generation and the reactive demand at bus 29. A negative sensitivity can be observed from 42 seconds. When the voltage instability accelerates at 97 seconds, the sensitivity measure becomes very high, as the increase in total reactive generation and the reduction of reactive demand at bus 29 are both very steep. Compared to the performance of our proposed approach in Figure 7, it can be seen that the sensitivity-based method might detect the unstable condition slightly earlier. However, we need an effective filtering algorithm and a long time window to smooth the transient effects caused by OEL switching and obtain an accurate assessment.

For the simulation scenario of the Nordic 32 bus test system, the load bus to be monitored is bus 47, nearest to bus 4047 where the generator is tripped. The total reactive generation and the reactive demand at bus 47 are shown in Figure 14. In this case, a negative sensitivity occurs clearly at 160 seconds. Compared to the result in Figure 10, it can be seen that our proposed approach triggers an alarming signal earlier (around 125 seconds). Besides, in this case, the effectiveness of the sensitivity-based method might be reduced because of large transients caused by OLTC switching and the unstable oscillations near the final voltage collapse. It should be noted that in other studies,<sup>10,11</sup> the authors have used a QSS method, which could not present accurately the effect of fast transients.

## 5 | DISCUSSION AND CONCLUSION

Depleted reactive power margin is considered an alarming signal for impending voltage instability. This paper has proposed a framework to assess the reactive output level from generators, based on real-time measurement of system voltages. The proposed analytical model does not require any dynamic model of the generators, loads, or OEL relays. The simulations performed with 2 test systems—the New England and the Nordic 32 bus test systems—show that the event of voltage collapse can be predicted quite early and accurately. In the case of Nordic 32 bus test system, the critical condition was detected even before the first OEL action. The simulations in Section 4 also show the reliability of the proposed algorithm. Even without input filtering, the transition of reactive output level from a normal to a critical state can still be observed. As OCs for different classes have large overlaps, it is difficult to achieve very high classification accuracy. However, with the proposed multiclass classification approach and the use of probability/score estimates, the reliability of voltage stability assessment can be guaranteed. A comparison with the sensitivity-based algorithm<sup>10</sup> showed that the proposed method is much less affected by the transients caused by OLTCs and OELs.

The results obtained also underline the need for a wide-area protection scheme against voltage instability. Simulations with the Nordic 32 bus system show that an impending voltage collapse can be detected when all the bus voltages are still beyond 0.9 pu, whereas in the other case, no load shedding is required, even when several bus voltages have reached 0.85 pu. This will be the focus of the author's future work. Future work may also focus on the corrective action that can be deduced from the trained classifiers. The proposed approach can also be tested with other AI classifiers such as the random forest and the bagged trees.

## ACKNOWLEDGEMENTS

This research is funded by Vietnam National Foundation for Science and Technology Development (NAFOSTED) under grant number 102.05-2013.27.

## REFERENCES

1. Technical analysis of the August 14, 2003, blackout: What happened, why, and what did we learn? North American Electric Reliability Council; 2003.
2. Lai LL, Zhang HT, Mishra S, Ramasubramanian D, Lai CS, Xu FY. Lessons learned from July 2012 Indian blackout. Paper presented at: 9th IET International Conference on Advances in Power System Control, Operation and Management; 2012; Hong Kong, China. 1–6.
3. Nguyen-Duc H, Cao-Duc H, Nguyen-Dinh C, Nguyen-Xuan-Hoang V. Simulation of a power grid blackout event in Vietnam. Paper presented at: IEEE Power Engineering Society General Meeting; 2015; Denver, CO, USA. 1–5.
4. Cutsem TV, Vournas C. *Voltage Stability of Electric Power Systems*. In: Link S, ed. New York, NY: Springer; 1998.
5. Glavic M, Cutsem TV. A short survey of methods for voltage instability detection. Paper presented at: IEEE Power and Energy Society General Meeting; 2011; Detroit, MI, USA. 1–8.
6. Vu K, Begovic MM, Novosel D, Saha MM. Use of local measurements to estimate voltage-stability margin. *IEEE Trans Power Syst*. 1999;14(3):1029–1035. <https://doi.org/10.1109/59.780916>
7. Wang Y, Pordanjani IR, Li W, Xu W, Chen T, Vaahedi E, Gurney J. Voltage stability monitoring based on the concept of coupled single-port circuit. *IEEE Trans Power Syst*. 2011; 26(4):2154–2163. <https://doi.org/10.1109/TPWRS.2011.2154366>
8. Dmitrova E, Fredericia D, Wittrock ML, Johannsson H, Nielsen A. Early prevention method for power system instability. *IEEE Trans Power Syst*. 2015;30(4):1784–1792.
9. Xu J, Huang L, Sun Y, et al. Voltage instability detection based on the concept of short circuit capacity. *Int Trans Electr Energy Syst*. 2016;26(2):444–460. <https://doi.org/10.1002/etep.2098>
10. Glavic M, Cutsem TV. Wide-area detection of voltage instability from synchronized phasor measurements. Part I: principle. *IEEE Trans Power Syst*. 2009;24(3):1408–1416. <https://doi.org/10.1109/TPWRS.2009.2023271>
11. Glavic M, Cutsem TV. Wide-area detection of voltage instability from synchronized phasor measurements. Part II: simulation results. *IEEE Trans Power Syst*. 2009;24(3):1417–1425. <https://doi.org/10.1109/TPWRS.2009.2023272>
12. Leelaruij R, Vanfretti L, Uhlen K, Gjerde JO. Computing sensitivities from synchrophasor data for voltage stability monitoring and visualization. *Int Trans Electr Energy Syst*. 2015;25(6):933–947. <https://doi.org/10.1002/etep.1869>

13. Capitanescu F, Van Cutsem T. Unified sensitivity analysis of unstable or low voltages caused by load increases or contingencies. *IEEE Trans Power Syst.* 2005;20:321–329. <https://doi.org/10.1109/tpwrs.2004.841243>
14. Bao G, Morison G, Kundur P. Voltage stability evaluation using modal analysis. *IEEE Trans Power Syst.* 1992;7(4):1529-1542.
15. Beiraghi M, Ranjbar A. Online voltage security assessment based on wide-area measurements. *IEEE Trans Power Delivery.* 2013;28(2):989-997.
16. Leonardi B, Ajarapu V. Development of multilinear regression models for online voltage stability margin estimation. *IEEE Trans Power Syst.* 2011;26(1):374-383.
17. Milosevic B, Begovic M. Voltage-stability protection and control using a wide-area network of phasor measurements. *IEEE Trans Power Syst.* 2003;18(1):121-127. <https://doi.org/10.1109/TPWRS.2002.805018>
18. Fabozzi D, Cutsem TV. Simplified time-domain simulation of detailed long-term dynamic models. Paper presented at: IEEE Power Energy Society General Meeting; 2009; Calgary, AB, Canada. 1-8.
19. Capitanescu F, Cutsem TV. Evaluation of reactive power reserves with respect to contingencies. *Bulk Power System Dynamics and Control V.* Onomichi, Japan; 2001:377–386.
20. Gomez FR, Rajapakse AD, Annakkage UD, Fernando IT. Support vector machine-based algorithm for post-fault transient stability status prediction using synchronized measurements. *IEEE Trans Power Syst.* 2011;26(3):1474-1483. <https://doi.org/10.1109/TPWRS.2010.2082575>
21. Hashiesh F, Mostafa HE, Khatib AR, Helal I, Mansour MM. An intelligent wide area synchrophasor based system for predicting and mitigating transient instabilities. *IEEE Trans Smart Grid.* 2012;3(2):645-652. <https://doi.org/10.1109/TSG.2012.2187220>
22. Guo T, Milanovi JV. Probabilistic framework for assessing the accuracy of data mining tool for online prediction of transient stability. *IEEE Trans Power Syst.* 2014;29(1):377-385. <https://doi.org/10.1109/TPWRS.2013.2281118>
23. Xie L, Chen Y, Liao H. Distributed online monitoring of quasi-static voltage collapse in multi-area power systems. *IEEE Trans Power Syst.* 2012;27:2271–2279. <https://doi.org/10.1109/tpwrs.2012.2191310>
24. Sun K, Likhate S, Vittal V, Kolluri V, Mandal S. An online dynamic security assessment scheme using phasor measurements and decision trees. *IEEE Trans Power Syst.* 2007;22(4):1935-1943.
25. Diao R, Sun K, Vittal V. et al. Decision tree-based online voltage security assessment using PMU measurements. *IEEE Trans Power Syst.* 2009;24. <https://doi.org/10.1109/tpwrs.2009.2016528>
26. Yue X, Venkatasubramanian V. Algorithms for detection of static voltage instability in power systems using synchrophasors. Paper presented at: 43rd Hawaii International Conference on System Sciences; 2010; Honolulu, HI, USA. 1-7.
27. Kaci A, Kamwa I, Dessaint LA, Guillon S. Synchrophasor data baselining and mining for online monitoring of dynamic security limits. *IEEE Trans Power Syst.* 2014;29(6):2681-2695. <https://doi.org/10.1109/TPWRS.2014.2312418>
28. Sajan K, Kumar V, Tyagi B. Genetic algorithm based support vector machine for on-line voltage stability monitoring. *Int J Electr Power Energy Syst.* 2015;73:200-208. <http://www.sciencedirect.com/science/article/pii/S0142061515002070>
29. IEEE. Blackout experiences and lessons, best practices for system dynamic performance, and the role of new technologies, Technical Report, IEEE PES Working Group on Power Grid Blackouts, Power System Dynamic Performance Committee; 2007. IEEE PES Special Publication 07TP190.
30. Capitanescu F. Assessing reactive power reserves with respect to operating constraints and voltage stability. *IEEE Trans Power Syst.* 2011;26(4):2224-2234. <https://doi.org/10.1109/TPWRS.2011.2109741>
31. Lopes BIL, de Souza AZ. On multiple tap blocking to avoid voltage collapse. *Electr Power Syst Res.* 2003;67(3):225-231. [https://doi.org/10.1016/S0378-7796\(03\)00128-7](https://doi.org/10.1016/S0378-7796(03)00128-7)
32. Moulin LS, da Silva APA, El-Sharkawi MA, Marks RJ. Support vector machines for transient stability analysis of large-scale power systems. *IEEE Trans Power Syst.* 2004;19(2):818-825. <https://doi.org/10.1109/TPWRS.2004.826018>
33. Wu T-F, Lin C-J, Weng RC. Probability estimates for multi-class classification by pairwise coupling. *J Mach Learn Res.* 2004;5:975-1005. <http://dl.acm.org/citation.cfm?id=1005332.1016791>
34. Chang C-C, Lin C-J. LIBSVM: a library for support vector machines. *ACM Trans Intell Syst Technol.* 2011;2:27:1-27:27. <http://www.csie.ntu.edu.tw/~cjlin/libsvm>
35. Hastie T, Tibshirani R, Friedman J. *The elements of statistical learning.* Springer Series in Statistics. New York, NY, USA: Springer New York Inc.; 2001.
36. Zimmerman RD, Murillo-Sanchez CE, Thomas RJ. Matpower: steady-state operations, planning, and analysis tools for power systems research and education. *IEEE Trans Power Syst.* 2011;26(1):12-19. <https://doi.org/10.1109/TPWRS.2010.2051168>
37. Abba-Aliyu S. Voltage stability and distance protection zone3. *Master's Thesis.* 2003.
38. Capitanescu F, Cutsem TV. Preventive control of voltage security margins: a multicontingency sensitivity-based approach. *IEEE Trans Power Syst.* 2002;17(2):358-364. <https://doi.org/10.1109/TPWRS.2002.1007904>

**How to cite this article:** Nguyen Duc H, Kamwa I, Dessaint L-A, Cao-Duc H. A novel approach for early detection of impending voltage collapse events based on the support vector machine. *Int Trans Electr Energ Syst.* 2017;27:e2375. <https://doi.org/10.1002/etep.2375>

## TEXT REQUIREMENTS AND GUIDELINES

1. The **UD's Journal of Science and Technology** agrees to publish only genuine articles written with practical and scientific values in the fields of science and technology, which have not yet been published in any other journal or magazine before.
2. The article should not exceed *5 pages* and should be a uniform manuscript typed in the *Time new Roman font* with size *10pt* on pages size: *190mm x 265mm*, including figures, charts, diagrams and reference materials. All margins (top, bottom, left, right) are *10mm*. The line spacing is *1 line* and the paragraph spacing is *3pt*. The body of the article consists of *2 columns* with a middle space of *0.5cm*.
3. The following contents should be included in the article:
  - **Abstract:** This should be written both in English and in Vietnamese, about 150 words in length and it needs to present all the basic results and ideas of the article. It should be followed by a "New Words" section containing at least 5 words or phrases.
  - **Introduction:** This should reflect the current research conditions in the country and throughout the world.
  - **Solutions.**
  - **Study Results and Comments.**
  - **Conclusions.**
  - **References.**
4. The references deal with only the quoted materials of the article in the following order:
  - For the materials quoted from books, theses and reports, the order is arranged as follows:  
[...] The author's, publisher's name, *the title of the book (thesis or report)*, publishing house, and publishing year
  - For the materials quoted from articles, the order is arranged as follows:  
[...] The author's name, the title of the article, *the name of the journal*, volume (No.), publishing-house, and publishing year, page number (from page ... to page ...).
5. The journal accepts only clearly -typed articles with clear charts and figures, in appropriation to the text requirements (both printed manuscripts and files). The articles which are not accepted for publication will not be returned to the authors.
6. The author's full name, address, telephone number, email and signature should be added below the article.
7. An article format guide at <http://tapchikhcn.udn.vn> in the "Text Requirements and Guidelines" section can be used by the author as a model to write the article.
8. For information and manuscript submission, please contact:
  - **UD's Journal of Science and Technology,**
  - *41 Le Duan Street, Danang City*
  - *Tel.: 0236.3817.788, Fax: 0236.3823.683*
  - *E-mail: tapchikhcn@ud.edu.vn, http://tapchikhcn.udn.vn*

English Versions prepared by:

*Phan Thi Be*

*Nguyen Thi Quynh Hoa*

Computer Manuscripts by:

*Truong Bach Tue*

Cover Design by:

*La Thanh Hien*

Press License No. 510/GP-BVHTT Date Nov. 25th, 2002 and  
Amendments and Alterations to License No 1487/GP-BTTTT Date Sept. 15th, 2011.

Re. granted License No 07/GP-BTTTT Date Jan. 07th, 2016

Printed at Trung Khoa Company Limited, 118 Le Loi St., Da Nang City

Copyright Printed and Submitted on December, 2017

ISSN 1859-1531



BỘ GIÁO DỤC VÀ ĐÀO TẠO  
ĐẠI HỌC ĐÀ NẴNG

# Tap chí Khoa học và Công nghệ

THE UNIVERSITY OF DANANG

## JOURNAL OF SCIENCE AND TECHNOLOGY

12 (121)  
2017

12 (121). 2017

ISSN 1859-1531

UNIVERSITY OF DANANG

# JOURNAL OF SCIENCE AND TECHNOLOGY

15 ISSUES PER YEAR

## EDITOR-IN-CHIEF

Prof. Tran Van Nam, Ph.D.

## VICE EDITOR-IN-CHIEF

Ass.Prof. Doan Quang Vinh, Ph.D.

## EDITORIAL HEAD

Ass.Prof. Vo Trung Hung, Ph.D.

## ADMIN.HEAD

Truong Le Bich Tram, Ph.D.

## EDIT.SECRETARY

Huynh Thi Tam Thuong, M.A.

## EDITORIAL BOARD

Prof. Dao Hung Cuong, Ph.D.

Prof. Bui Van Ga, Dr.of Sc.

Prof. Tran Van Nam, Ph.D.

Prof. Nguyen The Hung, Ph.D.

Prof. Le Kim Hung, Ph.D.

Prof. Truong Ba Thanh, Ph.D.

Prof. Le The Gioi, Ph.D.

Prof. Nguyen Truong Son, Ph.D.

Prof. Vo Xuan Tien, Ph.D.

Ass.Prof. Nguyen Ngoc Vu, Ph.D.

Ass.Prof. Doan Quang Vinh, Ph.D.

Ass.Prof. Vo Trung Hung, Ph.D.

Ass.Prof. Nguyen Le Hung, Ph.D.

Ass.Prof. Dinh Minh Diem, Ph.D.

Ass.Prof. Nguyen Dinh Lam, Ph.D.

Ass.Prof. Phan Cao Tho, Ph.D.

Ass.Prof. Truong Hoai Chinh, Ph.D.

Ass.Prof. Hoang Ngoc Dong, Ph.D.

Ass.Prof. Tran Van Quang, Ph.D.

Ass.Prof. Le Quang Son, Ph.D.

Ass.Prof. Luu Trang, Ph.D.

Ass.Prof. Nguyen Bao Hoang Thanh, Ph.D.

Ass.Prof. Tran Quoc Chien, Dr.of Sc.

Ass.Prof. Le Tu Hai, Ph.D.

Ass.Prof. Vo Van Minh, Ph.D.

Ass.Prof. Nguyen Manh Toan, Ph.D.

Ass.Prof. Vo Thi Thuy Anh, Ph.D.

Ass.Prof. Nguyen Ngoc Chinh, Ph.D.

Ass.Prof. Nguyen Van Long, Ph.D.

## Editorial Office:

41 Le Duan St., Danang City

Tel.: 0236.3 817 788, 0236.3 824 787

E-mail: tapchikhcn@ud.edu.vn

**Licence:** 510/GP-BVHTT (25.11.2002)

1487/GP-BTTTT (15.9.2011)

07/GP-BTTTT (07.01.2016)

ISSN 1859-1531

BỘ GIÁO DỤC VÀ ĐÀO TẠO  
ĐẠI HỌC ĐÀ NẴNG

# Tap chí Khoa học và Công nghệ

TẠP CHÍ XUẤT BẢN 15 KỶ/NĂM

## TỔNG BIÊN TẬP

GS.TS. Trần Văn Nam

## PHÓ TỔNG BIÊN TẬP

PGS.TS. Đoàn Quang Vinh

## TRƯỞNG BAN BIÊN TẬP

PGS.TS. Võ Trung Hùng

## TRỊ SỰ

TS. Trương Lê Bích Trâm

## THƯ KÝ

ThS. Huỳnh Thị Tâm Thương

## BAN BIÊN TẬP

GS.TS. Đào Hùng Cường

GS.TSKH. Bùi Văn Ga

GS.TS. Trần Văn Nam

GS.TS. Nguyễn Thế Hùng

GS.TS. Lê Kim Hùng

GS.TS. Trương Bá Thanh

GS.TS. Lê Thế Giới

GS.TS. Nguyễn Trường Sơn

GS.TS. Võ Xuân Tiến

PGS.TS. Nguyễn Ngọc Vũ

PGS.TS. Đoàn Quang Vinh

PGS.TS. Võ Trung Hùng

PGS.TS. Nguyễn Lê Hùng

PGS.TS. Đinh Minh Diệm

PGS.TS. Nguyễn Đình Lâm

PGS.TS. Phan Cao Thọ

PGS.TS. Trương Hoài Chính

PGS.TS. Hoàng Ngọc Đồng

PGS.TS. Trần Văn Quang

PGS.TS. Lê Quang Sơn

PGS.TS. Lưu Trang

PGS.TS. Nguyễn Hoàng Bảo Thanh

PGS.TSKH. Trần Quốc Chiến

PGS.TS. Lê Tự Hải

PGS.TS. Võ Văn Minh

PGS.TS. Nguyễn Mạnh Toàn

PGS.TS. Võ Thị Thúy Anh

PGS.TS. Nguyễn Ngọc Chinh

PGS.TS. Nguyễn Văn Long

## Trụ sở Toà soạn:

41 Lê Duẩn, Thành phố Đà Nẵng

ĐT: 02363 817 788, 02363 824 787

E-mail: tapchikhcn@ud.edu.vn

**GPXB:** 510/GP-BVHTT (25.11.2002)

1487/GP-BTTTT (15.9.2011)

07/GP-BTTTT (07.01.2016)

# BI-LEVEL OPTIMIZATION MODEL BASED EVALUATION OF WHOLESALE ELECTRICITY PRICE INTERVALS CONSIDERING THE WIND POWER UNCERTAINTY AND ELASTIC DEMAND

Pham Nang Van<sup>1</sup>, Nguyen Duy Cung<sup>2</sup>, Nguyen Duc Huy<sup>1</sup>

<sup>1</sup>Hanoi University of Science and Technology (HUST); van.phamnang@hust.edu.vn, huy.nguyenduc1@hust.edu.vn

<sup>2</sup>Student at Hanoi University of Science and Technology (HUST)

**Abstract** - In the electricity market operation, wholesale electricity prices or Locational Marginal Prices (LMP) vary according to electric demand (including consumption power consumed, bidding prices and the level of price-sensitivity) as well as the penetration level of the wind power. The variable domain identification of LMP plays a very important role for market participants to assess and mitigate the risk on account of the uncertainty of wind power output forecasting. Traditionally, the Monte Carlo simulation (MCS) method can be used in order to determine the variable intervals of LMP. However, in this paper, the authors deploy a bi-level optimization model to calculate the upper and lower bounds of LMP when considering the uncertainty of wind power and elastic demand. The objective function of the upper-level optimization problem is to maximize (or minimize) LMP at a node whereas the objective function of the lower-level optimization problems is to calculate the optimal power generation of the units participating in supplying the load.

**Key words** - Wholesale electricity market; mathematical program with equilibrium constraints (MPEC); mixed-integer linear programming (MILP); wind power uncertainty; elastic demand.

## 1. Introduction

Currently, many countries around the world, including Vietnam, have been operating wholesale electricity markets. In the wholesale electricity market, the market participants are generation companies (GENCOS) and distribution companies (DISCOS). The market operator collects generating offers by producers, load bids by consumers and clears the market by maximizing the social welfare [1]-[2].

The uncertainty from wind output has brought unprecedented challenges to the optimal operation of the electricity market. The power system operation has been dealing with the uncertainty of load, different from load uncertainty; however, wind output is characterized with large uncertainties and low prediction precision [3]. On the other hand, load demand has an intrinsic pattern and thus the load prediction, especially, in short-term, has a significantly high forecast accuracy [3]. Therefore, the optimal operation and dispatching model considering stochastic wind power output has been a hot topic for research.

Reference [4] studied the effect of wind integration and wind uncertainty on power system reliability, using an ARMA model to analyze short-term wind forecast. Reference [5] studied the impact of stochastic wind power on the unit commitment (UC) problem and constructed a UC stochastic optimization problem with the objective to minimize the expected operation cost. In reference [6], the influence of distribution generation on a heavily loaded distribution system with a wind forecast model based on statistics is tackled. A mixed-integer stochastic optimization model is established in [7] where the wind uncertainty is modeled with ARMA as well as Latin hypercube sampling and a scenario reduction method is adopted to simplify the computation.

The first step to investigate the effect of uncertainty is to model the uncertain wind output by using a variety of methods, for instance, probability distribution model [8], fuzzy model [9] and interval number model [10]. In the next steps, different optimization models are applied to find the solution.

To make payments in the electricity market, locational marginal prices (LMP) are calculated. The difference in LMPs between two nodes of a branch depends upon the congestion and losses on that branch [2]. The locational marginal pricing methodology is widely used in electricity markets to determine the electricity prices and to evaluate the transmission congestion cost [11]-[12]. Step change characterizes of LMP under system load variation has been identified and discussed [13]. Moreover, the concept of critical load level (CLL) is defined and employed for load frequency control [13]. Based on a similar idea, the investigation of the impact of variable wind power outputs on LMPs must be worth launching. It is important to find a method to efficiently obtain the wholesale electricity price intervals under the variation of wind power output and elastic demand.

This paper proposes an approach to determine the intervals of LMP using a bi-level optimization model, which is similar to the interval number-based optimization model regarded as the optimization of optimization. In addition, the impact of the uncertainty of wind power as well as the level for demand-bid price sensitivity is also analyzed.

The next sections of the article are organized as follows. In section 2, the authors present bi-level optimization model to determine LMP intervals. In addition, the authors also describe the solution to this bi-level optimization problem including the procedure of transferring it into a Mathematical Program with Equilibrium Constraints (MPEC) problem and the conversion from MPEC to a Mixed-Integer Linear Programming (MILP). Section 3 demonstrates the simulation results and numerical analyses of PJM 5-bus system. Some conclusions are given in section 4.

## 2. LMP interval under wind power uncertainty

### 2.1. Market clearing model

Economic Dispatch (ED) considering elastic demands in wholesale electricity market is carried out by Independent System Operators (ISOs) to clear market as well as determine LMPs and output of generating units. In this paper, the DCOPF-based approach without losses is employed to model the electricity market and estimate LMPs. This DCOPF is a linear programming (LP) problem

presented as follows:

$$\min \sum_{i=1}^N (c_{Gi} P_{Gi} + c_{Wi} P_{Wi} - c_{Di} P_{Di}^E) \quad (1)$$

$$s.t \sum_{i=1}^N (P_{Gi} + P_{Wi}) = \sum_{i=1}^N (P_{Di}^F + P_{Di}^E) : \lambda \quad (2)$$

$$-Limit_l \leq \sum_{i=1}^N GSF_{l-i} (P_{Gi} + P_{Wi} - P_{Di}^F - P_{Di}^E) \quad (3)$$

$$\leq Limit_l : \mu_l^{\min}, \mu_l^{\max}, \forall l = \overline{1, M}$$

$$P_{Gi}^{\min} \leq P_{Gi} \leq P_{Gi}^{\max} : \omega_i^{\min}, \omega_i^{\max}, \forall i = \overline{1, N} \quad (4)$$

$$0 \leq P_{Wi} \leq P_{Wi}^{\max} : \phi_i^{\min}, \phi_i^{\max}, \forall i = \overline{1, N} \quad (5)$$

$$0 \leq P_{Di}^E \leq P_{Di}^{E\max} : \phi_i^{\min}, \phi_i^{\max}, \forall i = \overline{1, N} \quad (6)$$

where  $N$  is the number of buses;  $M$  is the number of lines;  $c_{Gi}$  and  $c_{Wi}$  are energy prices offered by conventional generation and wind power, respectively;  $P_{Gi}$  and  $P_{Wi}$  are power outputs of the conventional generating unit and wind power, respectively;  $c_{Di}$  is the price bid by demand  $i$ ;  $P_{Di}^E$  and  $P_{Di}^F$  are the elastic power and fixed power of demand  $i$ , respectively;  $GSF$  is the generation shift factor matrix;  $P_{Gi}^{\min}$  and  $P_{Gi}^{\max}$  are the upper and lower bounds of the convention generation output;  $P_{Wi}^{\max}$  is the maximum available wind power output;  $P_{Di}^{E\max}$  is the maximum price-sensitivity demand at bus  $i$ ; and the variables on the right side of the colon are the dual variables associated with the equality and inequality constraints on the left.

The LMP at bus  $i$  can be calculated from the Lagrange function of the above ED problem. This function and LMP are given by

$$\begin{aligned} \psi = & \sum_{i=1}^N (c_{Gi} P_{Gi} + c_{Wi} P_{Wi} - c_{Di} P_{Di}^E) \\ & - \lambda \sum_{i=1}^N (P_{Gi} + P_{Wi} - P_{Di}^F + P_{Di}^E) \\ & - \sum_{l=1}^M \mu_l^{\min} \left( \sum_{i=1}^N GSF_{l-i} (P_{Gi} + P_{Wi} - P_{Di}^F - P_{Di}^E) + Limit_l \right) \\ & - \sum_{l=1}^M \mu_l^{\max} \left( Limit_l - \sum_{i=1}^N GSF_{l-i} (P_{Gi} + P_{Wi} - P_{Di}^F - P_{Di}^E) \right) \\ & - \sum_{i=1}^N \omega_i^{\min} (P_{Gi} - P_{Gi}^{\min}) - \sum_{i=1}^N \omega_i^{\max} (P_{Gi}^{\max} - P_{Gi}) \\ & - \sum_{i=1}^N \phi_i^{\min} P_{Wi} - \sum_{i=1}^N \phi_i^{\max} (P_{Wi}^{\max} - P_{Wi}) \\ & - \sum_{i=1}^N \phi_i^{\min} P_{Di}^E - \sum_{i=1}^N \phi_i^{\max} (P_{Di}^{E\max} - P_{Di}^E) \end{aligned} \quad (7)$$

$$LMP_i = \frac{\partial \psi}{\partial P_{Di}^F} = \lambda + \sum_{l=1}^M GSF_{l-i} (\mu_l^{\min} - \mu_l^{\max}) \quad (8)$$

## 2.2. LMP interval and its bi-level optimization form

Traditionally, the intervals of LMP are usually evaluated using Monte Carlo Simulation (MCS) approach. However, this approach requires a huge amount of computation time in comparison with the bi-level optimization approach in terms of the same level of accuracy.

The problem for calculation LMP interval is formulated as follows:

$$Upper \ Level : \max LMP_i \text{ (or } \min LMP_i) \quad (9)$$

$$s.t \text{ Lower level : ED optimization model } \{(1)-(6)\} \quad (10)$$

$$\underline{P}_{wf,i} \leq P_{Wi}^{\max} \leq \overline{P}_{wf,i} \quad (11)$$

where  $\underline{P}_{wf,i}$  and  $\overline{P}_{wf,i}$  is the forecast upper and lower bounds of the maximum wind power output. In other words, interval constraints are used to model the maximum wind power output in the upper level.

In the above formulation, we see that if there are  $N$  buses in the power system,  $2N$  optimization runs should be carried out.

## 2.3. Formulation as a MPEC

Given that the lower level ED is an LP problem, the bi-level can be transformed into a Mathematical Program with Equilibrium Constraints (MPEC) by recasting the lower level problem as its Karush-Kuhn-Tucker (KKT) optimality conditions, which are added to the upper level problem as the additional complementary constraints [14] - [16]:

$$OBJ: (9) \quad (12)$$

$$s.t. \text{ Constraints in (2) and (11)} \quad (13)$$

$$c_{Gi} = \lambda + \sum_{l=1}^M GSF_{l-i} (\mu_l^{\min} - \mu_l^{\max}) + (\omega_i^{\min} - \omega_i^{\max}) \quad (14)$$

$$c_{Wi} = \lambda + \sum_{l=1}^M GSF_{l-i} (\mu_l^{\min} - \mu_l^{\max}) + (\phi_i^{\min} - \phi_i^{\max}) \quad (15)$$

$$c_{Di} = \lambda + \sum_{l=1}^M GSF_{l-i} (\mu_l^{\min} - \mu_l^{\max}) - (\phi_i^{\min} - \phi_i^{\max}) \quad (16)$$

$$0 \leq \mu_l^{\min} \perp Limit_l + \sum_{i=1}^N GSF_{l-i} (P_{Gi} + P_{Wi} - P_{Di}^F - P_{Di}^E) \geq 0 \quad (17)$$

$$0 \leq \mu_l^{\max} \perp Limit_l - \sum_{i=1}^N GSF_{l-i} (P_{Gi} + P_{Wi} - P_{Di}^F - P_{Di}^E) \geq 0 \quad (18)$$

$$0 \leq \omega_i^{\min} \perp P_{Gi} - P_{Gi}^{\min} \geq 0 \quad (19)$$

$$0 \leq \omega_i^{\max} \perp P_{Gi}^{\max} - P_{Gi} \geq 0 \quad (20)$$

$$0 \leq \phi_i^{\min} \perp P_{Wi} \geq 0 \quad (21)$$

$$0 \leq \phi_i^{\max} \perp P_{Wi}^{\max} - P_{Wi} \geq 0 \quad (22)$$

$$0 \leq \phi_i^{\min} \perp P_{Di}^E \geq 0 \quad (23)$$

$$0 \leq \phi_i^{\max} \perp P_{Di}^{E\max} - P_{Di}^E \geq 0 \quad (24)$$

## 2.4. Mixed-Integer Linear Programming (MILP)

The MPEC model depicted in (12) – (24) is nonlinear on account of the slack complementarity constraints (17) – (24). These slack complementary constraints are compactly written as  $0 \leq F(x) \perp x \geq 0$ , which is stated equivalently in vector form as:

$$F(x) \geq 0, x \geq 0, F(x)^T x = 0 \quad (25)$$

With the method in [15], however, this MPEC problem can be converted to a mixed-integer linear programming (MILP), which can be solved by CPLEX [18]. The MILP model is presented as follows:

$$\text{OBJ: (9)} \quad (26)$$

$$\text{s.t. Constraints in (13), (14), (15) and (16)} \quad (27)$$

$$0 \leq \mu_l^{\min} \leq M_\mu^{\min} v_{\mu,l}^{\min} \quad (28)$$

$$0 \leq \text{Limit}_l + \sum_{i=1}^N \text{GSF}_{l-i} (P_{Gi} + P_{Wi} - P_{Di}^F - P_{Di}^E) \leq M_\mu^{\min} (1 - v_{\mu,l}^{\min}) \quad (29)$$

$$0 \leq \mu_l^{\max} \leq M_\mu^{\max} v_{\mu,l}^{\max} \quad (30)$$

$$0 \leq \text{Limit}_l - \sum_{i=1}^N \text{GSF}_{l-i} (P_{Gi} + P_{Wi} - P_{Di}^F - P_{Di}^E) \leq M_\mu^{\max} (1 - v_{\mu,l}^{\max}) \quad (31)$$

$$0 \leq \omega_i^{\min} \leq M_\omega^{\min} v_{\omega,i}^{\min} \quad (32)$$

$$0 \leq P_{Gi} - P_{Gi}^{\min} \leq M_\omega^{\min} (1 - v_{\omega,i}^{\min}) \quad (33)$$

$$0 \leq \omega_i^{\max} \leq M_\omega^{\max} v_{\omega,i}^{\max} \quad (34)$$

$$0 \leq P_{Gi}^{\max} - P_{Gi} \leq M_\omega^{\max} (1 - v_{\omega,i}^{\max}) \quad (35)$$

$$0 \leq \phi_i^{\min} \leq M_\phi^{\min} v_{\phi,i}^{\min} \quad (36)$$

$$0 \leq P_{Wi} \leq M_\phi^{\min} (1 - v_{\phi,i}^{\min}) \quad (37)$$

$$0 \leq \phi_i^{\max} \leq M_\phi^{\max} v_{\phi,i}^{\max} \quad (38)$$

$$0 \leq P_{Wi}^{\max} - P_{Wi} \leq M_\phi^{\max} (1 - v_{\phi,i}^{\max}) \quad (39)$$

$$0 \leq \phi_i^{\min} \leq M_\phi^{\min} v_{\phi,i}^{\min} \quad (40)$$

$$0 \leq P_{Di}^E \leq M_\phi^{\min} (1 - v_{\phi,i}^{\min}) \quad (41)$$

$$0 \leq \phi_i^{\max} \leq M_\phi^{\max} v_{\phi,i}^{\max} \quad (42)$$

$$0 \leq P_{Di}^{E \max} - P_{Di}^E \leq M_\phi^{\max} (1 - v_{\phi,i}^{\max}) \quad (43)$$

where  $M_\mu^{\min}, M_\mu^{\max}, M_\omega^{\min}, M_\omega^{\max}, M_\phi^{\min}, M_\phi^{\max}, M_\phi^{\min}, M_\phi^{\max}$  are large enough constants and  $v_{\mu,l}^{\min}, v_{\mu,l}^{\max}, v_{\omega,i}^{\min}, v_{\omega,i}^{\max}, v_{\phi,i}^{\min}, v_{\phi,i}^{\max}$  are the auxiliary binary variables [14].

## 3. Results and discussions

In this section, the bi-level optimization approach is

performed on the modified PJM 5-bus system [17]. The MILP problem is solved by CPLEX 12.7 under MATLAB environment.

### 3.1. System data

The test system is modified from the PJM 5-bus system [10], as shown in Figure 1. Two wind plants (WF1 and WF2) with the same capacity are added into the system at buses A and C while one original generator is removed from bus A. The total fixed and maximum elastic demand is 1200 MW equally distributed among buses B, C and D.

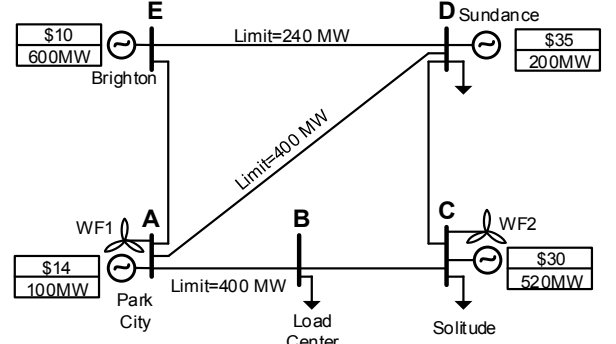


Figure 1. PJM 5-bus system with two wind farms

### 3.2. Impact from wind power uncertainty

This subsection shows the impact of wind power forecast uncertainty on LMP interval. The simulation parameters are shown in Table 1. In addition, the only fixed demand is considered in this subsection.

Table 1. Uncertain parameters of wind power

Wind Power Model	Normal Distributed
WF wind power mean (MW)	180
WF2 wind power mean (MW)	180
Wind power standard deviation range (%)	0-30%

It should be emphasized that the findings calculated in this work are exactly the same in comparison with the MCS method (with 5000 samples), while the simulation time for bi-level optimization-based approach is dramatically lower than that of MCS. Table 2 shows results achieved across all buses from both approaches when the standard deviation equals 15% from the mean.

Table 2. LMP result intervals from MCS method and Bi-level optimization method

Bus	Bi-vel optimization method	MCS method
A	[15.24, 16.98]	[15.24, 16.98]
B	[23.68, 28.18]	[23.68, 28.18]
C	[26.70, 30.00]	[26.70, 30.00]
D	[35.00, 39.94]	[35.00, 39.94]
E	[10, 10]	[10, 10]

Table 3 shows LMP intervals when the indicator of wind forecast uncertainty ( $\sigma$ ) changes. According to the results shown in Table 3, in general, when the standard deviation of forecasting wind power increases, the difference between the upper and lower bound of LMP at every bus also rises. Moreover, these results also reveals

that despite the variation of wind power uncertainty, the LMP intervals at bus C remain unchanged.

**3.3. Impact from Demand-Bid Price Sensitivity**

To investigate the influence of variation in the level of demand price sensitivity, [11] proposed the coefficient which is defined as Eq. (43).

$$R_i = \frac{P_{Di}^{E \max}}{P_{Di}^F + P_{Di}^{E \max}} \quad (44)$$

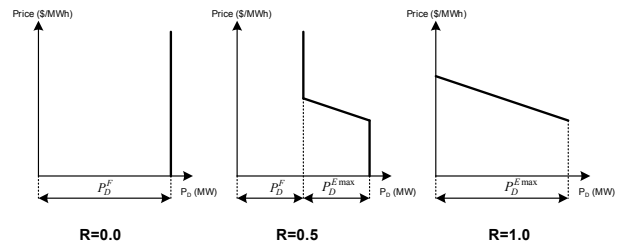
From the formula (43), the R values range from 0.0 (100% fixed demand) to 1.0 (100% price-sensitive demand).

Figure 2 illustrates the construction of R for the special cases R = 0.0, R = 0.5 and R = 1.0.

In this paper, it is assumed that the ratio R of four demands is similar. Additionally, the forecast mean value of both wind powers is 180 MW and it follows a normal distribution with a standard deviation of 10% from the mean.

Table 4 presents the LMP internal results with the

various R values from the proposed approach. According to this Table, the R ratio markedly affects the locational marginal prices at every bus in terms of the maximum and minimum values as well as the difference between these two items. In particular, when R varies from 0.4 to 0.6, there is a decline in the maximum and the minimum values of LMP at bus D; however, these values of LMP at bus E grows considerably. Furthermore, when the R ratio equals 0.6, 0.8 and 1.0, respectively, the LMP intervals remain stable at all buses.



**Figure 2.** Illustration of the R ratio construction for the experimental control of demand-bid price sensitivity

**Table 3.** LMP interval results with the various standard deviation

Bus	LMP interval						
	$\sigma = 0\%$	$\sigma = 5\%$	$\sigma = 10\%$	$\sigma = 15\%$	$\sigma = 20\%$	$\sigma = 25\%$	$\sigma = 30\%$
A	[15.24, 15.24]	[15.24, 15.83]	[15.24, 16.98]	[15.24, 16.98]	[15.24, 23.45]	[15.24, 23.45]	[15.24, 23.45]
B	[28.18, 28.18]	[23.68, 28.18]	[23.68, 28.18]	[23.68, 28.18]	[23.68, 28.18]	[23.68, 28.18]	[23.68, 28.18]
C	[30, 30]	[26.70, 30.00]	[26.70, 30.00]	[26.70, 30.00]	[26.70, 30.00]	[26.70, 30.00]	[26.70, 30.00]
D	[35, 35]	[35, 35]	[35.00, 39.94]	[35.00, 39.94]	[35.00, 39.94]	[35.00, 39.94]	[35.00, 39.94]
E	[10, 10]	[10, 10]	[10, 10]	[10, 10]	[10.00, 19.94]	[10.00, 19.94]	[10.00, 19.94]

**Table 4.** LMP interval results with R different demand-bid price sensitivity

Bus	LMP interval					
	R = 0	R = 0.2	R = 0.4	R = 0.6	R = 0.8	R = 1
A	[15.24, 16.98]	[15.65, 15.83]	[14.00, 15.23]	[14, 14]	[14, 14]	[14, 14]
B	[23.68, 28.18]	[23.68, 25.00]	[19.39, 22.29]	[18.51, 25.00]	[18.51, 25.00]	[18.51, 25.00]
C	[26.70, 30.00]	[26.70, 27.67]	[21.47, 25.00]	[20.24, 25.00]	[20.24, 25.00]	[20.24, 25.00]
D	[35.00, 39.94]	[35, 35]	[27.17, 32.46]	[25, 25]	[25, 25]	[25, 25]
E	[10, 10]	[10, 10]	[10, 10]	[10.66, 11.68]	[10.66, 11.68]	[10.66, 11.68]

**4. Conclusion**

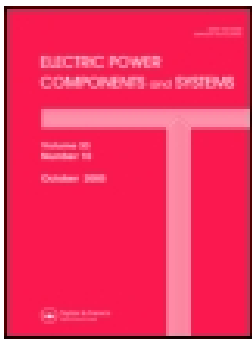
This paper presents an approach to determine the intervals of locational marginal prices (LMPs) based on bi-level optimization model. Moreover, authors also present the conversion of this model to a mathematical program with equilibrium constraints (MPEC), then to a mixed-integer linear programming (MILP), which can be easily solved by available software tools. The results of this bi-level optimization problem reveal that the wind uncertainty and the demand-bid price sensitivity level have a remarkable impact on LMP intervals. In the computational aspect, the bi-level optimization-based method is more efficient compared with Monte-Carlo simulations although the calculated results using both approaches are identical.

**REFERENCES**

- [1] Pham Nang Van, Nguyen DucHuy, Nguyen Van Duong, Nguyen The Huu, "A tool for unit commitment schedule in day-ahead pool-based electricity markets", *Journal of Science and Technology, The University of Danang*, no. 6, pp. 21-25, June, 2016.
- [2] Pham Nang Van, Nguyen Dong Hung, Nguyen Duc Huy, "The impact of TCSC on transmission costs in wholesale power markets considering bilateral transactions and active power reserves", *Journal of Science and Technology, The University of Danang*, no. 12, pp. 24-28, December, 2016.
- [3] Zou J, Lai X, Wang N, Time series model of stochastic wind power generation, *Power System Technology*, pp. 2416-2421, 2014.
- [4] Zhang Y, Ka WC, "The impact of wind forecasting in power system reliability", *Third international electric utility deregulation and restructuring and power technologies*, Nanjing.
- [5] Tuohy A, Meibom P, Denny E, "Unit commitment for systems with significant wind penetration", *IEEE Trans. Power Syst*, vol. 24, pp. 592-601, 2009.

- [6] Kroposki B, Sen PK, Malmedal K, "Selection of distribution feeders for implementing distributed and renewable energy applications", *IEEE Rural electric power conference*, Fort Collins, CO, 2009.
- [7] Yan Y, Wen F, Yang S, "Generation scheduling with fluctuating wind power", *Automation of Electric Power Systems*, vol. 34, pp. 79-88, 2010.
- [8] Juan M. Morales, Antonio J. Conejo and Juan Perez-Ruiz, "Simulating the impact of wind production on locational marginal prices", *IEEE Trans. Power Systems*, vol. 26, no. 2, pp. 820-828, May 2011.
- [9] Hu Y, *Study on wind power storage technology and the intelligent dispatch model*, Master thesis, Lanzhou University of Technology, 2013.
- [10] Xin Fang, Qinran Hu, Fangxing Li, Beibei Wang and Yang Li, "Coupon-based demand response considering wind power uncertainty: a strategic bidding model for load serving entities", *IEEE Trans. Power Syst.*, vol. 31, no. 5, pp.1025-1037, May 2016.
- [11] Hongyan Li, Leigh Tesfatsion, "ISO Net surplus collection and allocation in wholesale power markets under LMP", *IEEE Trans. Power Systems*, vol. 26, pp. 627-641, April 2011.
- [12] V. Sarkar and S. A. Khaparde, "Optimal LMP Decomposition for the ACOPF Calculation", *IEEE Trans. Power Systems*, vol. 26, pp. 1714-1723, May 2011.
- [13] F. Li and R. Bo, "Congestion and price prediction under load variation", *IEEE Trans. Power Syst.*, vol. 24, no. 2, pp. 911-922, May 2009.
- [14] L. Baringo and A. J. Conejo, "Strategic offering for a wind power producer", *IEEE Trans. Power Syst.*, vol. 28, no. 4, pp.1645-1654, November 2013.
- [15] Zhi-Quan Luo, Jong-Shi Pang and Daniel Ralph, *Mathematical Programs with Equilibrium constraints*, Cambridge University Press, 2004.
- [16] R.C.Bansal, *Optimization Methods for Electric Power Systems: An Overview*, International Journal of Emerging Electric Power Systems, 2005.
- [17] Fangxing Li, Rui Bo, "Small test systems for Power System Economic Studies", *IEEE PES General Meeting*, pp. 1-4, 2010.
- [18] CPLEX optimization studio. [Online] Available: <https://www.ibm.com/bs-en/marketplace/ibm-ilog-cplex>

(The Board of Editors received the paper on 25/4/2017, its review was completed on 15/5/2017)



## An Approach to Solve Transient Stability-Constrained Optimal Power Flow Problem Using Support Vector Machines

Huy Nguyen-Duc, Linh Tran-Hoai & Huy Cao-Duc

To cite this article: Huy Nguyen-Duc, Linh Tran-Hoai & Huy Cao-Duc (2017): An Approach to Solve Transient Stability-Constrained Optimal Power Flow Problem Using Support Vector Machines, Electric Power Components and Systems, DOI: [10.1080/15325008.2017.1292328](https://doi.org/10.1080/15325008.2017.1292328)

To link to this article: <http://dx.doi.org/10.1080/15325008.2017.1292328>



Published online: 28 Mar 2017.



Submit your article to this journal [↗](#)



View related articles [↗](#)



View Crossmark data [↗](#)

# An Approach to Solve Transient Stability-Constrained Optimal Power Flow Problem Using Support Vector Machines

Huy Nguyen-Duc,<sup>1</sup> Linh Tran-Hoai,<sup>1</sup> and Huy Cao-Duc<sup>2</sup>

<sup>1</sup>School of Electrical Engineering, Hanoi University of Science and Technology, Hanoi, Vietnam

<sup>2</sup>Department of Power System Development, Vietnam Institute of Energy, Hanoi, Vietnam

## CONTENTS

- 1. Introduction
- 2. Background
- 3. Proposed Framework
- 4. Test Results
- 5. Conclusion
- Funding
- References

---

**Abstract**—The Transient Stability-Constrained Optimal Power Flow (TSC-OPF) is a challenging optimization problem, and is the subject of several recent researches. This paper proposes a novel approach to solve TSC-OPF. In the proposed framework, Support Vector Machines (SVMs) are used to classify whether an operating condition satisfies predefined transient contingencies. A novel classification strategy is proposed to ensure the optimal solution satisfies all considered contingencies with certain security margin. Besides, the weight coefficients of the SVM are used as sensitivity measures in order to help optimization solver find solutions more effectively. The proposed approach is demonstrated for the New England system and the IEEE 300 bus system.

---

## 1. INTRODUCTION

The power systems nowadays are operating closer to their stability limits. As a consequence, the risk of various instability phenomena is now higher. The power system stability requires more attention during the production planning and optimization procedures. If the stability constraints can be incorporated into various operation planning problems such as Optimal Power Flow (OPF) and Unit Commitment, it would help power engineers determine operating conditions which are optimal in terms of minimal cost, and are also secure under probable contingency events. Due to the complexity of the power system models, several types of instability dynamics can occur. The power system dynamics and stability phenomena can be classified into three main categories: Rotor angle stability, voltage stability, and frequency stability [1]. The assessment of transient rotor angle stability requires detailed time-domain simulation, which is a very computationally extensive process. An alternative to time-domain simulations is the transient energy function method [2]. In [3], the transient energy-based data have been shown to improve the accuracy of transient stability classification. However, the energy function method is only directly applicable for simple

Keywords: power system dynamics, power system stability, power system optimization, computational intelligence, support vector machines, optimal power flow

Received 2 September 2015; accepted 23 January 2017

Address correspondence to Huy Nguyen-Duc, School of Electrical Engineering, Hanoi University of Science and Technology, Hanoi 100000, Vietnam. E-mail: [ngduchuy@gmail.com](mailto:ngduchuy@gmail.com)

Color versions of one or more of the figures in the article can be found online at [www.tandfonline.com/uemp](http://www.tandfonline.com/uemp).

model of the generator. The extension of this method for higher-order model of the synchronous generator, with its governor and excitation control, remains a challenge.

Transient stability-constrained optimal power flow (TSC-OPF) is one research subject that has received increasing attention [4–7]. The basic objective of TSC-OPF is to determine an optimal operating condition, in which the generators can remain synchronized following severe contingencies. This research topic is becoming more relevant in deregulated markets, in which power system operating points are subject to more variation and uncertainties. The method to solve TSC-OPF problem is based on two main approaches. In the first approach, the power system differential equations are discretized. The resulting finite difference equations are included into the OPF problem as equality constraints. This approach has been proposed in [7, 8], and also has been proposed for the Transient Stability-Constrained Unit Commitment [9]. The main drawback of this approach is that the OPF problem size is increased drastically, with only few contingencies considered. Recent studies in this approach proposed to use advanced computing platform to speed up the computation time [10, 11].

In the second approach, the simulation of power system dynamics is carried out separately from the OPF process. During the OPF, the transient stability boundary (TSB) is evaluated using an independent simulation software [12, 13]. With this approach, high-order model of power system dynamics can be considered easily. In fact, a dedicated power system simulation software can be used, which allows user to model many different generator control systems. With this approach, however, there is a need to derive an accurate sensitivity measure of the TSB with respect to optimization variables. The sensitivity evaluation has been proposed in [13, 14], using a finite difference method.

The above analysis shows that the second approach has several advantages, especially when the TSC-OPF problem is carried out for large-scale system comprising several types of devices and control models. The main obstacle to improving the efficiency of the second approach is how sensitivity measures can be accurately determined.

Along with TSC-OPF research, the approaches for TSB approximation have also been studied. It has been shown in earlier studies that artificial neural networks (ANNs) can estimate with fairly high accuracy of the power system, critical clearing times (CCTs)—a very commonly used measure for TSB [15]. Besides the ANNs, other mediums for classification are also proposed, such as polynomial representation, support vector machines (SVMs), least absolute shrinkage and selection operator (LASSO), and ridge regression. If the CCT can be represented as an analytical expression of load flow

variables, this function can be used as transient stability constraints in the TSC-OPF. This idea has been proposed first in [16]. In fact, if ANNs can estimate with good accuracy the TSB, then they can also give measures of sensitivity of the TSB in function of their input. Therefore, a TSC-OPF framework can be formulated, in which the TSBs with respect to various disturbances can be described using different ANNs or SVMs. The approach has several advantages: The TSC-OPF problem size is only increased slightly compared to conventional OPF formulation; moreover, the TSC-OPF can tackle multiple contingency constraints very easily.

The benefit of having sensitivity measures of TSB with regard to operating variables expands beyond the TSC-OPF framework. During real-time operation, based on the measured input variables, power engineers can deduce accurate dispatching orders that would mitigate the risk of probable insecure operating conditions. Some operating rules and strategies can be deduced from the obtained ANN and SVM.

In this work, a new approach to solve TSC-OPF is proposed. SVMs are trained to classify operating states based on transient stability criterion, with several contingencies considered. In the OPF framework, the weight coefficients of the SVM are used as a sensitivity measure to determine the search direction. Compared to previous research [16], the SVM is used as a classifier, instead of an approximator. With this approach, the computation burden for the creation of training instances is significantly reduced. The paper is organized as follows: Section 2 presents background on the mathematical formulation of TSC-OPF, and approaches to determine the TSB based on ANN and SVM. Section 3 presents the proposed approach to solve TSC-OPF based on SVM. Some test results are presented in Section 4, and conclusions are given in Section 5.

## 2. BACKGROUND

### 2.1. Transient Stability-Constrained Optimal Power Flow

The conventional OPF problem can be described as follows:

$$f(P_g) \rightarrow \min \quad (1)$$

such that:

$$P_g - P_L - P(V, \theta) = 0 \quad (2)$$

$$Q_g - Q_L - Q(V, \theta) = 0 \quad (3)$$

$$V_{\min} \leq V \leq V_{\max} \quad (4)$$

$$P_{g,\min} \leq P_g \leq P_{g,\max} \quad (5)$$

$$Q_{g,\min} \leq Q_g \leq Q_{g,\max} \quad (6)$$

Constraints (2–3) represent the network power flow equations, and constraints (4–6) represent the physical limits of optimization variables. Transient Stability OPF (or security-constrained OPF in general) extends the OPF formulation by adding constraints related to the stability criteria. At a given operating point, the maximum clearing time for all faults must be higher than a specified value, determined by relay response and circuit breaker time, with some safety margin. In an analytical form, these criteria can be expressed as

$$CCT_k(P_g, Q_g, V, \theta) \geq CCT_{\min}, \quad k = [1, N] \quad (7)$$

where  $k$  denotes the  $k^{\text{th}}$  contingency, and  $N$  is the total number of contingencies considered. The threshold  $CCT_{\min}$  in Eq. (7) denotes a minimum required value for the CCT, which must be at least longer than the operating time of the protective relaying system and circuit breaker time, plus some security margin. There is, however, no analytical function for CCT, since time-domain simulations need to be carried out to determine the values of CCT.

## 2.2. Approximation of Transient Stability Boundary Using Neural Networks

There have been extensive works on the approximation of the TSBs using NNs. In most cases, the CCT is chosen as the transients stability boundary [15]. Reference [17] shows that an ANN with generator active and reactive output as input space can estimate with very high accuracy the CCT of a single machine infinite bus system. Reference [18] proposes to use a Multi layer Perception Network to estimate the CCT of the IEEE 39 bus system, with good accuracy. Study in [19] showed that with bus voltages and angles as input features, the SVM can estimate with high accuracy the system CCT. Instead of using ANN to estimate the CCT of operating conditions, one can also train the ANN and other alternative artificial intelligence engines to classify whether an operating condition will be transiently stable with a given fault. Reference [20] is one of the first studies in this approach, in which an SVM is used as a classifier.

Researches on the approximation of CCT have proposed several combinations of load flow variables as input vectors for the ANN, such as active and reactive power output ( $P_g$ ,  $Q_g$ ), and bus voltage magnitudes and angles ( $V_m$ ,  $V_a$ ). Overall, the generator active output ( $P_g$ ) and either generator voltage or reactive output ( $V_g$  or  $Q_g$ ) are commonly chosen as

input variables. In fact, there are good reasons to use these two inputs:

- $P_g$  has a quasi-linear relationship with regard to the TSB. This can be explained easily using the equal area criterion [8].
- A generator set point voltages  $V_g$  also have a small effect on the CCT of the three-phase fault at its terminal. This can be quantitatively explained using the equal area criterion [19]: High set point voltage requires high field current, which leads to higher value of transient e.m.f ( $E'_q$ ). As a result, the decelerating areas tend to be larger.
- In OPF and optimal commitment problems,  $P_g$  and  $V_g$  are the control variables.

## 2.3. Support Vector Machines

As discussed in the previous section, recent works have focused on using various artificial intelligence engines such as ANN, SVM, LASSO, and ridge regression to estimate the TSB [16, 20, 21]. In most researches, the CCT is used as a TSB. For the purpose of classification, the SVMs are often used. The idea of a linear SVM can be described briefly as follows:

$$f(x) = \text{sign}(\mathbf{w}^T x + b) \quad (8)$$

This classifier separates the input feature space into two classes by a hyperplane. One class corresponds to  $f(x^+) = 1$ , and the other class corresponds to  $f(x^-) = -1$ . The vector  $\mathbf{w}$  is called the weight vector, and  $b$  is the bias term. The minimum distance between two input values belonging to two different classes is

$$m_D(x) = \mathbf{w}^T (x^+ - x^-) = \frac{2}{\|\mathbf{w}\|} \quad (9)$$

The task of training the SVM is to maximize the margin  $\frac{2}{\|\mathbf{w}\|}$ , which is equivalent to minimizing  $\|\mathbf{w}\|$ . The optimization problem is formulated as follows:

$$\min_{w, b, \xi} \frac{1}{2} \mathbf{w}^T \mathbf{w} + C \sum_{i=1}^l \xi_i \quad (10)$$

subject to:

$$\begin{cases} y_i(\mathbf{w}^T \phi(x_i) + b) & \geq 1 - \xi_i \\ \xi_i & \geq 0 \end{cases} \quad (11)$$

The slack variables  $\xi_i$  are introduced in the optimization problem, in order to allow some misclassification. The coefficient  $C$  in (10) is used as a penalty factor for classification errors. In Eq. (11), the function  $\phi(x)$  represents a nonlinear mapping, which maps the input vector  $x$  into a higher-dimensional space. With an appropriate selection of the kernel function, the classification problem can be linearly

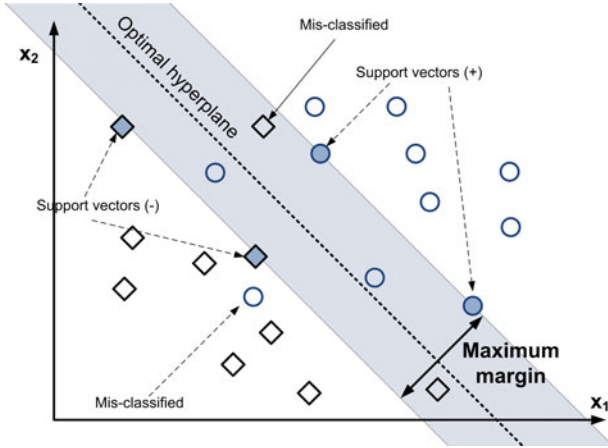


**FIGURE 1.** Concept of SVMs. The optimal hyperplane separates two classes of instances: square and circle. The dark filled instances are called support vectors.

separable in the new higher dimensional space. Without loss of generality, the concept of SVM can be illustrated in case of a linear kernel function, as shown in Figure 1. The obtained optimal hyperplane separates the input space with a maximum possible margin. Instances which satisfy  $\mathbf{w}^T \mathbf{x} + b > 1$  and  $\mathbf{w}^T \mathbf{x} + b < -1$  belong to classes “+1” and “-1,” respectively. The instances for which  $\mathbf{w}^T \mathbf{x} + b = \pm 1$  are called the support vectors. The weight coefficients  $\mathbf{w}$  reveal the importance of input variables. Some misclassification can be tolerated by adjusting the penalty on error term  $C$  in Eq. (10). Compared to other classifiers, such as ANNs, the SVM has several advantages: it is based on Sequential Quadratic Programming, which yields unique solution, without issues with local minima. [22].

### 3. PROPOSED FRAMEWORK

An important parameter for the training of SVM is the soft margin constant  $C$  in Eq. (10). For linearly separable data, there exists a linear boundary that separates samples belonging to “-1” class and those belonging to “+1” class. However, in practical classification problems, data are often not separable (even with nonlinear kernels). Hence, the soft margin term  $C$  and the error margin  $\xi$  are introduced to allow a certain misclassification.

It is necessary at this point to discuss whether the problem of CCT classification in power systems is separable. Reference [19] has proved that for a Single Machine Infinite Bus system, where the generator is modeled by constant transient voltage ( $E'_g$ ) behind transient reactance ( $X'_d$ ), there exists an analytical function of the CCT with respect to pre-fault active power and  $E'_g$ . Hence, a classification engine can be deduced

with 100% accuracy. The above observation can be extended to multimachine case. However, the CCT of one machine can also depend on the power output of nearby generators.

Another problem associated with CCT estimation accuracy is the use of simulation time step. For best the CCT estimation accuracy, a small simulation time step is needed. Consequently, the process of CCT estimation will take a lot of computation time. To achieve a compromise between accuracy and computation burden, a variable time step solver is required, as proposed in previous research [23].

The above analysis shows that with proper selection of input features, the CCT approximation problem can be done with 100% accuracy, *i.e.* the CCT classification problem might be separable using SVM. However, doing so would require small integration time step solvers, large input space, and also a highly nonlinear kernel function and activation function, if SVM and ANN are used respectively.

On the other hand, in the determination of CCT, a certain security margin is often tolerated. For example, if the power system operating condition can guarantee a CCT  $CCT_i = T_0 + \varepsilon_i$  for all contingencies  $i$ , and  $\varepsilon_i$  are small security margins, the operating condition can be considered secure.

The above analysis has led to the proposed framework for this paper, which could be stated as follows: Find the optimal operating point for a power system, in which all contingencies must have CCTs that satisfy:

$$CCT_i = CCT_{\min,i} + \varepsilon_i \quad (12)$$

where  $CCT_i$  is the actual clearing time for contingency  $i$ ;  $CCT_{\min,i}$  is its minimum allowable value, and  $\varepsilon_i$  is a positive security margin that is bounded:  $\varepsilon_i \leq \varepsilon_0$ . The flowchart for the creation of training instance is depicted in Figure 2. Instances with CCT greater than  $CCT_{\min,i} + \varepsilon_0$  are labeled as “+1,” whereas instances with CCT smaller than  $CCT_{\min,i}$  are labeled as “-1”. The criteria for determining whether a simulation is stable or non-stable are based on the angle difference between each machine and the center of inertia (COI) angle

$$\delta_i(t_s) - \frac{\sum_{k=1}^{n_g} H_k \delta_k(t_s)}{\sum_{k=1}^{n_g} H_k} \leq 100^\circ, \quad k = 1, \dots, n_g \quad (13)$$

where  $t_s$  is a predefined simulation time. The angle threshold of  $100^\circ$  for transient stability evaluation is often used in the literature [24]. This criterion is quite conservative, but it allows to account for both first-swing and multi-swing instability. To account for multi-swing instability, one can simply choose a longer simulation time  $t_s$ . The specific value of  $t_s$  depends on the dynamic performance of each system. If the studied system exhibits poor damping of power oscillations, multi-swing instability might occur [25], and consequently a longer  $t_s$  should be used.

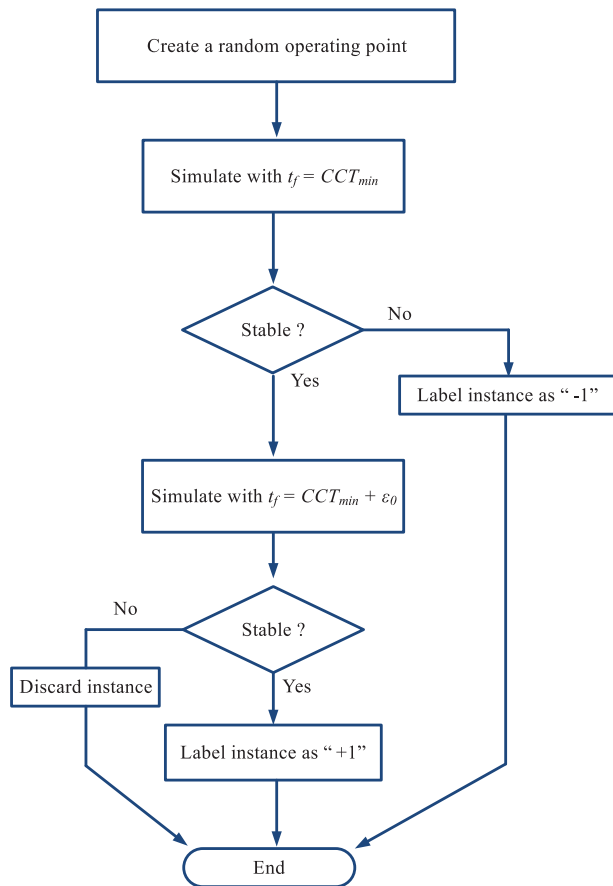


**FIGURE 2.** Framework for the creation of training instances.

As can be seen in Figure 2, since the training instances from two classes have CCT difference of at least  $\varepsilon_0$ , the classification accuracy can be improved significantly. This framework is applied to train SVM for all considered contingencies in the TSC-OPF problem. Each contingency constraint is represented by a single SVM. Assuming a linear SVM is used, the corresponding Transient Stability criteria to be included in the TSC-OPF formulation are as follows:

$$\mathbf{w}_i^T x + b_i \geq 0 \quad (14)$$

where  $\mathbf{w}_i$  and  $b_i$  are the weight vector and bias obtained after training the SVM for contingency  $i$ , and  $x$  is the vector of optimization variables. Hence, each transient stability constraint is represented by a single additional constraint in the OPF formulation. The proposed framework has the following advantages compared to previous approaches to solve TSC-OPF:

- Each transient stability constraint is represented by a single additional constraint. Therefore, the computational burden of the TSC-OPF does not increase considerably, compared to the conventional OPF.

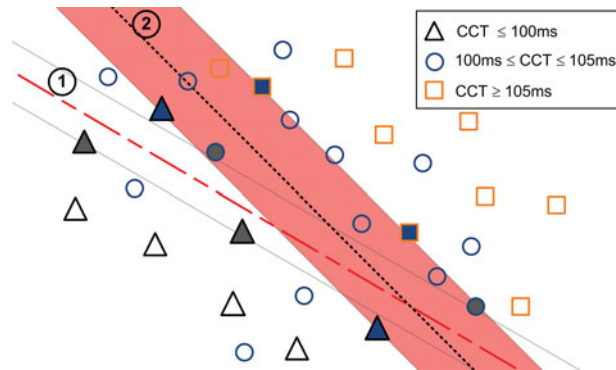


**FIGURE 3.** Illustration of the proposed classification approach: If one performs a classification between instances with  $CCT \leq 100$  ms and those with  $CCT \geq 100$  ms, the resulting separating hyperplane is 1, with quite a few errors. On the other hand, if a classification is made between instances with  $CCT \leq 100$  ms and those with  $CCT \geq 105$  ms, the resulting hyperplane is now 2, which separates with much higher accuracy.

- With a tolerance  $\varepsilon_0$ , the classification accuracy can be improved significantly. With a sufficiently large  $\varepsilon_0$ , the classification error can be reduced to 0%. In fact, a small tolerance (5–10 ms) is chosen in this work, to guarantee the stability of the OPF solution without too much conservativeness. As can be seen in Figure 3, the proposed classification approach can guarantee a higher security margin. All samples in the right-hand side of the hyperplane 2 have CCT of at least  $CCT_{min}$ . If the resulting hyperplane becomes a binding constraint in the TSC-OPF problem (hence, the optimal solution should lie in the hyperplane 2), the optimized operating condition will most likely have a CCT between  $CCT_{min}$  and  $CCT_{min} + \varepsilon_0$ . One important parameter for the database generation and training is the selection of the parameter  $\varepsilon_0$ . Increasing  $\varepsilon_0$  will improve the classification accuracy, but also will make the classification engine more conservative. The choice of  $\varepsilon_0$  should be decided by the power system planning engineer, considering the required stability margin as well as the required reliability in transient stability evaluation.
- The approach using classification would require less training samples than the approach using approximation, as in [16, 26], since it is not needed to determine the exact value of CCT. Only two simulations are needed to determine the label for a training instances. As a result, the transient stability evaluation can be done faster than CCT-based approaches, which would require 4–5 simulations [27].

- The approach can tackle both first-swing and multi-swing instability. To deal with multi-swing instability, one can choose a longer simulation time.

## 4. TEST RESULTS

### 4.1. The IEEE 39 Bus (New England) System

The proposed framework is first applied for the New England system, with 10 generators and 39 buses. For training samples, generator's output and load demand are varied randomly as in the following equations:

$$P_L^j(k) = P_L^j.[1 + 2\Delta P.(0.5 - \epsilon_{PL}(k))] \quad (15)$$

$$Q_L^j(k) = Q_L^j.[1 + 2\Delta Q.(0.5 - \epsilon_{QL}(k))] \quad (16)$$

$$P_G^j(k) = P_G^j.[1 + 2\Delta P_G.(0.5 - \epsilon_{PG}(k))] \quad (17)$$

$$V_G^j(k) = V_G^j.[1 + 2\Delta V_G.(0.5 - \epsilon_{VG}(k))] \quad (18)$$

The transient stability contingencies considered in this work are three-phase faults at generators' terminals. The proposed data generation and training method are applied to each contingency considered. With each fault, a total of 500 operating conditions are created randomly using Eq. (15). Each operating condition is checked for limit violations and then its transient stability is evaluated using the framework in Figure 2. For input features, the generators active and reactive output are selected. Classification results obtained with different input and kernel functions are shown in Table 1. The LibSVM package [28] has been used for training and testing of SVM.

The result presented in Table 1 has shown that a linear classifier can be enough for the classification of CCT, with proper selection of  $\epsilon_0$ . Although a nonlinear kernel can give 100% classification accuracy, the implementation of its corresponding analytical function in the form of Eq. (7) is much

Input	Kernel type	Margin $\epsilon_0$ (ms)	Accuracy (%)
$P_g$	Linear	2	97.36
$P_g$	Linear	5	97.97
$P_g$	Linear	10	98.31
$P_g$	Polynomial	10	100.0
$P_g, Q_g$	Linear	5	99.02
$P_g, Q_g$	Linear	10	99.25

**TABLE 1.** Classification accuracy with different  $\epsilon_0$  and kernel functions, machine G7

Gen.	Desired CCT (ms)	$\epsilon_0$	Actual CCT (ms)
3	200	10	208.6
5	180	10	180.5
7	190	10	194.3
8	200	10	208.0
9	100	5	108.6

**TABLE 2.** TSC-OPF result for single contingency

more complicated than with a linear kernel. The same test has been carried out for other generators faults, with quite similar result.

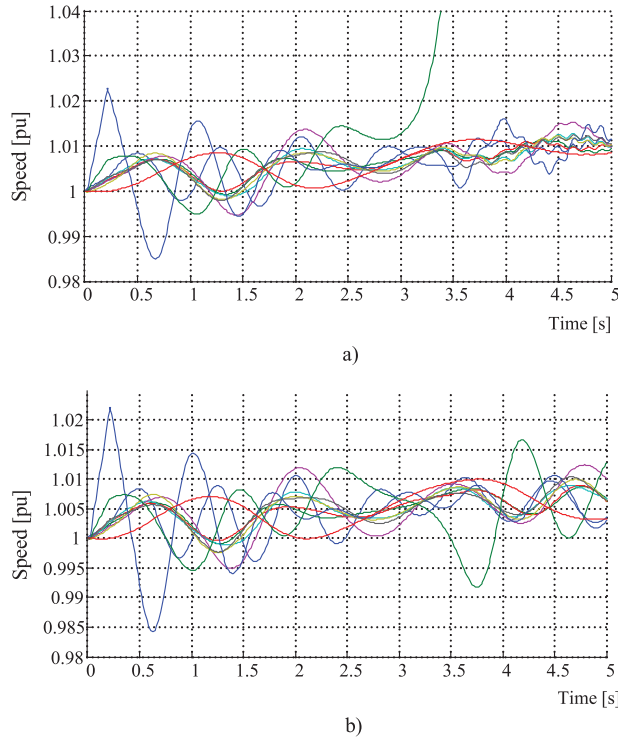
With the transient stability criterion being represented by one linear constraint, obtained from the trained SVM, a TSC-OPF framework can be formulated. With each fault considered in the TSC-OPF, the corresponding generator's production cost is deliberately reduced to a small value. As a result, the TSC-OPF will try to increase this generator active power, so that transient stability will be reduced. Therefore, the transient stability constraint of this generator in the form of Eq. (7) will become a binding constraint. The CCT of the optimal solution (which should be  $CCT_{\min}$ ) is then re-evaluated to determine the effectiveness of the proposed algorithm. This procedure is carried out for 5 generators: 3, 5, 7, 8 and 9.

Table 2 presents the CCTs of 5 different TSC-OPF solutions, each was run with one single contingency constraint. Table 3 presents the CCT results of the TSC-OPF solution obtained when the transient stability constraints for all 5 contingencies are considered. In all cases, it can be seen that the proposed algorithm yielded OPF results that satisfied all transient stability constraints, within the predefined error boundary.

The stabilizing effect of the TSC-OPF is also verified by time-domain simulation. Figure 4 shows system speed responses with a 200-ms fault at generator 8 terminal. This is a multi-swing instability contingency. As can be seen in Figure 4(b), the optimal operating condition obtained from the TSC-OPF is stable with this fault.

Gen.	Desired CCT (ms)	$\epsilon_0$	Actual CCT (ms)
3	200	10	202
5	180	10	189
7	190	10	198
8	200	10	203
9	100	5	102

**TABLE 3.** TSC-OPF result with multiple contingency constraints, case New England



**FIGURE 4.** Speed responses with a 200-ms three-phase fault at generator 8. (a) Speed response of 200-ms fault at generator 8, OPF solution. (b) Speed response of 200-ms fault at generator 8, TSC-OPF solution.

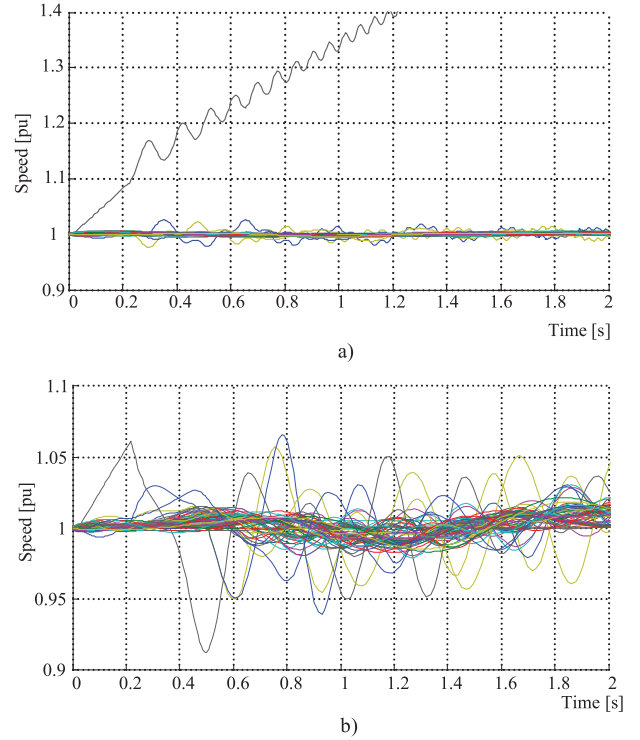


**FIGURE 5.** Verification of transient stability criteria at generator 21 bus. (a) Speed response with 200-ms fault at G21, OPF solution. (b) Speed response with 200-ms fault at G21, TSC-OPF solution.

Gen.	OPF		TSC-OPF	
	$P_g$	$Q_g$	$P_g$	$Q_g$
1	613.29	140.00	421.42	140.00
2	616.71	300.00	618.59	145.86
3	<b>725.00</b>	<b>300.00</b>	<b>693.34</b>	<b>277.57</b>
4	599.15	108.50	604.35	182.70
5	<b>508.00</b>	<b>140.87</b>	<b>496.91</b>	<b>167.00</b>
6	603.44	216.02	537.62	122.27
7	<b>580.00</b>	<b>59.71</b>	<b>580.00</b>	<b>127.52</b>
8	<b>564.00</b>	<b>2.40</b>	<b>553.42</b>	<b>137.75</b>
9	<b>865.00</b>	<b>34.44</b>	<b>850.40</b>	<b>49.77</b>
10	631.04	101.67	943.35	-11.59
Obj. (\$/h)	1.99E+04		2.22E+04	

**TABLE 4.** Load flow result, TSC-OPF vs OPF, case New England

Table 4 compares the generator active and reactive output of OPF and TSC-OPF solutions. Dispatch results for the concerned generators are shown in bold. The results also reveal the re-scheduling effect of TSC-OPF. Apart from generator 3, all other considered generators increase their reactive output in the TSC-OPF solution. This could be explained by the

fact that higher field current tends to increase the CCT, as discussed in Section 2.2. It is also worth noting that generator 7 does not need to reduce its active output at all in order to satisfy the stability constraints. This result shows that besides generator active power, which is an obvious control variable in generation re-scheduling to satisfy transient stability constraints, the generator reactive output can also be used.

#### 4.2. The IEEE 300 Bus System

The proposed TSC-OPF approach is also applied for the IEEE 300 bus system. The load flow and generator cost data for this system are available in MATPOWER [29]. The dynamic data for this system were created with IEEE AC4A excitation model and TGOV1 governors. The contingencies considered for this system are 3-phase faults at generators 6, 20, 21, and 40. A CCT margin of 8 ms is chosen for all generator contingencies. After the TSC-OPF solution is obtained, the CCT of all contingencies is verified with time-domain simulations. Figure 5 shows time-domain simulation results of the three-phase fault at bus 21, with OPF and TSC-OPF solutions.

The CCT of all considered contingencies are shown in Table 5. It can be seen that the TSC-OPF solution satisfies all transient stability constraints, with relatively small margins.

Gen.	Target CCT (ms)	$\varepsilon_0$	Actual CCT (ms)
6	140	8	140.6
20	140	8	146.0
21	200	8	202.6
40	120	8	121.4

**TABLE 5.** TSC-OPF result with multiple contingency constraints, case IEEE 300

Two application examples for the New England system and the IEEE 300 bus system show that with the proposed framework, both first-swing and multi-swing stability constraints can be considered.

## 5. CONCLUSION

This paper presents a novel approach to solve TSC-OPF problem. In the proposed framework, the SVM are used to classify contingencies. With the proposed approach for CCT classification, it can be guaranteed that the optimal solution of the TSC-OPF will satisfy the required minimum CCT, with some predefined positive security margin. The approach has several advantages: Compared to the previous approach based on CCT approximation, the training time for SVM is significantly reduced. The proposed approach can tackle multicontingency-constrained OPF. Moreover, the transient stability constraints are described as linear constraints. Therefore, the additional computational burden is negligible. It is worth noting that the implementation of TSC-OPF based on commercial software is quite simple, since several commercial OPF solvers such as PSS/E already support the inclusion of additional constraints in linear form.

Besides the transient stability constraints based on critical fault clearing time, the proposed approach can also be expanded to consider other types of constraints, such as those related to voltage stability and small signal instability. This will be the subject of the authors' future research.

## FUNDING

This research is funded by the Vietnam National Foundation for Science and Technology Development (NAFOSTED) under grant number 102.05-2013.27.

## REFERENCES

[1] Kundur, P., Paserba, J., Ajarapu, V., Andersson, G., Bose, A., Canizares, C., Hatziargyriou, N., Hill, D., Stankovic, A., Taylor, C., Van Cutsem, T., and Vittal, V., "Definition and classification

of power system stability IEEE/CIGRE joint task force on stability terms and definitions," *IEEE Trans. Power Syst.*, Vol. 19, pp. 1387–1401, August 2004.

[2] Pai, M. A., *Energy Function Analysis for Power System Stability*, 1989.

[3] Geeganage, J., Annakkage, U., Weekes, T., and Archer, B., "Application of energy-based power system features for dynamic security assessment," *IEEE Trans. Power Syst.*, Vol. 30, pp. 1957–1965, July 2015.

[4] Yuan, Y., and Sasaki, H., "A solution of optimal power flow with multicontingency transient stability constraints," *IEEE Trans. Power Syst.*, Vol. 18, No. 3, pp. 1094–1102, 2003.

[5] Zarate-Milano, R., Cutsem, T., Milano, F., and Conejo, A., "Securing transient stability using time domain simulations within an optimal power flow," *IEEE Trans. Power Syst.*, Vol. 25, No. 1, pp. 243–253, 2010.

[6] Xin, D. G. H., Huang, Z., Zhuang, K., and Cao, L., "Application of stability constrained optimal power flow in the east China system," *IEEE Trans. Power Syst.*, Vol. 25, No. 3, pp. 1423–1433, 2010.

[7] Pizano-Martinez, A., Fuerte-Esquivel, C. R., and Ruiz-Vega, D., "Global transient stability-constrained optimal power flow using an OMIB reference trajectory," *IEEE Trans. Power Syst.*, Vol. 25, pp. 392–403, February 2010.

[8] Pizano-Martinez, A., Fuerte-Esquivel, C., and Ruiz-Vega, D., "A new practical approach to transient stability-constrained optimal power flow," *IEEE Trans. Power Syst.*, Vol. 26, No. 3, pp. 1686–1696, 2011.

[9] Jiang, Q., Zhou, B., and Zhang, M., "Parallel augmented Lagrangian relaxation method for transient stability constrained unit commitment," *IEEE Trans. Power Syst.*, Vol. 28, pp. 1140–1148, May 2013.

[10] Geng, G., Ajarapu, V., and Jiang, Q., "A hybrid dynamic optimization approach for stability constrained optimal power flow," *IEEE Trans. Power Syst.*, Vol. 29, No. 5, pp. 2138–2149, 2014.

[11] Jiang, Q., and Geng, G., "A reduced-space interior point method for transient stability constrained optimal power flow," *IEEE Trans. Power Syst.*, Vol. 25, pp. 1232–1240, August 2010.

[12] Tu, X., Dessaint, L.-A., and Kamwa, I., "Fast approach for transient stability constrained optimal power flow based on dynamic reduction method," *IET Gener. Transm. Distrib.*, Vol. 8, No. 7, pp. 1293–1305, 2013.

[13] Xu, Y., Dong, Z. Y., Zhao, J., Xue, Y., and Hill, D., "Trajectory sensitivity analysis on the equivalent one-machine-infinite-bus of multi-machine systems for preventive transient stability control," *IET Gener. Transm. Distrib.*, Vol. 9, No. 3, pp. 276–286, 2015.

[14] Hou, G., and Vittal, V., "Determination of transient stability constrained interface real power flow limit using trajectory sensitivity approach," *IEEE Trans. Power Syst.*, Vol. 28, No. 3, pp. 2156–2163, 2013.

[15] Weerasoory, S., *Application of Neural Networks for Classification and Identification in Power Systems*. PhD thesis, University of Washington, Seattle, WA, 1992.

[16] Jayasekara, B., and Annakkage, U., "Transient security assessment using multivariate polynomial approximation," *Electr. Power Syst. Res.*, Vol. 77, No. 5–6, pp. 704–711, 2007.

- [17] Wehenkel, L., "Machine learning approaches to power-system security assessment," *IEEE Expert*, Vol. 12, No. 5, pp. 60–72, 1997.
- [18] Karami, A., "Power system transient stability margin estimation using neural networks," *Int. J. Elect. Power Energy Syst.*, Vol. 33, pp. 983–991, May 2011.
- [19] Jayasekara, B., and Annakkage, U., "Derivation of an accurate polynomial representation of the transient stability boundary," *IEEE Trans. Power Syst.*, Vol. 21, No. 4, pp. 1856–1863, 2006.
- [20] Moulin, L., da Silva, A. P., El-Sharkawi, M. A., and R. J. M. II, "Support vector machines for transient stability analysis of large scale power systems," *IEEE Trans. Power Syst.*, Vol. 19, No. 2, pp. 818–825, 2004.
- [21] Ly, J., Pawlak, M., and Annakkage, U., "Prediction of the transient stability boundary using the LASSO," *IEEE Trans. Power Syst.*, Vol. 28, No. 1, pp. 281–288, 2013.
- [22] Haykin, S., *Neural Networks: A Comprehensive Foundation*, 2nd ed., Upper Saddle River, NJ: Prentice Hall PTR, 1998.
- [23] Tu, X., Dessaint, L.-A., and Nguyen-Duc, H., "Transient stability constrained optimal power flow using independent dynamic simulation," *IET Gener. Transm. Distrib.*, Vol. 7, No. 3, pp. 244–253, 2013.
- [24] Gan, D., Thomas, R., and Zimmerman, R., "Stability-constrained optimal power flow," *IEEE Trans. Power Syst.*, Vol. 15, No. 2, pp. 535–540, 2000.
- [25] Kundur, P., *Power System Stability and Control*. EPRI Power Systems Engineering Series, McGraw-Hill, 1994.
- [26] Jayasekara, U., and Annakkage, B., "Incorporating dynamic security into market dispatch using accurate transient stability constraints," *IEEE Power Engineering Society General Meeting*, 2006.
- [27] Pavella, M., Ernst, D., and Ruiz-Vega, D., *Transient Stability of Power System, a Unified Approach to Assessment and Control*. Kluwer Academic Publishers, 1999.
- [28] Chang, C.-C., and Lin, C.-J., "LIBSVM: A library for support vector machines," *ACM Transactions on Intelligent Systems and Technology*, Vol. 2, pp. 27:1–27:27, 2011.
- [29] Zimmerman, R. D., Murillo-Sanchez, C. E., and Thomas, R. J., 'MATPOWER: Steadystate operations, planning and

analysis tools for power systems research and education," *IEEE Trans. Power Syst.*, Vol. 26, No. 1, pp. 12–19, 2011.

## BIOGRAPHIES

**Huy Nguyen-Duc** received the B.S. degree from the Department of Electric Power systems, Hanoi University of Science and Technology (HUST), Hanoi, Vietnam, in 2001, and the Ph.D. degree in Electrical Engineering from the Department of Electrical Engineering, École de Technologie Supérieure, Montréal, Québec, Canada, in 2011. He is currently with the Department of Electric Power systems at HUST. He is a member of the IEEE. His fields of interest are power system operation and control, and applications of artificial intelligence techniques in power systems.

**Linh Tran-Hoai** is an Associate Professor in the School of Electrical Engineering of Hanoi University of Science and Technology. He received the M.Sc. degree in Applied Informatics in 1997, the Ph.D. and the habilitation degrees in Electrical Engineering in 2000 and 2005, respectively, from the Warsaw University of Technology, Poland. His current research concentrates on the application of artificial intelligence in modern instrumentation devices and in power system controls.

**Huy Cao-Duc** graduated from the Hanoi University of Science and Technology in 2014. From 2014 until now, he is a planning engineer at the Vietnam Institute of Energy, Ministry of Industry and Trade (MOIT), Vietnam. His research interest includes power system stability and power system modeling.

# MULTI-PERIOD LINEARIZED OPTIMAL POWER FLOW MODEL INCORPORATING TRANSMISSION LOSSES AND THYRISTOR CONTROLLED SERIES COMPENSATORS

Pham Nang Van<sup>1</sup>, Le Thi Minh Chau<sup>1</sup>, Pham Thu Tra My<sup>2</sup>, Pham Xuan Giap<sup>2</sup>, Ha Duy Duc<sup>2</sup>, Tran Manh Tri<sup>2</sup>

<sup>1</sup>Hanoi University of Science and Technology (HUST); van.phamnang@hust.edu.vn, chau.lethiminh@hust.edu.vn

<sup>2</sup>Student at Department of Electric Power Systems, Hanoi University of Science and Technology (HUST)

**Abstract** - This paper presents multi-period linearized optimal power flow (MPLOPF) with the consideration of transmission network losses and Thyristor Controlled Series Compensators (TCSC). The transmission losses are represented using piecewise linear approximation based on line flows. In addition, the nonlinearity due to the impedance variation of transmission line with TCSC is linearized deploying the big-M based complementary constraints. The proposed model in this paper is evaluated using PJM 5-bus test system. The impact of a variety of factors, for instance, the number of linear blocks, the location of TCSC and the ramp rate constraints on the power output and locational marginal price (LMP) is also analyzed using this proposed model.

**Key words** - Multi-period linearized optimal power flow (MPLOPF); mixed-integer linear programming (MILP); transmission losses; Thyristor Controlled Series Compensators (TCSC); big-M

## 1. Introduction

Electricity networks around the world are experiencing extensive change in both operation and infrastructure due to the electricity market liberalization and our increased focus on eco-friendly generation. Managing and operating power systems with considerable penetration of renewable energy sources (RES) is an enormous challenge and many approaches are applied to cope with RES integration, mainly the management of intermittency. In addition to increasing power reserves, energy storage systems (ESS) can be invested to mitigate the uncertainty of RES. The increasing application of ESS as well as problems including time-coupled formulations such as power grid planning, N-1 secure dispatch and optimal reserve allocation for outage scenarios have led to extended optimal power flow (OPF) model referred to as multi-period OPF problems (MPOPF) [1]-[2].

Typically, the MPOPF problem is approximated using the DC due to its convexity, robustness and speed in the electricity market calculation [3]. To improve the accuracy of the MPOPF model, transmission power losses have been integrated. This is significant because the losses typically account for 3% to 5% of total system load [4]. When power losses are incorporated in the MPOPF model, this model becomes nonlinear. To address the nonlinearity, reference [3] deploys the iterative algorithm based on the concept of fictitious nodal demand (FND). The disadvantage of this approach is that the MPOPF problem must be iteratively solved. Reference [5] presents another approach in which branch losses are linearized. The branch losses can be expressed as the difference between node phase angles or line flows [4]. The main drawback of this model is that it can lead to “artificial losses” without introducing binary variables [5].

Moreover, the TCSC is increasingly leveraged in power systems to improve power transfer limits, to enhance

power system stability, to reduce congestion in power market operations and to decrease power losses in the grid [6]. When integrating TCSC in the MPOPF problem, this model becomes nonlinear and non-convex since the TCSC reactance becomes a variable to be found [7]. At present, there are several strong solvers like CONOPT, KNITRO for solving this nonlinear optimization problem [8]. However, directly solving nonlinear optimization problems cannot guarantee the global optimal solution. References [9]-[10] demonstrate the relaxation technique to solve the nonlinear optimization problem in power system expansion planning considering TCSC investment. Furthermore, the iterative method is used to determine optimal parameter of TCSC in reference [11].

The main contributions of the paper are as follows:

- Combining different linearized techniques to convert the nonlinear MPOPF to the mixed-integer linear MPOPF.
- Analysing the impact of some factors such as the number of loss linear segments, the location of TCSC as well as the ramp rate of the units on the locational marginal price (LMP) and generation output.

The next sections of the article are organized as follows. In section 2, the authors present general mathematical formulation of multi-period optimal power flow (MPOPF) model incorporating losses and TCSC. The different linearization techniques are specifically presented in section 3 and 4. Section 5 demonstrates multi-period linearized optimal power flow (MPLOPF) model. The simulation results, numerical analyses of PJM 5-bus system are given in section 6. Section 7 provides some concluding remarks.

## 2. General mathematical formulation

For normal operation conditions, the node voltage can be assumed to be flat. A multi-period optimal power flow (MPOPF) considering network constraints can be modeled for all hour  $t$ , all buses  $n$ , all generators  $i$ , and all lines  $(s, r)$  as follows:

$$\min_{P, \delta} \sum_{i \in T} \sum_{i \in I} \sum_{b \in G_i(t)} \lambda_{gi}(b, t) \cdot P_{gi}(b, t) \quad (1)$$

Subject to

$$\sum_{i:(i,n) \in M_g} P_{gi}(t) - \sum_{j:(j,n) \in M_d} P_{dj}(t) - P_n(\delta, t) = 0 \quad (2)$$

$$\forall n \in N, \forall t \in T$$

$$\max \{P_{sr}(\delta, t); P_{rs}(\delta, t)\} \leq P_{sr}^{ub}; \forall (s, r) \in \Omega^l, \forall t \in T \quad (3)$$

$$0 \leq P_{gi}(b, t) \leq P_{gi}^{ub}(b, t); \forall i \in I, \forall b \in G_i(t), \forall t \in T \quad (4)$$

$$P_{gi}^{lb} \leq P_{gi}(t) \leq P_{gi}^{ub}; \forall i \in I, \forall t \in T \quad (5)$$

$$P_{gi}(t) - P_{gi}(t-1) \leq R_i^{up}; \forall i \in I, \forall t \in T \quad (6)$$

$$P_{gi}(t-1) - P_{gi}(t) \leq R_i^{dn}; \forall i \in I, \forall t \in T \quad (7)$$

The objective function in (1) represents the total system cost in T hours (here, T = 24 h). The constraints (2) enforce the power balance at every node and every hour. The constraints (3) enforce the line flow limits at every hour. The constraints (4) and (5) are operating constraints that specify that a generator's power output as well as power output of each energy block must be within a certain range. The other constraints included in the formulation above are the ramp-up constraints (6) and ramp-down constraints (7).

If the reactance of branch  $x_{sr}$  is taken as a variable due to TCSC installation, in the range of  $[x_{sr}^{\min}, x_{sr}^{\max}]$ , it yields a new model:

$$\min_{P, \delta, x_{sr}} \sum_{t \in T} \sum_{i \in I} \sum_{b \in G_i(t)} \lambda_{gi}(b, t) \cdot P_{gi}(b, t) \quad (8)$$

Subject to

$$x_{sr}^{\min} \leq x_{sr} \leq x_{sr}^{\max} \quad (9)$$

$$(2)-(7) \quad (10)$$

The above general model is nonlinear. Sections 3 and 4 present different linearization methods to convert this model to the linear form.

### 3. Linearization of the network losses

In this section, the subscript  $t$  is dropped for notational simplicity. However, it could appear in every variable and constraint. Additionally, the expressions presented below apply to every transmission line; therefore, the indication  $\forall (s, r) \in \Omega^l$  will be explicitly omitted.

The real power flows in the line  $(s, r)$  determined at bus  $s$  and  $r$ , respectively, are given by

$$P_{sr}(\delta_s, \delta_r) = G_{sr} [1 - \cos(\delta_s - \delta_r)] - B_{sr} \sin(\delta_s - \delta_r) \quad (11)$$

$$P_{rs}(\delta_s, \delta_r) = G_{sr} [1 - \cos(\delta_s - \delta_r)] + B_{sr} \sin(\delta_s - \delta_r) \quad (12)$$

The real power loss in the line  $(s, r)$ ,  $P_{sr}^{loss}(\delta_s, \delta_r)$  can be attained as follows:

$$P_{sr}^{loss}(\delta_s, \delta_r) = P_{sr}(\delta_s, \delta_r) + P_{rs}(\delta_s, \delta_r) \cong G_{sr} (\delta_s - \delta_r)^2 \quad (13)$$

In the lossless DC model, the real power flow in the line  $(s, r)$  at bus  $s$  is approximately calculated as in (14):

$$F_{sr}(\delta_s, \delta_r) \cong -B_{sr} (\delta_s - \delta_r) = \frac{1}{X_{sr}} (\delta_s - \delta_r) \quad (14)$$

Substituting (14) in (13), the real power loss in the line  $(s, r)$  is expressed as in (15):

$$P_{sr}^{loss}(\delta_s, \delta_r) = G_{sr} (X_{sr} F_{sr})^2 = \frac{R_{sr}}{1 + (R_{sr} / X_{sr})^2} F_{sr}^2 \quad (15)$$

Equation (15) can be further simplified. The resistance  $R_{sr}$  is usually much smaller than its reactance  $X_{sr}$ , particularly in high voltage lines. Consequently, (15) can be further reduced to (16)

$$P_{sr}^{loss}(\delta_s, \delta_r) = R_{sr} F_{sr}^2 \quad (16)$$

The first advantage of (16) compared to (13) is that power flows in lines neither built nor operative are zero. Another advantage of (16) is its possible application to model losses in HVDC lines.

The quadratic losses function (16) can be expressed using piecewise linear approximation according to absolute value of the line flow variable as follows:

$$P_{sr}^{loss}(\delta_s, \delta_r) = R_{sr} \sum_{l=1}^L \alpha_{sr}(l) |F_{sr}(l)| \quad (17)$$

To complete the piecewise linearization of the power flows and line loss, the following constraints are necessary to enforce adjacency blocks:

$$\omega_{sr}(l) \cdot \Delta P_{sr}^{\max} \leq |F_{sr}(l)|; \quad l = 1, \dots, L-1 \quad (18)$$

$$|F_{sr}(l)| \leq \omega_{sr}(l-1) \cdot \Delta P_{sr}^{\max}; \quad l = 2, \dots, L \quad (19)$$

$$\omega_{sr}(l) \leq \omega_{sr}(l-1); \quad l = 2, \dots, L-1 \quad (20)$$

$$|F_{sr}(l)| \geq 0; \quad l = 1, \dots, L \quad (21)$$

$$\omega_{sr}(l) \in \{0, 1\}; \quad l = 1, \dots, L-1 \quad (22)$$

Constraints (18) and (19) set the upper limit of the contribution of each branch flow block to the total power flow in line  $(s, r)$ . This contribution is non-negative, which is expressed in (21) and limited upper by  $\Delta P_{sr}^{\max} = P_{sr}^{ub} / L$ , the "length" of each segment of line flow (18). A set of binary variables  $\omega_{sr}(l)$  is deployed to guarantee that the linear blocks on the left will always be filled up first; therefore, this model eliminates the fictitious losses. Finally, constraints (22) state that the variables  $\omega_{sr}(l)$  are binary.

A linear expression of the absolute value in (17) is needed, which is obtained by means of the following substitutions:

$$|F_{sr}| = F_{sr}^+ + F_{sr}^- \quad (23)$$

$$F_{sr} = F_{sr}^+ - F_{sr}^- \quad (24)$$

$$0 \leq F_{sr}^- \leq (1 - \theta_{sr}) P_{sr}^{ub} \quad (25)$$

$$0 \leq F_{sr}^+ \leq \theta_{sr} P_{sr}^{ub} \quad (26)$$

In (24), two slack variables  $F_{sr}^+$  and  $F_{sr}^-$  are used to replace  $F_{sr}$ . Constraints (25) and (26) with binary variable  $\theta_{sr}$  ensure that the right-hand side of (23) equals its left-hand side.

Moreover, the slopes of the blocks of line flow  $\alpha_{sr}(l)$  for all transmission lines can be given by Eq. (27).

$$\alpha_{sr}(l) = (2l-1) \Delta P_{sr}^{\max} \quad (27)$$

It is emphasized that the number of linear segments will radically affect the accuracy of the optimal problem solution. Moreover, this linear technique is independent of the reference bus selection and thereby eliminating discrimination in the electricity market operation.

Using the above expressions, the real power flow in line  $(s, r)$  computed at bus  $s$  and  $r$  can be recast as follows, respectively:

$$P_{sr}(\delta_s, \delta_r) = \frac{1}{2} P_{sr}^{loss}(\delta_s, \delta_r) + F_{sr} \quad (28)$$

$$= \frac{1}{2} R_{sr} \sum_{l=1}^L \alpha_{sr}(l) |F_{sr}(l)| + F_{sr}$$

$$P_{rs}(\delta_s, \delta_r) = \frac{1}{2} P_{sr}^{loss}(\delta_s, \delta_r) - F_{sr} \quad (29)$$

$$= \frac{1}{2} R_{sr} \sum_{l=1}^L \alpha_{sr}(l) |F_{sr}(l)| - F_{sr}$$

The power withdrawn into a node  $n$ ,  $P_n(\delta, t)$  can be written as

$$P_n = \sum_{k:(n,k) \in \Omega'} \left[ \frac{1}{2} R_{nk} \sum_{l=1}^L \alpha_{nk}(l) |F_{nk}(l)| + F_{nk} \right] \quad (30)$$

A linear substitution for the function in (3) can be found by the following equivalent constraints without increasing the number of rows

$$\frac{1}{2} R_{sr} \sum_{l=1}^L \alpha_{sr}(l) |F_{sr}(l)| + |F_{sr}| \leq P_{sr}^{ub} \quad (31)$$

Rewriting Eq. (31), the constraints (3) are expressed as follows

$$\sum_{l=1}^L \left[ \frac{1}{2} R_{sr} \alpha_{sr}(l) + 1 \right] |F_{sr}(l)| \leq P_{sr}^{ub} \quad (32)$$

#### 4. Linearization of a bilinear function

When  $x_{sr}$  is taken as a variable, constraint (14) also makes the MPOPF model nonlinear since this constraint is a bilinear function. To overcome the nonlinearity of this constraint, we introduce a new variable  $F_{sr}$ , instead of variable  $x_{sr}$ . After obtaining the optimal solution with variable  $(P, F, \delta)$ , the optimal reactance can be uniquely determined according to Eq. (33)

$$x_{sr} = \frac{\delta_s - \delta_r}{F_{sr}} \quad (33)$$

Therefore, the constraint (9) becomes:

$$x_{sr}^{\min} \leq x_{sr} = \frac{\delta_s - \delta_r}{F_{sr}} \leq x_{sr}^{\max} \quad (34)$$

It is noted that the sign of  $F_{sr}$  cannot be determined beforehand. Moreover, if the denominator  $F_{sr}$  is zero, the numerator  $\delta_s - \delta_r$  must be zero. As a result, (34) can be converted into the expression (35) depending on the sign of  $F_{sr}$ .

$$\begin{cases} \text{if } F_{sr} > 0 & F_{sr} \cdot x_{sr}^{\min} \leq \delta_s - \delta_r \leq F_{sr} \cdot x_{sr}^{\max} \\ \text{if } F_{sr} = 0 & \delta_s - \delta_r = 0 \\ \text{if } F_{sr} < 0 & F_{sr} \cdot x_{sr}^{\max} \leq \delta_s - \delta_r \leq F_{sr} \cdot x_{sr}^{\min} \end{cases} \quad (35)$$

These condition constraints can be combined by leveraging binary variables  $y_{sr}$  and big-M based complementary constraints as follows [12]. In our model, M is taken to be  $\pi/2$  due to system stability requirement [13].

$$\begin{cases} -My_{sr} + F_{sr} \cdot x_{sr}^{\min} \leq \delta_s - \delta_r \leq F_{sr} \cdot x_{sr}^{\max} + My_{sr} \\ -M(1 - y_{sr}) + F_{sr} \cdot x_{sr}^{\max} \leq \delta_s - \delta_r \leq F_{sr} \cdot x_{sr}^{\min} + M(1 - y_{sr}) \end{cases} \quad (36)$$

It is important to stress that linear technique using the above binary variable is exact while the linearized technique in Section 3 is approximately presented.

#### 5. Multi-period linearized optimal power flow (MPLOPF) model with losses and TCSC

The MPLOPF model with losses and TCSC has the following form:

$$\min_{P, F, \delta} \sum_{t \in T} \sum_{i \in I} \sum_{l \in G_i(t)} \lambda_{gi}(b, t) \cdot P_{gi}(b, t) \quad (37)$$

Subject to

$$\sum_{i:(i,n) \in M_g} P_{gi}(t) - \sum_{j:(j,n) \in M_d} P_{dj}(t) = \begin{cases} \left[ \frac{1}{2} R_{nk} \sum_{l=1}^L \alpha_{nk}(l) [F_{nk}^+(l, t) + F_{nk}^-(l, t)] \right] \\ \left[ \sum_{l=1}^L F_{nk}^+(l, t) - \sum_{l=1}^L F_{nk}^-(l, t) \right] \end{cases}; \forall n, \forall t \quad (38)$$

$$\sum_{l=1}^L \left[ \frac{1}{2} R_{sr} \alpha_{sr}(l) + 1 \right] [F_{sr}^+(l, t) + F_{sr}^-(l, t)] \leq P_{sr}^{ub} \quad (39)$$

$$\omega_{sr}(l, t) \cdot \Delta P_{sr}^{\max} \leq F_{sr}^+(l, t) + F_{sr}^-(l, t); \quad l = 1, \dots, L-1 \quad (40)$$

$$F_{sr}^+(l, t) + F_{sr}^-(l, t) \leq \omega_{sr}(l-1, t) \cdot \Delta P_{sr}^{\max}; \quad l = 2, \dots, L \quad (41)$$

$$\omega_{sr}(l, t) \leq \omega_{sr}(l-1, t); \quad l = 2, \dots, L-1; \quad (42)$$

$$F_{sr}^+(l, t) \geq 0; F_{sr}^-(l, t) \geq 0; \omega(l, t) = \{0; 1\} \quad (43)$$

$$0 \leq \sum_{l=1}^L F_{sr}^+(l, t) \leq \theta(t) P_{sr}^{ub}; \quad \forall (s, r) \in \Omega^l, \forall t \in T \quad (44)$$

$$0 \leq \sum_{l=1}^L F_{sr}^-(l, t) \leq [1 - \theta(t)] P_{sr}^{ub}; \quad \forall (s, r) \in \Omega^l, \forall t \in T \quad (45)$$

$$\begin{cases} -My_{sr}(t) + F_{sr}(t) x_{sr}^{\min} \leq \delta_s(t) - \delta_r(t) \\ \delta_s(t) - \delta_r(t) \leq F_{sr}(t) x_{sr}^{\max} + My_{sr}(t) \\ -M[1 - y_{sr}(t)] + F_{sr}(t) x_{sr}^{\max} \leq \delta_s(t) - \delta_r(t) \\ \delta_s(t) - \delta_r(t) \leq F_{sr}(t) x_{sr}^{\min} + M[1 - y_{sr}(t)] \end{cases} \quad (46)$$

$$(4) - (7) \quad (47)$$

Regarding the computational complexity of the model, the number of continuous variable is  $24 \cdot N^{GEN} \cdot N_i^{GEN} + 24 \cdot (N^{BUS} - 1) + 2.24 \cdot N^{LIN} \cdot L$  and the number of binary variables is  $24 \cdot N^{LIN} \cdot (L-1) + 2.24 \cdot N^{LIN}$ .

After the MPLOPF problem is solved, the marginal cost at the node  $i$  in hour  $t$  can be determined by the following expression [3]:

$$LMP_i = LMP_E - LF_i \cdot LMP_E + \sum_l SF_{l-i} \cdot \mu_l \quad (48)$$

#### 6. Results and discussions

In this section, the multi-period linearized optimal power flow model is performed on the modified PJM 5-bus system [3]. The MPLOPF problem is solved by CPLEX 12.7 [15] under MATLAB environment.

### 6.1. System data

The test system is shown in Figure 1. The total peak demand in this system is 1080 MW and the total load is equally distributed among buses B, C and D. The daily load curve is depicted in Figure 2. Two small size generators on bus A have the capability to quickly start up. The ramp rate for the other generators is 50% of the rated power output [14].

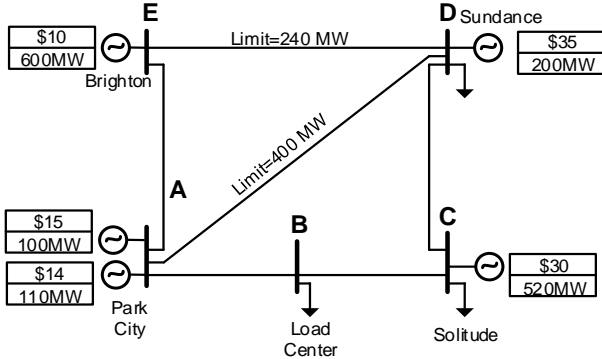


Figure 1. PJM 5-bus system and generation parameters

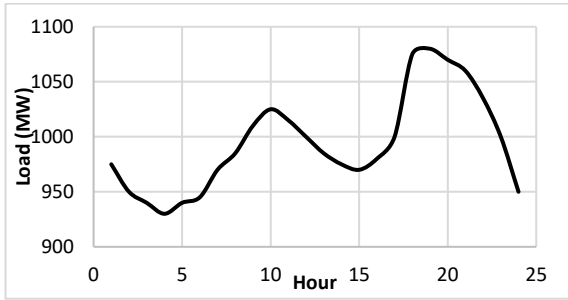


Figure 2. Daily load curve for PJM system

### 6.2. Impact from the number of linear blocks

Table 1. The effects of number of linear blocks

Linear blocks	Objective (\$)	Total losses (MW)	Time (s)
2	3844.43	316.69	1.71
4	3824.04	244.83	2.97
6	3822.96	238.56	5.28
8	3820.70	230.41	8.42
10	3820.55	229.49	12.35
11	3820.51	229.49	14.61

The number of linear blocks can significantly affect the solution time as well as the model accuracy listed in Table 1. The key idea in this paper is to find the number of linear blocks which give the best balance between the model accuracy and the solution time. In this case, 10 is an appropriate number in terms of objective value, total losses and calculation time.

### 6.3. Impact from losses

Table 2 compares the results of power output at 10 AM using the proposed model. These results are also compared with those of POWERWORLD software using the ACOPF model [16]. When comparing to POWERWORLD software, the calculated results using the proposed model considering losses are more accurate and less different than that of the model neglecting losses.

Table 2. Generating output results at 10 AM

Bus	Lossless (MW)	Losses (MW)	POWERWORLD (MW)
A1	110	110	110
A2	100	100	100
C	19.95	30.1	27.83
D	195.05	194.8	197.2
E	600	600	600

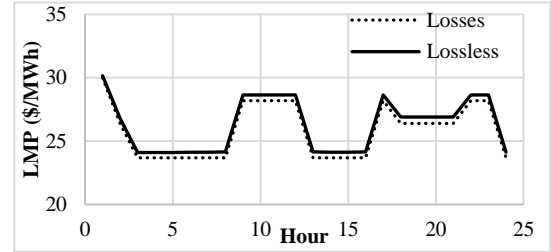


Figure 3. LMP at bus B at different hours without losses and with losses

The results of LMP calculations at node B for 24 hours using the proposed model with and without losses are given in Figure 3. This figure illustrates that the effect of power losses on LMP is very little. This result is consistent because the power losses account for about 1% of the total load for this PJM 5-bus system, therefore the marginal generating units as well as congested lines are the same in both cases.

### 6.4. Impact from TCSC location

It is assumed that power losses are not considered and the ramp rate of the generating units (not including units at node A) are taken as 25% of the maximum power output. Also, the compensation level of TCSC varies from 30% to 70%.

Figure 4 depicts the power output of generator at node C for 24 hours for different locations of TCSC. During the period from 1 AM to 3 AM, the power output of the unit at node C nearly remains when the location of TCSC varies. In addition, the power output of this unit is highest in 24 hours when TCSC is located in line A-B.

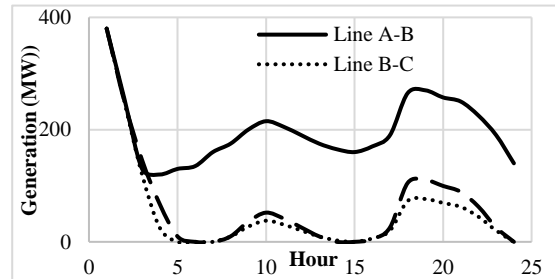


Figure 4. The dependence of Generating output of Unit at bus C on TCSC location

### 6.5. Impact from ramp rate constraints

Figure 5 shows the power output of generator located at node C when changing the ramp rate of generators and it is assumed that TCSC is not applied to the power grid. From the 5 AM to 24 PM, the power output of this unit is the same for ramp rates of 25%, 35% and 50%. At the same time, the output of this unit is the highest for ramp rate 100% of the maximum power.

Figure 6 depicts the effect of TCSC placement on the power output with different ramp rate scenarios at 10 AM. We see that the power output of generator at node C does not change as the ramp rate of the units changes in case of placing TCSC on line A-B. However, when TCSC is not installed, the ramp rate of units has a significant effect on the unit's output, increasing from 30,097 MW for the ramp rate of 50% to 223,37 MW for the ramp rate of 100%. Thus, using TCSC also reduces the impact of the ramp rate on the power output.

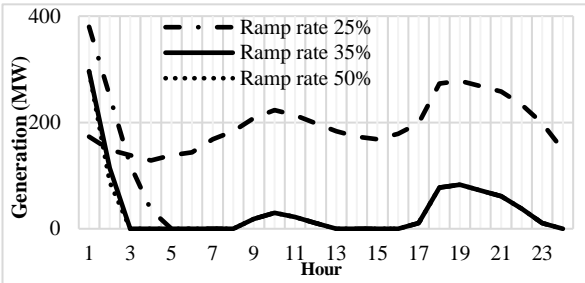


Figure 5. The dependence of generating output of Unit at bus C on Ramp rate without TCSC

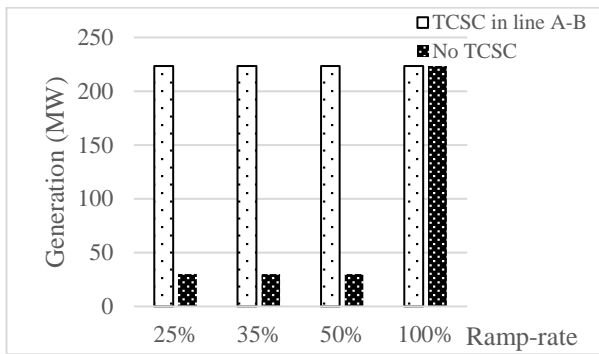


Figure 6. The dependence of power output of Unit at bus C on Ramp rate with TCSC in line A-B at 10 AM

## 7. Conclusion

This paper presents multi-period linearized optimal power flow (MPLOPF) model based mixed-integer linear programming (MILP). This MPLOPF integrates line losses and Thyristor Controlled Series Compensator (TCSC). The different linearization techniques, such as piecewise linear approximation and big-M based complementary constraints are deployed to convert multi-period nonlinear OPF problem to multi-period linearized OPF model. The calculated results using the proposed model are compared to those of the commercial POWERWORLD software and this proves the validation of the proposed model. Additionally, the influences of the number of linear blocks, line losses, location of TCSC and ramp rate are analyzed. The results reveal that these factors can importantly impact on LMP, generating output of units as well as revenue of participants in electricity markets.

## NOMENCLATURE

The main mathematical symbols used throughout this paper are classified below.

Constants:

$\alpha_{sr}(l)$  Slope of the  $l$ th segment of the linearized power flow in line  $(s, r)$

$\lambda_{gi}(b, t)$  Offered price of the  $b$ th linear block of the energy bid by the  $i$ th generating unit in hour  $t$

$B_{sr}$  Imaginary part of the admittance of line  $(s, r)$

$G_{sr}$  Real part of the admittance of line  $(s, r)$

$R_{sr}$  Resistance of the line  $(s, r)$

$X_{sr}$  Reactance of the line  $(s, r)$

$P_{dj}(t)$  Power consumed by the  $j$ th load in hour  $t$

$L$  Number of the blocks of the loss linearization

$P_{sr}^{ub}$  Transmission limit of line  $(s, r)$

$P_{gi}^{ub}$  Upper bound on the power output of the  $i$ th producer

$P_{gi}^{lb}$  Lower bound on the power output of the  $i$ th producer

$R_i^{up}$  Ramp-up limit of the  $i$ th unit

$R_i^{dn}$  Ramp-down limit of the  $i$ th unit

$x_{sr}^{\min}$  Lower bound of the reactance of the line with TCSC

$x_{sr}^{\max}$  Upper bound of the reactance of the line with TCSC

$N^{BUS}$  Number of nodes

$N^{GEN}$  Number of generators

$N^{LIN}$  Number of transmission lines

$N_i^{GEN}$  Number of energy blocks of unit  $i$

Variables:

$P_{gi}(b, t)$  Power output corresponding to the  $b$ th block of the  $i$ th unit in hour  $t$

$P_n(\delta, t)$  Power withdrawal at bus  $n$  in hour  $t$

$P_{sr}(\delta, t)$  Power flow in line  $(s, r)$  at node  $s$  in hour  $t$

$P_{rs}(\delta, t)$  Power flow in line  $(s, r)$  at node  $r$  in hour  $t$

$\delta_s(t)$  Voltage angle at node  $s$  in hour  $t$

$F_{sr}(t)$  Power flow in line  $(s, r)$  in hour  $t$  without losses

$P_{sr}^{loss}(\delta, t)$  Power losses in line  $(s, r)$  in hour  $t$

$\omega_{sr}(l)$  Binary variable relating to the line flow linearization

$y_{sr}(t)$  Binary variable corresponding the big-M based complementary constraints

$x_{sr}(t)$  The reactance of the line with TCSC in hour  $t$

$LF_i$  Loss factor at bus  $i$

$SF_{l-i}$  Sensitivity of branch power flow  $l$  with respect to injected power  $i$

$\mu_l$  Shadow price of transmission constraint on line  $l$

Sets:

$I$  Set of indices of the generating units

$G_i(t)$  Set of blocks energy bid offered by the  $i$ th unit in hour  $t$

$N$  Set of indices of the network nodes

$\Omega^l$  Set of transmission lines

## ACKNOWLEDGMENT

This research is funded by the Hanoi University of Science and Technology (HUST) under project number T2017-PC-093.

## REFERENCES

- [1] D. Kourounis, A. Fuchs, and O. Schenk, "Towards the next generation of multiperiod optimal power flow solvers", *IEEE Trans.*

- Power Syst.*, vol. 8950, pp. 1–10, 2018.
- [2] P. N. Van, N. D. Huy, N. Van Duong, and N. T. Huu, “A tool for unit commitment schedule in day-ahead pool based electricity markets”, *J. Sci. Technol. Univ. Danang*, vol. 6, pp. 21–25, 2016.
- [3] F. Li, S. Member, R. Bo, and S. Member, “DCOPF-Based LMP Simulation : Algorithm, comparison with ACOPF and sensitivity”, *IEEE Trans. Power Syst.*, vol. 22, no. 4, pp. 1475–1485, 2007.
- [4] D. Z. Fitiwi, L. Olmos, M. Rivier, F. de Cuadra, and I. J. Pérez-Arriaga, “Finding a representative network losses model for large-scale transmission expansion planning with renewable energy sources”, *Energy*, vol. 101, pp. 343–358, 2016.
- [5] J. M. Arroyo and A. J. Conejo, “Network-constrained Multiperiod auction for a pool-based electricity market”, *IEEE Trans. Power Syst.*, vol. 17, no. 4, pp. 1225–1231, 2002.
- [6] P. N. Van, N. D. Hung, and N. D. Huy, “The impact of TCSC on transmission costs in wholesale power markets considering bilateral transactions and active power reserves”, *J. Sci. Technol. Univ. Danang*, vol. 12, pp. 24–28, 2016.
- [7] G. Y. Yang, G. Hovland, R. Majumder, and Z. Y. Dong, “TCSC allocation based on line flow based equations via mixed-integer programming”, *IEEE Trans. Power Syst.*, vol. 22, no. 4, pp. 2262–2269, 2007.
- [8] Alireza Soroudi, *Power System Optimization Modeling in GAMS*. Springer, 2017.
- [9] O. Ziaee, O. Alizadeh Mousavi, and F. Choobineh, “Co-optimization of transmission expansion planning and TCSC placement considering the correlation between wind and demand scenarios”, *IEEE Trans. Power Syst.*, vol. 8950, no. c, pp. 1–1, 2017.
- [10] M. Farivar and S. H. Low, “Branch Flow Model: Relaxations and Convexification (Parts I, II)”, pp. 1–11, 2012.
- [11] P. N. Van and L. M. Khanh, “The optimal location and compensation level of Thyristor Controlled Series Compensator (TCSC) in Wholesale Electricity Markets considering Active Power Reserves”, *J. Sci. Technol. Tech. Univ. Vietnam*, 2017.
- [12] T. Ding, R. Bo, W. Gu, and H. Sun, “Big-M Based MIQP Method for Economic Dispatch With Disjoint Prohibited Zones”, *IEEE Trans. Power Syst.*, vol. 29, no. 2, pp. 976–977, 2014.
- [13] T. Ding, R. Bo, F. Li, and H. Sun, “Optimal Power Flow with the Consideration of Flexible Transmission Line Impedance”, *IEEE Trans. Power Syst.*, vol. 31, no. 2, pp. 1655–1656, 2016.
- [14] Y. Wei, H. Cui, X. Fang, and F. Li, “Strategic scheduling of energy storage for load serving entities in locational marginal pricing market”, *IET Gener. Transm. Distrib.*, vol. 10, no. 5, 2016.
- [15] IBM, “IBM ILOG CPLEX Optimization Studio Community Edition”.
- [16] <https://www.powerworld.com/>

(The Board of Editors received the paper on 18/4/2018, its review was completed on 04/5/2018)

# CONTENTS

ISSN 1859-1531 – THE UNIVERSITY OF DANANG, JOURNAL OF SCIENCE AND TECHNOLOGY, NO. 12(109).2016

## ENGINEERING AND TECHNOLOGY

---

Misalignment fading effects on performance of amplify-and-forward relaying FSO systems using SC-QAM signals over log-normal atmospheric turbulence channels <i>Duong Huu Ai, Do Trong Tuan, Ha Duyen Trung</i>	1
Photocatalytic degradation of phenol over Ag-TiO <sub>2</sub> -SiO <sub>2</sub> nano powder under sunlight irradiation <i>Han Van Dang, Vien Minh Le, Ky Phuong Ha Huynh</i>	6
Evaluating effectiveness of microwave heating and conventional heating for liquid fuel <i>Tran Thi Thu Huong</i>	11
Effects of red Y <sub>2</sub> O <sub>3</sub> :Eu <sup>3+</sup> phosphor in silicone lens on the color rendering ability of white led lamps <i>Anh Q. D. Nguyen, Vinh H. Nguyen</i>	16
Web service QoS prediction using service-based auto-encoder model <i>Le Van Thinh, Nguyen Xuan Hau</i>	20
The impact of TCSC on transmission costs in wholesale power markets considering bilateral transactions and active power reserves <i>Pham Nang Van, Nguyen Dong Hung, Nguyen Duc Huy</i>	24
A subproblem method for accurate thin shell models between conducting and nonconducting regions <i>Dang Quoc Vuong</i>	29
A design of frequency reconfigurable CPW-fed antenna using PIN diode for wireless applications <i>Hoang Thi Phuong Thao, Vu Van Yem</i>	34

## NATURAL SCIENCES

---

Isolation of stigmasterol from methanolic extract of stem and foliage of <i>Abrus precatorius</i> Linn <i>Ngo Minh Khoi, Tran Manh Luc</i>	39
Primary study on biological activities and chemical constituents of <i>Anoectochilus roxburghii</i> wall. of Vietnam <i>Ngo Thi Phuong, Bui Kim Anh, Giang Thi Kim Lien, Nguyen Thi Thanh Huong, Le Ngoc Hung, Nguyen Tuan Anh, Le Minh Ha</i>	43
Synthesizing and characterizing optical property of MOF-5 doped with trivalent europium <i>Bui Xuan Vuong</i>	46

## SOCIAL SCIENCES

---

A primary research on open innovation activities of SMEs in Vietnam <i>Tang Due Au</i>	50
---	----

## HUMAN SCIENCES

---

Some differences between the Ede language and the Vietnamese language <i>Nguyen Ngoc Chinh, Niê H'Loanh, Ngo Thi Huong Giang</i>	54
A study of the translation of fairy tales from English into Vietnamese - a Cognitive sociolinguistics perspective <i>Tran Quang Hai, Tran Thi Xuan Tham</i>	59
An investigation into the layout features of texts introducing museums in London <i>Nguyen Thi Thuy Hang, Nguyen Thi Quynh Hoa</i>	64
Loss and Gain phenomena in the English translations of conceptual metaphors of "Human status" in Trinh Cong Son's songs <i>Dinh Thi Minh Hien, Trinh Thi Thu Thao</i>	70
Stylistic devices used in song lyrics expressing patriotism in the two song books All American Patriotic and American Patriotic Songs <i>Nguyen Thi Quynh Hoa, Van Thi Bach Giang</i>	74
Developing intercultural awareness and attitudes of Vietnamese learners of English: case studies <i>Ho Si Thang Kiet</i>	80
An investigation into semantic features of wishing verbs in English and Vietnamese <i>Luu Quy Khuong, Ngo Thi Truc Mai</i>	85

# THE IMPACT OF TCSC ON TRANSMISSION COSTS IN WHOLESALE POWER MARKETS CONSIDERING BILATERAL TRANSACTIONS AND ACTIVE POWER RESERVES

Pham Nang Van<sup>1</sup>, Nguyen Dong Hung<sup>2</sup>, Nguyen Duc Huy<sup>1</sup>

<sup>1</sup>Hanoi University of Science and Technology (HUST); van.phamnang@hust.edu.vn; ngduchuy@gmail.com

<sup>2</sup>Student at Department of Electric Power Systems, HUST

**Abstract** - In the electricity market operation, calculating transmission charges is a critical issue. Transmission costs relate to the issue of how much is paid and by whom, for the use of transmission system. For short-run transmission charges, difference of location marginal prices (LMP) on a network branch has much influence on the market participants, including bilateral transactions. When there is congestion in power systems, difference of location marginal prices on the branch becomes bigger. One of the measures to overcome network congestion is using thyristor controlled series capacitor (TCSC). In addition, the presence of price-sensitive loads, bilateral transactions and requirement of active power reserves in power systems complicate matters associated with transmission charges in the wholesale electricity market. In this paper, a method for determining the optimal location of TCSC has been suggested and the impact of TCSC compensation levels on transmission charges of bilateral contracts in the wholesale electricity market is analyzed. The calculated results are illustrated on a 6-bus system.

**Key words** - Location marginal prices (LMP); wholesale power markets; transmission costs; active power reserves; bilateral transactions; thyristor controlled series capacitor (TCSC); AC optimal power flow (ACOPF).

## 1. Introduction

Today, the electricity industry has changed from monopoly to competitive market mechanism in many countries around the world, including Vietnam. In the wholesale electricity market, the market participants are generation companies (GENCOS) and distribution companies (DISCOS). To maintain the frequency stability, sufficient active reserve must be ensured. Not only the reserve must be sufficient to make up for a generating unit failure, but the reserves must also be appropriately allocated among fast-responding and slow-responding units [5]. The reserve for frequency regulation is divided into 3 categories: regulation reserve (RR), spinning reserve (SR) and supplemental reserve (XR). Spinning reserve and supplemental reserve are components of contingency reserve (CR). Operation reserve encompasses contingency reserve (CR) and regulation reserve [5]. The market operator collects generating offers (increase in price), reserve offers by producers, load bids (decrease in price) by consumers and reserve bids by the market operator and clears the market by maximizing the social welfare [1]. Then, power output of generation units, power output of buying units and reserve capacity of generator units may be determined by one of the following methods: sequentially optimizing energy and reserve; co-optimization of energy and reserve [2]. Additionally, the firm bilateral and multilateral contracts are also incorporated into this optimization problem [3]. To make payments in the electricity market, location marginal price (LMP) are calculated. The difference in LMPs between

two nodes of a branch is due to congestion and losses on that branch [4].

One of the measures to reduce the power flow on transmission lines congested is the use of Thyristor controlled series compensator (TCSC). The TCSC has many benefits, for instance, increasing power transfer limits, reducing power losses, enhancing stability of the power system, reducing production costs of power plants and fulfilling contractual requirements [6]. Moreover, the transmission charges of market participants and of bilateral transactions can be affected when installing TCSCs.

Recently, there has been growing interest in allocation of FACTS devices for achieving diverse objectives for transmission network. The impact of thyristor controlled series compensator (TCSC) on congestion and spot pricing is presented in [8]. Priority list method for TCSC allocation for congestion management has been proposed in [9]. However, these works have not taken into account active power reserves. This paper proposes a simple and efficient approach to determine the optimal placement of TCSC to reduce congestion index of the power system. In addition, the impact of compensation level of TCSC on LMPs and transmission charges of bilateral transactions in the wholesale electricity market when co-optimizing energy and active power reserve is also analyzed.

The next sections of the article are organized as follows. In section 2, the authors present optimization models to determine optimal placement of TCSC. Mathematical model of simultaneous optimization of the energy market and the active power reserve market, as well as methods to calculate the LMP are presented in section 3. Section 4 presents the methods for determining transmission costs in the electricity market and transmission charges of bilateral transactions. The calculated example for a 6 bus power system is presented and compared in section 5. Some conclusions are given in section 6.

## 2. Thyristor Controlled Series Capacitor (TCSC)

### 2.1. Static modeling of TCSC

Figure 1 shows a simple transmission line represented by its lumped PI equivalent parameters connected between bus  $i$  and bus  $j$ . The real and reactive power flow from bus  $i$  to bus  $j$  can be written as [3]:

$$P_{ij} = U_i^2 G_{ij} - U_i U_j \left[ G_{ij} \cos(\delta_{ij}) + B_{ij} \sin(\delta_{ij}) \right] \quad (1)$$

$$Q_{ij} = -U_i^2 (B_{ij} + B_{sh}) - U_i U_j \left[ G_{ij} \sin(\delta_{ij}) - B_{ij} \cos(\delta_{ij}) \right]$$

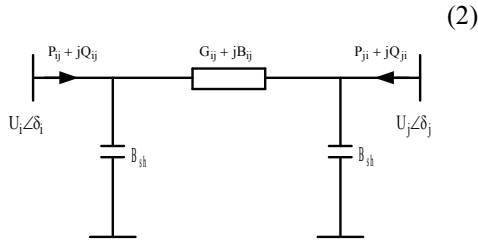


Figure 1. Model of transmission line

With a TCSC connected between bus  $i$  and bus  $j$ , the real and reactive power flow from bus  $i$  to bus  $j$  of a line are [6]:

$$P_{ij}^C = U_i^2 G'_{ij} - U_i U_j (G'_{ij} \cos \delta_{ij} + B'_{ij} \sin \delta_{ij}) \quad (3)$$

$$Q_{ij}^C = -U_i^2 (B'_{ij} + B_{sh}) - U_i U_j (G'_{ij} \sin \delta_{ij} - B'_{ij} \cos \delta_{ij}) \quad (4)$$

$$G'_{ij} = \frac{R_{ij}}{R_{ij}^2 + (X_{ij} - X_C)^2}; B'_{ij} = \frac{-(X_{ij} - X_C)}{R_{ij}^2 + (X_{ij} - X_C)^2} \quad (5)$$

The change in the line flow due to series capacitance can be represented as a line without series capacitance, with power injected at the receiving and sending ends of the line as shown in Figure 2 [6].

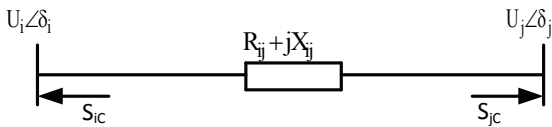


Figure 2. Injection model of TCSC

The real and reactive power injections at bus  $i$  and bus  $j$  can be expressed as follow [6]:

$$P_{iC} = U_i^2 \Delta G_{ij} - U_i U_j [\Delta G_{ij} \cos(\delta_{ij}) + \Delta B_{ij} \sin(\delta_{ij})] \quad (6)$$

$$P_{jC} = U_j^2 \Delta G_{ij} - U_i U_j [\Delta G_{ij} \cos(\delta_{ij}) - \Delta B_{ij} \sin(\delta_{ij})] \quad (7)$$

$$Q_{iC} = -U_i^2 \Delta B_{ij} - U_i U_j [\Delta G_{ij} \sin(\delta_{ij}) - \Delta B_{ij} \cos(\delta_{ij})] \quad (8)$$

$$Q_{jC} = -U_j^2 \Delta B_{ij} + U_i U_j [\Delta G_{ij} \sin(\delta_{ij}) + \Delta B_{ij} \cos(\delta_{ij})] \quad (9)$$

$$\Delta G_{ij} = \frac{X_C R_{ij} (X_C - 2X_{ij})}{(R_{ij}^2 + X_{ij}^2) [R_{ij}^2 + (X_{ij} - X_C)^2]} \quad (10)$$

$$\Delta B_{ij} = \frac{-X_C [R_{ij}^2 - X_{ij}^2 + X_C X_{ij}]}{(R_{ij}^2 + X_{ij}^2) [R_{ij}^2 + (X_{ij} - X_C)^2]} \quad (11)$$

## 2.2. Optimal location of TCSC

The severity of the system loading under normal cases can be described by a real power line performance index, as given below [3, 7],

$$PI = \sum_{m=1}^{NL} \frac{w_m}{2n} \left( \frac{P_{Lm}}{P_{Lm}^{\max}} \right)^{2n} \quad (12)$$

where  $P_{Lm}$  is the active power flow on line  $m$ ,  $P_{Lm}^{\max}$  is the limit of active power flow on line  $m$ .

In this paper, the value of  $n$  has been taken as 2 (to avoid masking effect) and weighting factors  $w_m = 1$  (the importance level of lines is similar).

To decrease congestion level of power transmission lines, TCSC should be placed in the line having the most negative sensitivity index  $b_k$  which is calculated below [7]:

$$b_k = \frac{\partial PI}{\partial X_{Ck}} \Big|_{X_{Ck}=0} \quad (13)$$

$$\frac{\partial PI}{\partial X_{Ck}} = \sum_{m=1}^{NL} w_m P_{Lm}^3 \left( \frac{1}{P_{Lm}^{\max}} \right)^4 \frac{\partial P_{Lm}}{\partial X_{Ck}} \quad (14)$$

$$\frac{\partial P_{Lm}}{\partial X_{Ck}} = \begin{cases} \left( SF_{mi} \frac{\partial P_i}{\partial X_{Ck}} + SF_{mj} \frac{\partial P_j}{\partial X_{Ck}} \right) & m \neq k \\ \left( SF_{mi} \frac{\partial P_i}{\partial X_{Ck}} + SF_{mj} \frac{\partial P_j}{\partial X_{Ck}} \right) + \frac{\partial P_j}{\partial X_{Ck}} & m = k \end{cases} \quad (15)$$

where  $SF_{mi}$ ,  $SF_{mj}$  is the sensitivity of branch power flow  $m$  with respect to injected power  $i$  and  $j$ , respectively.

## 3. Co-optimization of Energy and active power reserves

### 3.1. Objective function

The objective function of co-optimization problem of energy and reserves in the wholesale electricity market is to minimize the total cost to supply minus total consumer benefit. This objective function is expressed as Eq. (16).

$$\begin{aligned} & \sum_{i=1}^{N_G} \sum_{b=1}^{N_{Gi}} \lambda_{Gib} \cdot P_{Gib} \\ & + \sum_{i=1}^{N_G} \left( \lambda_{Gi}^{RR+} \cdot P_{Gi}^{RR+} + \lambda_{Gi}^{RR-} \cdot P_{Gi}^{RR-} + \lambda_{Gi}^{SR} \cdot P_{Gi}^{SR} + \lambda_{Gi}^{XR} \cdot P_{Gi}^{XR} \right) \\ & - \sum_{j=1}^{N_D} \sum_{k=1}^{N_{Dj}} \lambda_{Djk} \cdot P_{Djk} - \sum_{b=1}^{N_{RR+}} \lambda_b^{RR+} \cdot A_b^{RR+} - \sum_{b=1}^{N_{RR-}} \lambda_b^{RR-} \cdot A_b^{RR-} \\ & - \sum_{b=1}^{N_{CR}} \lambda_b^{CR} \cdot A_b^{CR} - \sum_{b=1}^{N_{OR}} \lambda_b^{OR} \cdot A_b^{OR} \end{aligned} \quad (16)$$

where  $\lambda_{Gib}$  is price of the energy block  $b$  offered by generating unit  $i$  (constant),  $P_{Gib}$  is power of the energy block  $b$  offered by generating unit  $i$  (variable),  $\lambda_{Gi}^{RR+}$  is price of Up Regulation Reserve (RR) offered by generating unit  $i$  (constant),  $\lambda_{Gi}^{RR-}$  is price of Down Regulation Reserve offered by generating unit  $i$  (constant),  $\lambda_{Gi}^{SR}$  is price of Spinning Reserve (SR) offered by generating unit  $i$  (constant),  $\lambda_{Gi}^{XR}$  is price of Supplemental Reserve (XR) offered by generating unit  $i$  (constant),  $P_{Gi}^{RR+}$  is Up Regulation Reserve Power offered by generating  $i$  (variable),  $P_{Gi}^{SR}$  is Spinning Reserve Power offered by generating  $i$  (variable),  $P_{Gi}^{XR}$  is Supplemental Reserve Power offered by generating  $i$  (variable),  $\lambda_{Djk}$  is price of the energy block  $k$  bid by demand  $j$  (constant),  $P_{Djk}$  is

power block b bid by demand j (variable),  $\lambda_b^{RR+}$  is price of Up Regulation Reserve block b bid by Area (constant),  $\lambda_b^{CR}$  is price of Contingency Reserve (CR) block b bid by Area (constant),  $\lambda_b^{OR}$  is price of Operation Reserve (OR) block b bid by Area (constant),  $A_b^{RR+}$  is Up Regulation Reserve Power block b bid by Area (variable),  $A_b^{CR}$  is Contingency Reserve Power block b bid by Area (variable),  $A_b^{OR}$  is Operation Reserve Power block b bid by Area (variable).

### 3.2. Constraints

#### 3.2.1. Network equations

The state of a power system of n buses is determined by 2n nodal equations:

$$P_i = P_{Gi} - P_{Di} = \left| \dot{U}_i \right| \left| \sum_{k=1}^n \dot{U}_j \right| (G_{ij} \cos \delta_{ij} + B_{ij} \sin \delta_{ij}) \quad (17)$$

$$Q_i = Q_{Gi} - Q_{Di} = \left| \dot{U}_i \right| \left| \sum_{k=1}^n \dot{U}_j \right| (G_{ij} \sin \delta_{ij} - B_{ij} \cos \delta_{ij})$$

#### 3.2.2. Reserve balance

For each area or zone, the reserve balance is shown according to the following expressions:

$$\sum_{i=1}^{N_G} P_{Gi}^{RR+} = A^{RR+} \quad (18)$$

$$\sum_{i=1}^{N_G} P_{Gi}^{RR-} = A^{RR-} \quad (19)$$

$$\sum_{i=1}^{N_G} (P_{Gi}^{SR} + P_{Gi}^{XR}) = A^{CR} \quad (20)$$

$$\sum_{i=1}^{N_G} (P_{Gi}^{RR+} + P_{Gi}^{SR} + P_{Gi}^{XR}) = A^{OR} \quad (21)$$

#### 3.2.3. Limits on generating active power of block b

$$0 \leq P_{Gib} \leq P_{Gib}^{\max} \quad (\forall i, b) \quad (22)$$

#### 3.2.4. Limits on generator power

The limits on generator active and reactive power of power plants, considering all kinds of reserves are expressed as Eq. (23) – (24).

$$0 \leq P_{Gi} + P_{Gi}^{RR+} + P_{Gi}^{SR} + P_{Gi}^{XR} \leq P_{Gi}^{\max} \quad (\forall i) \quad (23)$$

$$P_{Gi} - P_{Gi}^{RR-} \geq P_{Gi}^{\min} \quad (24)$$

$$Q_{Gi}^{\min} \leq Q_{Gi} \leq Q_{Gi}^{\max}$$

#### 3.2.5. Limits on reserve capacity of generating units

These constraints are shown as the following equations (25) – (28):

$$0 \leq P_{Gi}^{RR+} \leq P_{Gi \max}^{RR+} \quad (25)$$

$$0 \leq P_{Gi}^{RR-} \leq P_{Gi \max}^{RR-} \quad (26)$$

$$0 \leq P_{Gi}^{SR} \leq P_{Gi \max}^{SR} \quad (27)$$

$$0 \leq P_{Gi}^{XR} \leq P_{Gi \max}^{XR} \quad (28)$$

#### 3.2.6. Limits on elastic power of demand

In the wholesale electricity market, load is often represented by two components: constant load and price-sensitive load. Demand curve of the elastic demand can include multiple blocks and limits are expressed as Eq. (29) – (30).

$$P_{Dj}^{E \min} \leq P_{Dj}^E \leq P_{Dj}^{E \max} \quad (\forall j) \quad (29)$$

$$0 \leq P_{Djk}^E \leq P_{Djk}^{E \max} \quad (\forall j, k) \quad (30)$$

where  $P_{Dj}^E$  is the elastic power of demand j

#### 3.2.7. Limits on Area reserve power of block b

Area demand curves of reserve power can include several blocks and the MW size of each block, indexed by b, is expressed as Eq. (31) – (34).

$$0 \leq A_b^{RR+} \leq A_{b \max}^{RR+} \quad (31)$$

$$0 \leq A_b^{RR-} \leq A_{b \max}^{RR-} \quad (32)$$

$$0 \leq A_b^{CR} \leq A_{b \max}^{CR} \quad (33)$$

$$0 \leq A_b^{OR} \leq A_{b \max}^{OR} \quad (34)$$

#### 3.2.8. Spinning reserve percent constraint

For each area or zone, the spinning reserve (SR) usually accounts for at least SR% of contingency reserve (CR). This is due to the fact that the spinning reserve can only be provided by online units. Meanwhile, supplemental reserve (XR) is provided by online or offline fast-start units. This constraint is written as follows:

$$\sum_{i=1}^{N_G} P_{Gi}^{SR} \geq SR\% \cdot \sum_{i=1}^{N_G} (P_{Gi}^{SR} + P_{Gi}^{XR}) \quad (35)$$

#### 3.2.9. Branch flow limits

Branch flow limits are expressed as Eq. (36).

$$0 \leq S_{ij} = \sqrt{P_{ij}^2 + Q_{ij}^2} \leq S_{ij}^{\max} \quad (36)$$

#### 3.2.10. Voltage Limits

$$U_i^{\min} \leq U_i \leq U_i^{\max} \quad (37)$$

#### 3.2.11. Limits on bilateral contracts

When generating unit i and consumer j have a bilateral contract with contract power  $P^b$ , this constraint is expressed as equations (38)–(39):

$$P_{Gi} \geq P_{Gi}^b \quad (38)$$

$$P_{Dj} = P_{Dj}^E + P_{Dj}^F \geq P_{Dj}^b \quad (39)$$

where  $P_{Dj}^F$  is the constant power of demand j,  $P_{Gi}^b$  is the amount of power contract of generating unit i,  $P_{Dj}^b$  is the amount of power contract of demand j.

The above-mentioned AC-based optimal problem (ACOPF) be solved using successive linear programming (SLP) method [3].

### 3.3. LMP Calculation and Components

Location Marginal Price (LMP) is determined according to following equation [3].

$$LMP_i = LMP_E - LF_i \cdot LMP_E + \sum_l SF_{l-i} \cdot \mu_l \quad (40)$$

### 4. Transmission costs of bilateral transactions

The main objective of any transmission pricing method is to recover the transmission cost plus some profit. In order to recover operating costs, short-run marginal cost pricing (SMRC) based method is used in this paper [4]. SMRC is the difference in location marginal costs of supply bus and delivery bus. The location marginal costs of two buses can be determined from the solution of co-optimization energy and active power reserves shown in section 3. The transmission cost of bilateral contracts can be calculated by multiplying the power transaction with SRMC to obtain SRMC-based transmission charge [4].

In addition, the transmission pricing associated with each line or group of lines is also calculated. This transmission cost depends the power flow on a line proportion to power being transmitted by each transaction and determined through the use the linear Power Transfer Distribution Factor (PTDF). The PTDF can be defined as:

$$PTDF_{ij-mn} = \frac{\Delta P_{ij}}{\Delta P_{mn}^b} \quad (41)$$

where m and n are seller bus and buyer bus,  $\Delta P_{ij}$  is the change in power flow on line ij,  $\Delta P_{mn}^b$  is the change in power transfer of the bilateral transaction between m and n.

These PTDFs, which are computed at the base load flow condition, are utilized for computing change in transmission qualities at other operating conditions as well. The transmission costs (TC) paid by bilateral transactions are calculated as (42) and (43).

$$TC_{ij}^b = \Delta P_{ij-mn}^b (LMP_j - LMP_i) \quad (42)$$

$$TC^b = \sum_{ij} TC_{ij}^b \quad (43)$$

where  $\Delta P_{ij-mn}^b$  is the change in power flow on line ij when a power transfer of the bilateral transaction is changed between m and n.

## 5. Calculated results from a 6-bus system

### 5.1. Simulation Data

This section presents the calculated results using a 6 bus power system [3]. The energy offer prices of generating units and bid prices of price-sensitive demands include 5 blocks.

In terms of bilateral trade, two different bilateral transactions are carried out: between bus 1 and bus 6 with a contractual capacity of 20 MW, denoted as T1 (1, 6, 20); between node 2 and node 5 with a contractual capacity of 25 MW, denoted as T2 (2, 5, 25).

### 5.2. Optimal location of TCSC

The calculated  $b_k$  indices for the 6 bus system are shown in Table 1. From these results and the criteria for optimal location of TCSC expressed in section 2, TCSC is placed in line 2-6.

Table 1. Sensitivity  $b_k$

Line	$\frac{\partial P_i}{\partial X_{ck}}$	$\frac{\partial P_j}{\partial X_{ck}}$	$b_k$
1-2	-0.8830	0.8107	0.2679
1-4	-2.3154	2.2129	-0.8526
1-5	-1.2294	1.1625	0.0957
2-3	-0.0432	0.0401	0.0371
2-4	-4.5384	4.2975	1.4579
2-5	-0.6417	0.6118	-0.1375
<b>2-6</b>	<b>-1.4067</b>	<b>1.3546</b>	<b>-1.3442</b>
3-5	-0.9881	0.9188	-1.0195
3-6	-5.4084	5.2152	3.7894
4-5	-0.0713	0.0699	0.0456
5-6	0.0192	-0.0222	0.0189

When TCSC is located on the line 2-6, the impact of the control parameter of TCSC is shown in Figure 3. These results show that when the compensation level of TCSC is about 70% compared to the impedance of line 2-6, the PI index reaches the lowest value.

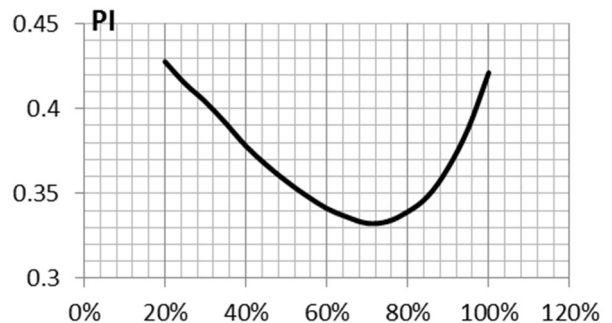


Figure 3. Effect of compensation level on PI indexes

### 5.3. Impact of TCSC on transmission cost

Without TCSC, transmission charges of two bilateral transactions are given in Table 2. Table 2 shows that although the capacity of bilateral contract T1 is less than that of T2, transmission cost of contract T2 is nearly 4 times as high as that of T1.

Table 2. Transmission cost of bilateral contracts

Line	LMP <sub>j</sub> - LMP <sub>i</sub> (\$/MWh)	T1 (1, 6, 20)		T2 (2, 5, 25)	
		(MW)	(\$/h)	(MW)	(\$/h)
1-2	0.36	8.37	3.012	-3.66	-1.319
1-4	0.83	6.35	5.271	-1.12	-0.928
1-5	1.67	5.82	9.719	4.46	7.448
2-3	-1.36	3.10	-4.216	3.87	-5.263
2-4	0.47	-5.21	-2.447	4.70	2.209

2-5	1.31	0.00	0.000	7.12	9.327
2-6	5.37	10.26	55.118	6.12	32.851
3-5	2.67	-2.54	-6.792	4.94	13.190
3-6	6.73	5.53	37.217	-0.99	-6.629
4-5	0.84	1.13	0.951	3.94	3.310
5-6	4.06	4.21	17.076	-4.62	-18.78
Total transmission cost	<b>114.9 \$/h</b>		<b>32.4 \$/h</b>		

When TCSC is located on the line 2-6, the difference in LMP between node 2 and 5 (bilateral contract T2) is lowest when the control parameter of TCSC is approximately 52%. Additionally, the transmission charge of this transaction are given in Figure 4.

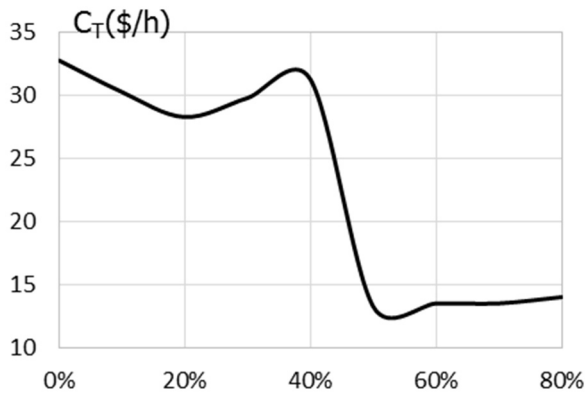


Figure 4. Effect of compensation level on transmission cost of transaction T2

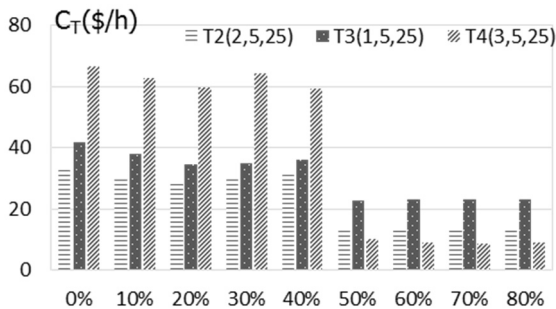


Figure 5. The impact of seller bus on transmission cost

The impact of the seller bus on transmission costs with different compensation levels is shown in Figure 5. The results show that with the same contractual capacity and the same compensation level, the position of seller bus can strongly affect transmission costs of the bilateral agreements.

## 6. Conclusion

This paper presents an approach to determine the optimal placement of TCSC to reduce congestion in the electric grid. Moreover, authors also presents the mathematical model of co-optimization problem of energy and active power reserve. The result of this optimization problem is location marginal price (LMP), the output capacity and reserve power of the generating units and the capacity of elastic loads. The influence of TCSC on LMPs, PI indices and transmission charges of bilateral agreements is also calculated and compared.

## REFERENCES

- [1] Hongyan Li, Leigh Tesfatsion, "ISO Net surplus collection and allocation in wholesale power markets under LMP", *IEEE Trans. Power Systems*, vol. 26, pp. 627-641, April 2011.
- [2] Marco Zugno, Antonio J. Conejo, "A robust optimization approach to energy and reserve dispatch in electricity markets", *European Journal of Operational Research*, 2015, page(s). 659-671.
- [3] Allen J. Wood, Bruce F. Wollenberg, Gerald B. Sheble, *Power generation, operation and control*, Wiley & Sons, Inc, New Jersey, 2014.
- [4] Kankar Bhattacharya, Math H.J. Bollen, Jaap E. Daalder, *Operation of restructured power systems*, Kluwer Academic Publishers, 2001.
- [5] Xingwang Ma, Yonghong Chen, Jie Wan, "MIDWEST ISO Co-Optimization based real-time dispatch and pricing of energy and ancillary services", 2009 IEEE General Meeting, July, 2009.
- [6] Xiao-Ping Zhang, Christian Rehtanz and Bikash Pal, *Flexible AC Transmission Systems: Modelling and Control*, Springer, 2012.
- [7] Seyed Abbas Taher, Hadi Besharat, "Transmission Congestion Management by Determining Optimal Location of FACTS Devices in Deregulated Power Systems", *American Journal of Applied Sciences* 5 (3), pp(s): 242-247, 2008.
- [8] N. Acharya and N. Mithulananthan, "Influence of TCSC on congestion and spot price in electricity market with bilateral contract", *Elect. Power Syst. Res.*, vol. 77, pp. 1010-1018, 2007.
- [9] N. Acharya and N. Mithulananthan, "Locating series FACTS devices for congestion management in deregulated electricity market", *Elect. Power Syst. Res.*, vol. 77, no. 3-4, pp. 352-360, 2007.

(The Board of Editors received the paper on 15/07/2016, its review was completed on 05/08/2016)

# Simulation of a Power Grid Blackout Event in Vietnam

Huy Nguyen-Duc\*, Huy Cao-Duc<sup>†</sup>, Chien Nguyen-Dinh<sup>‡</sup> and Viet Nguyen-Xuan-Hoang<sup>§</sup>

\*School of Electrical Engineering

Hanoi university of Science and Technology, 1 Daicoviet road, Hanoi

Email: huy.nguyenduc1@hust.edu.vn

<sup>†</sup> Power system department, Institute of Energy, Vietnam

Email: caohuy2310@gmail.com

<sup>‡</sup>Dispatching department, National Load Dispatch Center

Hanoi, Vietnam Email: dinhchien216@gmail.com

<sup>§</sup>School of Mechanical, Electrical and Electronic Engineering, HUTECH  
Hochiminh city, Vietnam

**Abstract**—This paper presents some results of our ongoing research on the dynamic performance of the Vietnam power system. The study involves simulations of N-1 events in the 500-220kV transmission system, especially the loss of an 500kV circuit, which in reality has caused a large scale blackout in the Southern grid of Vietnam, in May 2013. The simulations reveal some interesting results, regarding the operation of transmission line and generators protection systems. The sequence of relay operation can change the course of a large scale event drastically. The results provide us with new insight to revise relay settings that helps reduce the risk of cascade tripping.

## I. INTRODUCTION

The power system can be considered as one of the most sophisticated manufacturing process, involving several thousand of elements. To ensure the reliability of the power systems, the protection and control devices are needed to determine and isolate quickly the faulty elements that could potentially jeopardize the system security. Besides, good operating practices also contribute to the secure operation of power systems. However, large disturbances causing cascading events still occur, under some extra-ordinary circumstances.

Some of the most severe power grid failures in the recent years include the North America blackout in 2003 [1], the Italy blackout in September 2003 [2], the India power grid failure in 2012 [3]. Large scale cascading events normally originate from a failure of an important component, which subsequently leads to overloading of other component, causing cascaded tripping [4]. The analysis of power system operating conditions to determine critical contingencies is a very challenging task, since there are a lot of contingency simulations involved. It is not possible to eliminate totally the risk of blackout [4]. However, the understanding of the mechanism of cascading events certainly provide valuable information for grid planners and dispatchers, in order to reduce the risk of major grid failures.

In the power system dynamics and stability literatures, the mechanism of instability can be divided into three main categories [5]: Voltage instability, frequency instability and rotor angle instability. However, during the course of a large

scale cascading events, these dynamics often happen at the same time. Besides, the performance of the protective relaying system also plays a very important role. Under normal operating conditions, it is difficult to predict the interactions between numerous protective and control devices in the system. For this reason, the post-mortem analysis of the sequence of events and the root cause of major grid failures helps reveal important characteristic of the power system. This analysis helps improve the power system planning, and the setting of protective relays.

This paper presents our initial simulation results of a major grid blackout in Vietnam in May 22nd, 2013. The event was initialized by a permanent fault on a 500kV line in the Southern region of Vietnam. The tripping of this 500 circuit led to cascaded tripping of several other elements, including generators and transmission lines. The cascaded tripping separated the Southern grid from the North and the Central grid, and voltage collapse occurred in the Southern system. The methodology of this study is to carry out several simulations of the power system, with different scenarios (relay setting and loading condition), in order to find the most probable sequence of events.

The paper is organized as follows: Section II present some background information on the mechanism of blackout involving voltage collapse. Section III present the simulation models used in this study, including those of the generators, generator control systems and protective relays. Section IV presents typical simulation results. Some conclusion are given in Section V.

## II. POWER SYSTEM BLACKOUT AND VOLTAGE COLLAPSE

The blackout event in Vietnam in May 2013 was initialized by a permanent short-circuit fault on a 500kV transmission line. The tripping of this circuit has led to cascaded tripping of other transmission lines and generating units, causing the separation of the Southern grid from the Northern and Central grid. After the separation, the Southern grid experienced voltage collapse. The critical system condition caused several

protection relays to trip, which eventually led to the blackout in the Southern grid.

In many major power system disturbances and grid blackout, the voltage collapse phenomenon is identified as one important cause. A typical scenario for voltage collapse is as follows [6], [7]:

- Following a loss of a power system element, such as an important transmission line, or a large generating unit, the other element of the system is overloaded, leading to low voltage level at some system buses.
- Low voltage often leads to high current flows, which leads to overloading of power system components. At certain point, the overloaded component is tripped, which propagates the overload problem to other elements of the system.
- As the system elements are tripped, the lack of reactive support becomes more severe. Some generator Over Excitation Limiter relays may pick up.
- If the voltage problem is not mitigated in time, OEL relays will trip, leading to even more severe voltage problems. Moreover, when generators are tripped, the system may also experience low frequency problem.
- At some point, as the voltage level in the transmission network is too low, the transmission line distance relay may trip with Zone 3, or even Zone 2 element.

Depending on the strength of the system, the voltage collapse phenomenon can occur in a time frame of several minutes. The load response to voltage variation also plays an important role in the voltage dynamics.

### III. RELAY PERFORMANCE DURING MAJOR GRID FAILURES

In order to accurately assess the voltage instability process and the sequence of events, it is necessary to consider the operation of protective relays which can operate during the process. This section provides an overview of principal relaying component, and their models in PSS/E.

#### A. Over-current relay.

General principle of over-current protection relays is to send a tripping signal to current-interrupting devices when the measured current exceeds the predetermined value. Over-current relay operation often acts as a triggering event in the beginning of voltage stability process, and is direct cause of bifurcation. In this research, built-in model TIOCR1 of PSS/E was utilized to simulate the operation of over-current relays. Setting parameters of TIOCR1 models were calculated according to [8].

#### B. Distance protection relay

Distance protection relay is an impedance relay, which calculates apparent impedance from the voltage and current at relays location. If the measured impedance enters the protection zone, the relay will pick up and send tripping signals when its timer timed out.

The apparent impedance of distance relays depends greatly on measured voltage. Therefore, distance protection relays

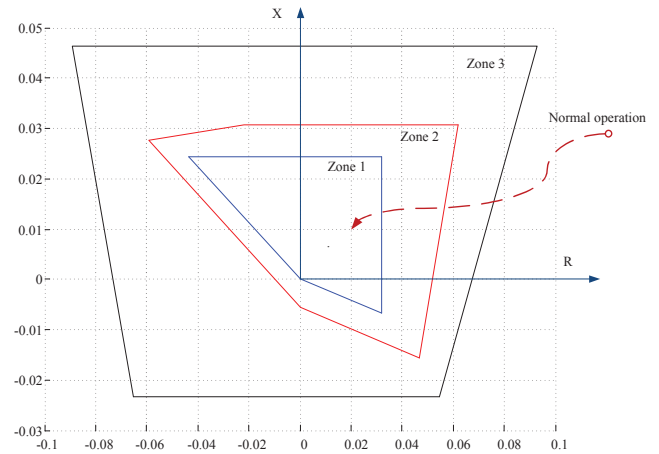


Fig. 1. Distance relay characteristic.

might operate during voltage instability process (which is correct, but inappropriate [9]). In our simulations, distance protection relays were simulated by PSS/E's built-in model RXR1 [10]. Setting parameters of RXR1 models were calculated according to [8]. The characteristics of model RXR1 are described in Fig. 1.

#### C. Out-of-step relay.

Out-of-step relay is also an impedance relay, used to prevent severe loss of synchronism between the generator and the power system. The relay sends tripping signal when it detects passage of the apparent impedance locus through an area of its characteristic. A rapid passage is interpreted as evidence of a fault. A passage which takes more than a defined time might indicate a power oscillation, or out-of-step condition [11].

Similar to distance protection relay, out-of-step relay is sensitive to voltage drop. Therefore, it may operate during voltage collapse. In this research, out of step relays is simulated by PSS/E model CIROS1 [10], with double lens impedance characteristic, as shown in Fig. 2.

#### D. Over-excitation limiter - OEL

Disturbances can make generators operate at the excitation level that higher than nominal. Those cases can lead to overload of generator field winding. Because of that, over excitation limiter (OEL) is utilized to reduce the field current, prevent overheating in generator field. While this action can protect the generator, OEL contributes to voltage stability since it make the reactive power burden to other generators. The operation of a generator's OEL, therefore, can lead to the operation of another generators OEL. Over-excitation limiter is simulated in PSS/E by the MAXEX1 model. The models characteristic is shown in Fig. 3. In this study, settings for OEL function are based on the IEEE guide C37.102 [12] and generators parameters.

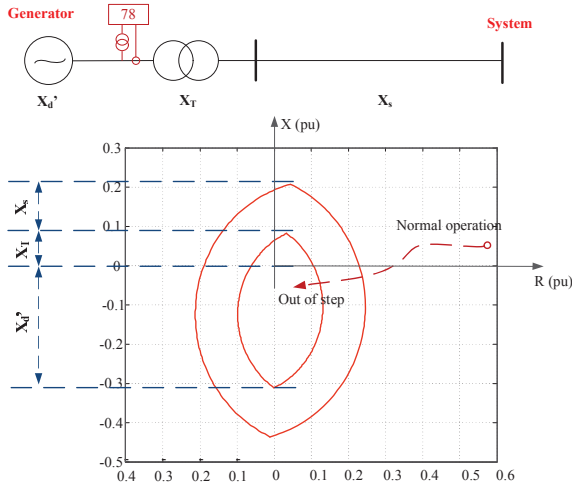


Fig. 2. Out of step relay characteristic.

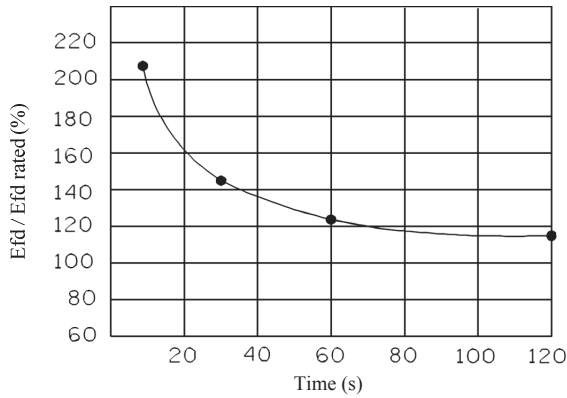


Fig. 3. OEL relay characteristic.

### E. Under-frequency load-shedding relay

When the interconnection lines are tripped, the power system can be divided into various separate islands, in which frequencies depend on the balance between load and available generation. If load exceeds generation, frequency will decrease, which, in some cases, causes a frequency collapse. To prevent frequency collapse and recover the island from under-frequency situation, under-frequency load-shedding relay is used. The relay drops a sufficient amount of load when measured frequency is less than predetermined value. Under-frequency load-shedding relay is simulated in PSS/E by LDSHxx type models. Setting parameters of LDSHxx models were calculated according to Vietnam Grid Code.

## IV. SIMULATION RESULTS

The simulation model is constructed in PSS/E, based on the typical operating condition of the Vietnam power system in late 2012/early 2013. There are approximately 1500 bus and 2000 branches, from 110kV to 500kV voltage level. Besides generators and generator control devices, relays models are also modeled for important network elements (transmission

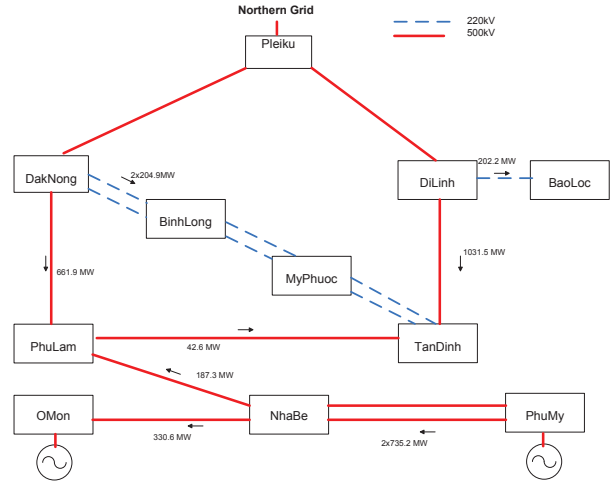


Fig. 4. Load flow condition prior to the grid disturbance.

lines and generators), especially those close to the studied region. The typical operating condition is shown in Fig. 4. In this operation mode, the circuit Di Linh - Tan Dinh is loaded at around 1000MW (approximately the SIL at 500kV voltage level). The tripping of this transmission line would therefore cause severe impact on the remaining circuits.

When the 500kV Di Linh - Tan Dinh circuit is tripped, the other transmission lines have to carry additional active power. Moreover, the remaining circuits would also have to operate above their SIL level, which creates additional reactive demand. As a result, the generating units connecting to this 500kV system would have to produce more reactive power.

Besides, the shortage of reactive power also affects the distance relay, since apparent impedances are reduced with voltage. Therefore distance relays might also be activated. It should be noted that the distance protection on the 500kV transmission line of Vietnam has a somewhat large zone 2, since it is calculated based on the assumption that all series compensators are bypassed. Under heavy load condition and low voltage, the zone 2 distance protection may be activated (phase-phase element).

For the simulation scenarios created in our study, distance relays on the Dak Nong - Phu Lam transmission lines and OEL protection of Phu My power plant (which connects to the Phu My 500kV substation) are activated when the Di Linh - Tan Dinh circuit is tripped.

### A. Stable scenario

In this scenario, the resistive element of the Zone 2 element of the Dak Nong-Phu Lam circuit was set to 1.56 times the reactance element. This setting is in the range of recommended setting by Siemens [8]. With this setting, the Dak Nong-Phu Lam circuit is tripped by Zone 2 element at 7.89s, which splits the Northern and the Southern system. The detailed sequence of events are as follows:

- At 2.00s, a permanent fault occurs on 500kV transmission line Di Linh-Tan Dinh, near 500kV Tan Dinh substation.

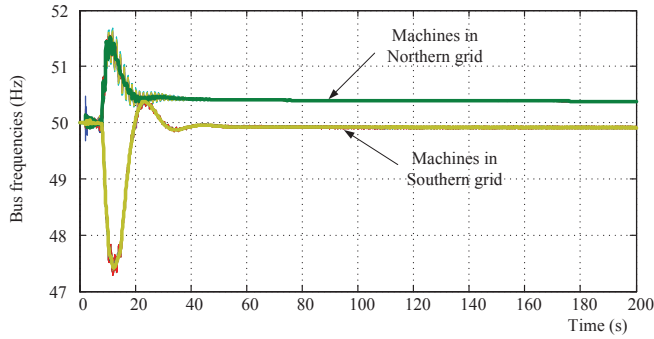


Fig. 5. Bus frequencies of the first scenario.

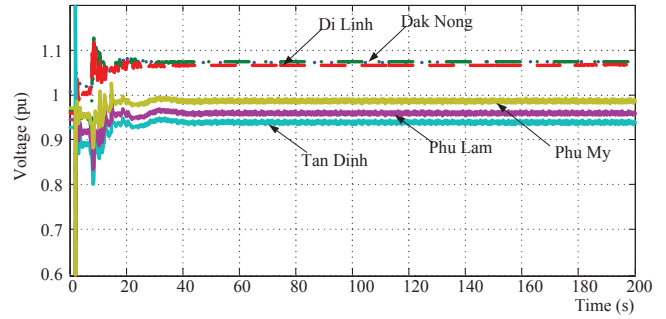


Fig. 7. Bus voltages, stable scenario.

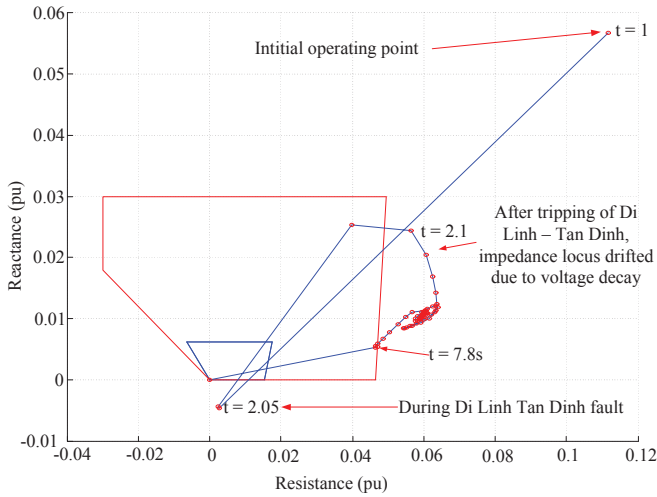


Fig. 6. Impedance locus of Phu Lam-DakNong 500kV line, stable scenario.

At 2.042s, Di Linh- Tan Dinh 500kV line trips. Voltages are recovered, but less than prior-fault voltages. The lack of reactive power in The South leads to the activation of some generator OELs, especially at the Phu My power plant.

- At 4.004s, over-current relay of 220kV transmission line Di Linh-Bao Loc activates. At 6.98s, this relay timer timed out. The 220kV transmission line Di Linh Bao Loc trips at 7.04s.
- At 7.56s, distance relay of 500kV Dak Nong- Phu Lam activates with apparent impedance in zone 2. The tripping signal is sent at 7.86. Dak Nong- Phu Lam line trips at 7.89s. Impedance locus observed by 500kV Dak Nong Phu Lam relay is shown in Fig. 6.
- The last interconnection between Northern and Southern power grid is 220kV transmission line Dak Nong- Binh Long. This line is soon tripped by distance relay at 8.152s. The power system divides into 2 separate islands.

After the separation, northern grid frequency increases to 51.5 Hz, then stabilizes at 50.4 Hz by generators governor action. At the same time, southern grid frequency decreases to 47.5 Hz due to the imbalance between load and available generation. From 10.39s to 17.32s, under-frequency load-

shedding relays in the South operate. The total amount of shed load is 2172 MW, which is roughly equal to the lack of active power in the South. The load shedding helps recover frequency in the Southern grid (Fig. 5). Some comments for this scenario are as follows:

- The power system split before OELs protection timed out.
- After system separation, thanks to the operations of load-shedding relays, the southern grid frequency is stabilized.
- After load-shedding has finished, the voltages in The South are recovered (Fig. 7). Therefore the OELs reset.

In this scenario, the blackout event did not occur. However, nearly 2000MW of load (which is approximately the amount of power imported from the Northern grid prior to the disturbance) has been shed.

### B. Unstable scenario

In this scenario, Zone 2 distance protection of Dak Nong-Phu Lam circuit has only slightly smaller resistive reach (1.55 times its reactance element). However, the resulting course of events has changed drastically:

- At 2.00s, a permanent fault occurs on 500kV transmission line Di Linh- Tan Dinh, near 500kV Tan Dinh substation. At 2.042s, Di Linh- Tan Dinh 500kV line trips. Voltages are recovered, but less than prior-fault voltages. The lack of reactive power in The South leads to the activation of some OELs, especially those at the Phu My powerplant.
- At 4.004s, over-current relay of 220kV transmission line Di Linh-Bao Loc activates. At 6.98s, this relay operates and send a tripping signal to the circuit breaker. The 220kV transmission line Di Linh Bao Loc trips at 7.04s
- At this point, the sequence of events are the same as in the first scenario. OELs of Phu My power plant and some other power plants are activated. The impedance locus of the Dak nong-Phu Lam circuit is also drifting slowly, but does not enter the protection zone (Fig. 8).
- Since the Dak Nong-Phu Lam circuit remains in service, the North-South interconnection is kept. However, several generating unit OEL are activating. Finally, at 41.58s, the OEL of PHUMY 2.1 plant trips, leading to a cascading relay operation in the South. From 41.58s to 88.93s, there are 13 OEL operated, reducing voltage profile of the South.

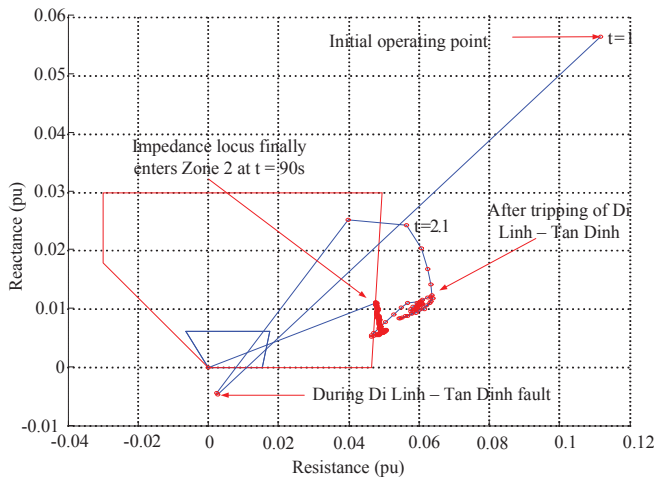


Fig. 8. Impedance locus of Phu Lam-DakNong 500kV line, unstable scenario

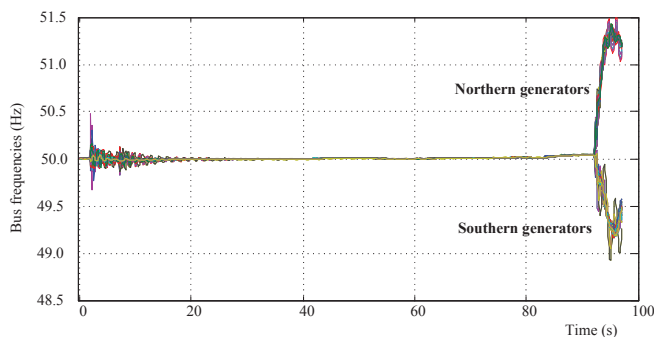


Fig. 9. Bus frequencies, unstable scenario.

- Voltage drop and overloading in 500kV transmission line Phu Lam- Dak Nong caused further reduction in apparent impedance observed by distance relay. Finally the 500kV Dak Nong- Phu Lam circuit is tripped at 92.18s.
- After that, at 92.56s, the last South-North interconnection line 220kV Dak Nong- Binh Long trips due to overloading. Voltage collapse phenomenon is observed in the southern area, since there are too little dynamic reactive support left at this time to maintain the transmission voltage.

The voltage collapse can be observed clearly in the Fig. 10. Voltages in the Southern regions reach as low as 0.4pu. The system frequency of this scenario is shown in Fig. 9. Due to low voltage, several other generators lose synchronism, and are tripped by out-of-step relays. Besides, several transmission lines are also tripped by distance protection relays. This result and the time frame to voltage collapse agree well with actual fault records.

## V. CONCLUSION

This paper presents our initial simulation results of a major grid blackout in Vietnam on May 22nd, 2013. The protective relaying system has been taken into account. The study reveals

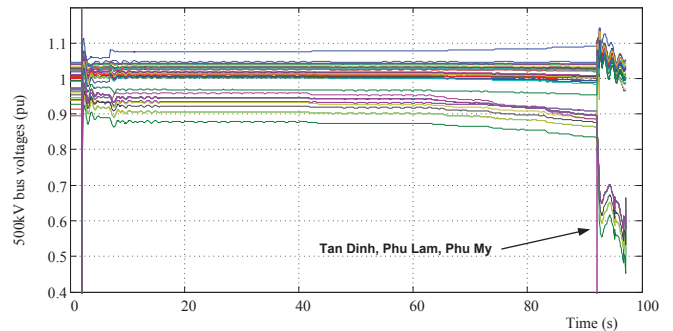


Fig. 10. 500kV bus voltages, unstable scenario.

that the sequence of relay operation can change drastically the final outcome of the power system contingency. In the studied scenarios, if the grid is separated prior to the operation of OELs relays, the blackout event could have been avoided.

It should be noted that the validation of all conclusion from this study is a very difficult task. In fact, the actual event data involve a large number of fault records, the exact sequence of which has not yet fully established. However, the unstable scenario in this study has the time frame to voltage collapse, and several relay operations which agree well with the main events during May 2013 grid disturbance.

## ACKNOWLEDGMENT

This research is funded by the Vietnam Ministry of Education and Training, under grant number B2014-01-76.

## REFERENCES

- [1] "Technical analysis of the august 14, 2003, blackout: What happened, why, and what did we learn?" North American Electric Reliability Council, Tech. Rep., July 2003.
- [2] UCTE, "Final report of the investigation committee on the 28 september 2003 blackout in italy," Tech. Rep., 2003.
- [3] L. L. Lai, H. T. Zhang, S. Mishra, D. Ramasubramanian, C. S. Lai, and F. Y. Xu, "Lessons learned from july 2012 indian blackout," in *9th IET International Conference on Advances in Power System Control, Operation and Management*, 2012.
- [4] IEEE, "Blackout experiences and lessons, best practices for system dynamic performance, and the role of new technologies," IEEE PES Working Group on Power Grid Blackouts, Power System Dynamic Performance Committee, Tech. Rep., 2007, IEEE PES Special Publication 07TP190.
- [5] IEEE/CIGRE Joint Task Force on Stability Terms and Definitions, "Definition and classification of power system stability," *IEEE Transactions on Power systems*, vol. 19, no. 2, pp. 1387–1401, 2004.
- [6] C. W. Taylor, *Power System Voltage Stability*. McGrawHill, 1994.
- [7] G. Morison, G. Bao, and P. Kundur, "Voltage stability analysis using static and dynamic approaches," *IEEE Transactions on Power systems*, vol. 8, no. 3, pp. 1159–1171, 1993.
- [8] SIEMENS, "Application for siprotec protection relays," Tech. Rep., 2005.
- [9] S. H. Horowitz and A. Phadke, "Blackouts and relaying considerations," *IEEE Power and Energy magazine*, 2006.
- [10] SIEMENS, "PSS/E program application guide," Tech. Rep., 2013.
- [11] W. Elmore, *Protective relaying: theory and applications*, C. Press, Ed., 2003.
- [12] IEEE, "IEEE guide for AC generator protection," IEEE Power Engineering Society, Tech. Rep., 2006, c37.102.